UNIVERSITY OF CALIFORNIA, SAN DIEGO

A Rab5 Endosomal Pathway Mediates Parkin-Dependent Mitochondrial Clearance

A dissertation submitted in partial satisfaction of the requirements
for the degree Doctor of Philosophy

in

Biomedical Sciences

by

Babette Hammerling

Committee in charge:

Professor Åsa Gustafsson, Chair
Professor Joan Heller Brown
Professor Ju Chen
Professor Amy Kiger
Professor JoAnn Trejo

2017

The Dissertation of Babette Hammerling is approved, and it is acceptable in quality and form for publication on microfilm and electronically:

_____

_____

_____

_____

_____

Chair

University of California, San Diego

2017

DEDICATION

I dedicate this dissertation to my family, for their lifetime of support and encouragement, and to my friends who have provided advice, encouragement, and help along the way.

TABLE OF CONTENTS

LIST OF ABBREVIATIONS

3D	3 dimensional
3-MA	3-Methyladenine
Ad-	Adenovirus
AAA	ATPases associated with diverse cellular activities
αMHC	α-myosin heavy chain
AMPK	Adenosine monophosphase(AMP)-activated protein kinase
ANOVA	Analysis of variance
APEX2	Apurinic/apyrimidinic endodeoxyribonuclease 2
Atg	Autophagy
ATP	Adenosine triphosphate
Baf A1	Bafilomycin A1
BAX/BAK	BCL2-associated X protein (BAX)/BCL2-antagonistic/killer (BAK)
BCL2	B-cell CLL/lymphoma 2
BNIP3	BCL2/adenovirus E1B 19 kDa protein-interacting protein 3
BNIP3L/Nix	BCL2/adenovirus E1B 19 kDa protein-interacting protein 3 Like
BSA	Bovine serum albumin
CCCP	Carbonyl cyanide m-chlorophenyl hydrazine
CCD	Charged coupled device
cDNA	Complementary DNA

Chmp	Charged multivesicular body protein
cKO	Conditional knockout
Clp	Caseinolytic mitochondrial matrix peptidase
CMA	Chaperone mediated autophagy
CNS	Central nervous system
Con	Control
CVD	Cardiovascular disease
DAB	Diaminobenzidine
DKO	Double knockout
DMEM	Dulbecco's modified eagle medium
DMSO	Dimethyl sulfoxide
DNA	Deoxyribonucleic acid
Drp1	Dynamin related protein 1
DTT	Dithiothreitol
EAP	ELL-associated protein
EDTA	Ethylenediaminetetraacetic acid
EE	Early endosome
EEA1	Early endosome antigen 1
EEE	Enlarged early endosome
EF	Ejection fraction
EGFP	Enhanced green fluorescent protein
EGFR	Epidermal growth factor receptor
EGTA	Ethylene glycol-bis(β-aminoethyl ether)-N,N,N',N'-tetraacetic

	acid
EHD3	EH domain containing 3
EM	Electron microscopy
ER	Endoplasmic reticulum
ERAD	Endoplasmic reticulum-associated protein degradation
ESCRT	Endosomal sorting complex required for transport
FBS	Fetal bovine serum
FCCP	Carbonyl cyanide-4-(trifluoromethoxy)phenylhydrazone
Fis1	Fission protein 1
FS	Fractional shortening
FUNDC1	FUN14 domain containing 1
GABARAP	Gamma-aminobutyric acid receptor-associated protein
GAPDH	Glyceraldehyde-3-phosphate dehydrogenase
GDP	Guanosine diphosphate
GFP	Green fluorescent protein
GTP	Guanosine triphosphate
h	Hour(s)
HAF-1	HAlF transporter
HEPES	4-(2-hydroxyethyl)-1-piperazineethanesulfonic acid
hMvb12	Human multivesicular body subunit 12
Hgs	Hepatocyte growth factor-regulated tyrosine kinase substrate
Hsp	Heat shock protein
Htra2/omi	HtrA Serine Peptidase 2

HW	Heart weight
I/R	Ischemia/reperfusion
ICLAC	International cell line authentication committee
ILV	Intraluminal vesicle
IMM	Inner mitochondrial membrane
IMS	Intermembrane space
LAMP1/2	Lysosome-associated membrane protein 1/2
LC3	Microtubule-associated protein 1 light chain 3
LC-MS/MS	Liquid chromatography-tandem mass spectrometry
LE	Late endosome
LM	Light microscopy
M199	Medium 199
MACS	Magnetic-activated cell sorting
MAPL	Mitochondrial-anchored protein ligase
Mdivi-1	Mitochondrial division inhibitor 1
MDV	Mitochondrial derived vesicle
MEF	Mouse embryonic fibroblast
Mfn1/2	Mitofusin 1/2
MI	Myocardial infarction
Miro	Mitochondrial rho GTPase 1
Mitoptosis	Mitochondrial apoptosis
Mnd2	Motor neuron degeneration 2
MOI	Multiplicity of infection

MOPS	3-(N-morpholino)propanesulfonic acid
MPP	Mitochondrial processing peptidase
mPTP	Mitochondria permeability transition pore
MS	Mass spectrometry
mtDNA	Mitochondrial DNA
MULAN	Mitochondrial ubiquitin ligase activator of NF-KB
MVB	Multivesicular body
Nbr1	Neighbor of BRCA1 gene 1
OCR	Oxygen consumption rate
OMM	Outer mitochondrial membrane
OPA1	Optic atrophy 1
P40PX	PX domain of p40
P62/Sqstm1	Sequestosome 1
PARL	Presenilin associated rhomboid like
PBS	Phosphate buffered saline
PCR	Polymerase chain reaction
pH	Potential of hydrogen
PI(3)P	Phosphatidylinositol 3-phosphate
PI3K	Phosphoinositide 3-kinase
PINK1	PTEN-induced putative kinase 1
PST	PBS plus 5% normal goat serum and 0.2% Tween20
qPCR	Quantitative polymerase chain reaction
RING	Really interesting new gene

RNAi	Ribonucleic acid interference
ROS	Reactive oxygen species
RPM	Revolutions per minute
SDS-PAGE	Sodium dodecyl sulfate-polyacrylamide gel electrophoresis
S.E.M.	Standard error of the mean
shRNA	short hairpin ribonucleic acid
sI/R	Simulated ischemia/reperfusion
siRNA	Small interfering ribonucleic acid
Sirt3	Sirtuin 3
Smac/Diablo	Second mitochondria-derived activator of caspase
SNARE	SNAP (soluble NSF attachment protein) receptor
Stam1/2	Signal transducing adaptor molecule 1/2
Stx17	Syntaxin 17
SV40	Simian vacuolating virus 40
TCA	Tricarboxylic acid cycle
TFEB	Transcription factor EB
TL	Tibia length
TOM	Translocase of the outer mitochondrial membrane
TORC1	Transcriptional coactivator for CREB1
Tsg101	Tumor susceptibility 101
UBA	Ubiquitin-associated domain
Ulk1/2	Unc-51 like autophagy activating kinase 1/2
Un	Untransfected

UPS	Ubiquitin proteasome system
UVRAG	UV radiation resistance associated gene
VDAC1	Voltage dependent anion channel 1
Vps	Vacuolar Protein Sorting
Vta1	Vesicle trafficking 1
WT	Wild type
YFP	Yellow fluorescent protein
Yme1l	Yme1 like 1 ATPase
ZVAD	N-benzyloxycarbonyl-val-ala-asp(O-Me)

LIST OF FIGURES

ACKNOWLEDGEMENTS

I would like to acknowledge Dr. Åsa Gustafsson for all of her support and assistance as my mentor over the past several years. She was generous enough to take me into her lab mid-way through my graduate career, and encouraged me to do my best work. Her patience and understanding has allowed me to grow into a better scientist who is more at ease with taking risks.

I would also like to thank all the members of the Gustafsson lab. Their assistance, jokes, and friendships not only aided me through the tougher times but also helped me to troubleshoot my experiments.

Additionally, I want to thank Jonathan Grinstein and Dekker Deacon, from my former lab, who spent countless hours with me in the TC talking about life, science, and grad school. They taught me everything from setting up proper experimental controls to life lessons, and I still recall their advice often.

Lastly, I want to thank the BMS staff, Gina, Leanne, Kathy, and Pat, for making BMS great and having everything run so smoothly. They promptly addressed problems and truly keep an eye out for every student in the program.

Parts of Chapter 1 were originally published in *the Journal of Molecular and Cellular Cardiology.* Hammerling, B. C., & Gustafsson, A. B. Mitochondrial quality control in the myocardium: cooperation between protein degradation and mitophagy. *Journal of Molecular and Cellular Cardiology.* 75: 122-130, 2014. © 2014 Elsevier Inc. The dissertation author was the primary investigator and author of this paper.

Parts of Chapters 2 through 7 were originally published in *Nature Communications*. Hammerling, B. C., Najor, R. H., Cortez, M. Q., Shires, S. E., Leon, L.

J., Gonzalez, E. R., Boassa, D., Phan, S., Thor, A., Jimenez, R. E., Li, H., Kitsis, R. N., Dorn II, G. W., Sadoshima, J., Ellisman, M. H., Gustafsson, A. G. A Rab5 Endosomal Pathway Mediates Parkin-Dependent Mitochondrial Clearance. *Nature Communications*. 8: 14050, 2017; doi:10.1038/ncomms14050 © 2017 Nature Publishing Group. The dissertation author was the primary investigator and author of this paper.

Parts of Chapters 2, 4, 6 and 7 were originally published in *Small GTPases*. Hammerling, B. C., Shires, S. E., Leon, L. J., Cortez, M. Q., Gustafsson, A. G. Isolation of Rab5-Positive Endosomes Reveals a New Mitochondrial Degradation Pathway Utilized by BINP3 and Parkin. *Small GTPases*. 1-8, 2017; doi: doi:10.1080/21541248.2017.1342749. © 2017 Taylor & Francis Online. The dissertation author was the primary investigator and author of this paper.

VITA

2011 Bachelor of Arts, Biological Sciences, Rutgers University, New Brunswick

2017 Doctor of Philosophy, Biomedical Sciences, University of California, San Diego

PUBLICATIONS

Hammerling, B.C., S.E. Shires, L.J. Leon, M.Q. Cortez, and A.B. Gustafsson. Isolation of Rab5-positive endosomes reveals a new mitochondrial degradation pathway utilized by BNIP3 and Parkin. Small GTPases: 1-8, doi:10.1080/21541248.2017.1342749, 2017.

Hammerling, B.C., R.H. Najor, M.Q. Cortez, S.E. Shires, L.J. Leon, E.R. Gonzalez, D. Boassa, S. Phan, A. Thor, R.E. Jimenez, H. Li, and R.N. Kitsis. A Rab5 endosomal pathway mediates Parkin-dependent mitochondrial clearance. Nature communications. 8:14050, 2017.

Hammerling, B.C. and Gustafsson, A.B. Mitochondrial Quality Control in the Myocardium: Cooperation Between Protein Degradation and Mitophagy. J Mol Cell Cardiol *75*, 122-130, 2014.

Masand, S.N., J. Chen, I.J. Perron, B.C. Hammerling, G. Loers, M. Schachner, and D.I. Shreiber. The effect of glycomimetic functionalized collagen on peripheral nerve repair. Biomaterials. 33:8353-8362, 2012.

ABSTRACTS

Hammerling, B.C., Cortez, M.Q., Hanna, R.A., and Gustafasson, Å.B., Parkin is Critical for the Clearance of Damaged Mitochondria via an Autophagy-Independent Pathway. Basic Cardiovascular Sciences Scientific Sessions 2016, Phoenix, Arizona, Jul 18-21, 2016.

Hammerling, B.C., Cortez, M.Q., Hanna, R.A., Gonzalez, E.R., and Gustafasson, Å.B., The E3 Ubiquitin Ligase Parkin Mediates Clearance of Damaged Mitochondria via Two Distinct Pathways. Selected for Best of BCVS poster presentation at American Heart Association Scientific Sessions 2015, Orlando, Florida, Nov 7-11, 2015.

Hammerling, B.C., Cortez, M.Q., Hanna, R.A., Gonzalez, E.R., and Gustafasson, Å.B., The E3 Ubiquitin Ligase Parkin Mediates Clearance of Damaged Mitochondria via Two

Distinct Pathways. Basic Cardiovascular Sciences Scientific Sessions 2015, New Orleans, Louisiana, Jul 13-16, 2015.

Hammerling, B.C., Cortez, M.Q., Hanna, R.A., Jimenez, R.E., and Gustafasson, Å.B., Identification of a Novel Pathway of Parkin-Mediated Mitochondrial Clearance in Cardiac Myocytes. Selected for Oral Abstract Presentation at American Heart Association Scientific Sessions, 2014, Chicago, Illinois, Nov 15-19, 2014.

Hammerling, B.C., Cortez, M.Q., Hanna, R.A., Jimenez, R.E., and Gustafsson, Å.B., Parkin Mediates Clearance of Dysfunctional Mitochondria via Multiple Pathways. Basic Cardiovascular Sciences Scientific Session 2014, Las Vegas, Jul 14-17, 2014.

PRESENTATIONS

Poster Presentation at Basic Cardiovascular Sciences (BCVS) (2014, 2015, 2016)
Oral Presentation at Genetics Training Program Annual Retreat (2016)
Poster Presentation: “Best of BCVS” at AHA Scientific Sessions (2015)
Oral Abstract Presentation at AHA Scientific Sessions, Late-Breaking Science Session (2014)
Oral Presentation at Pharmacological Research Discussions (Oct 2014, Oct 2015, Dec 2016)

AWARDS

American Heart Association Predoctoral Fellowship (Jan 2016- Dec 2017)
“Best of BCVS” Poster Award, American Heart Association (2015)
NIH Predoctoral Training Grant T32 GM008666 (2013-2014)

ABSTRACT OF THE DISSERTATION

A Rab5 Endosomal Pathway Mediates Parkin-Dependent Mitochondrial Clearance

by

Babette Hammerling

Doctor of Philosophy in Biomedical Sciences

University of California, San Diego, 2017

Professor Åsa Gustafsson, Chair

Mitochondria are critical for multiple cellular functions. However, damaged mitochondria pose a lethal threat to cells that necessitates their prompt removal, and failure to do so contributes to neurodegenerative and cardiovascular diseases. Degradation of mitochondria is an important cellular quality control mechanism and is mediated by two distinct pathways: one involving Parkin-mediated autophagy and the

other dependent on mitophagy receptors. Mitochondrial disposal via autophagy is dependent on damaged organelles being marked using several mechanisms including ubiquitylation by Parkin. Here I report a novel pathway for mitochondrial elimination that is dependent on functional Parkin but not on Drp1-mediated mitochondrial fission. This pathway is also distinct from Rab9- and Ulk1/2-mediated alternative autophagy. I show that mitochondria are sequestered by Rab5-positive early endosomes via the ESCRT machinery. These vesicles mature into late endosomes before delivery to lysosomes for degradation. Although this endosomal pathway is activated by stressors that also activate mitochondrial autophagy, endosomal-mediated mitochondrial clearance is initiated before autophagy. Moreover, in cells defective for autophagy, mitochondria are eliminated as promptly and completely through this endosomal pathway as in wild type cells. The autophagy protein Beclin1 regulates activation of Rab5 and endosomal-mediated degradation of mitochondria, suggesting crosstalk between these two pathways. Abrogation of Rab5 and the endosomal pathway results in the accumulation of damaged mitochondria and increases susceptibility to cell death in embryonic fibroblasts and cardiac myocytes. I also demonstrate that the mitophagy receptor BNIP3 can utilize the Rab5-endosomal pathway to clear mitochondria in cells, independent of Parkin. These data reveal a new mechanism for mitochondrial quality control mediated by Rab5 and early endosomes. Defects in this pathway could be involved in or contribute to a variety of disease states, and it may be possible to therapeutically target it in order to compensate for impaired autophagy that is a result of disease or aging.

CHAPTER 1: INTRODUCTION

1.1 Heart Disease and Mitochondria

It is estimated that there are currently 85.6 million Americans, greater than 1 in 3, who have at least one type of cardiovascular disease (CVD) (Mozaffarian et al., 2016). This number is expected to increase to 43.9% of the population by 2030. In addition to their broad prevalence, CVDs are the primary cause of mortality in 1 in 3 cases, as well as a contributing factor to 54% of deaths. The cost of treating these diseases is approximately $316.6 billion annually, which is projected to triple by 2030. Thus it is clear that CVDs present a significant and increasing burden on our health system and economy. Better therapies are needed to both prevent and treat such diseases.

Mitochondria are pivotal to the function of the heart, as these organelles provide the muscle with the ATP required for continuous heart contractions (Kubli and Gustafsson, 2012). In fact, mitochondria make up 30% of each myocyte's volume (Schaper et al., 1985). Insults to the heart can damage mitochondria, and in turn, damaged mitochondria can trigger cell death through the release of pro-death factors and production of reactive oxygen species (ROS) (Honda et al., 2005; Kubli and Gustafsson, 2012). For example, hypoxia, oxidative stress, DNA damage, cytosolic calcium overload, and loss of growth factors can all trigger mitochondrial-mediated cell death (Kubli and Gustafsson, 2012; Saelens et al., 2004). Mitochondria can initiate cell death through BCL2-associated X protein / BCL2-antagonistic/killer (BAX/BAK)-mediated membrane permeabilization or through opening of the mitochondrial permeability transition pore (mPTP). Cell death, in turn, is a primary hallmark of CVDs

such as myocardial infarction (MI), ischemia/reperfusion (I/R), and heart failure (Chiong et al., 2011). Since cardiac myocytes are terminally differentiated and have limited regenerative capabilities, permanent and excessive loss of individual myocytes can lead to cardiac dysfunction and development of heart failure (Thornburg et al., 2011). In order to protect against this, there are several levels of quality control that ensure damaged mitochondria are removed from the cell before they can activate cell death.

1.2 Mitochondrial Quality Control at the Protein Level

Mitochondria have a variety of quality control mechanisms at the protein and organelle level in order to maintain mitochondrial health and prevent cell death. Protein levels of control can be found in each of the four compartments of the mitochondria: the outer mitochondrial membrane (OMM), the intermembrane space (IMS), the inner mitochondrial membrane (IMM), and the mitochondrial matrix.

1.2.1 Protein Level of Quality Control in the Mitochondrion

The mitochondrion contains four compartments, and each of these has several enzymes that participate in protein quality control to ensure mitochondrial health. The ubiquitin proteasome degradation system (UPS), known for its role in the breakdown of cytosolic proteins, also contributes to degradation of mitochondrial proteins. These proteins are post-translationally modified by ubiquitination, extracted from the membrane, and delivered to the 26S proteasome, where they are finally degraded (Figure 1.1) (Livnat-Levanon and Glickman, 2011). There are two mitochondrial ubiquitin ligases that are localized on the cytosolic side of the OMM: March5 and

MULAN/MAPL (Kotiadis et al., 2014; Zhong et al., 2005). These proteins are responsible for ubiquitinating proteins that need to be degraded, which marks them for removal by the proteasome.

Protein quality control in the IMS is handled primarily by the protease HtrA2/Omi, the only soluble quality control protease found in this compartment (Baker and Haynes, 2011). HtrA2 deficiency results in mitochondrial malfunction, altered mitochondrial morphology, and ROS generation (Martins et al., 2004), which in turn damages mitochondrial DNA (mtDNA) (Goo et al., 2013). Knockout mice of HtrA2 have smaller hearts, and die by 30 days of age due to neurodegenerative disorder (Martins et al., 2004). The mutant mnd2 mice, possessing a missense mutation in HtrA2, also die young by day 30-40, but are rescued by wild-type HtrA2 gene expression in the central nervous system (Kang et al., 2013). Nevertheless, these rescued mice develop an accelerated aging phenotype in adulthood, display cardiac enlargement, and die by 12-17 months of age.

Quality control in the IMM is primarily dependent on two members of the AAA family: the m-AAA and i-AAA proteases. These protease complexes are embedded within the IMS, with their catalytic domains either exposed to the matrix (m-) or the intermembrane (i-) side. Deletion of a single gene encoding one of the two proteases in yeast impairs the mutants' respiratory capacity and results in aberrant mitochondrial morphology. Although these AAA proteases are present in cardiac mitochondria (Lau et al., 2012), little is known about their biological role or how these proteins are regulated under pathological conditions.

The greatest level of mitochondrial protein regulation and quality control occurs in the matrix of the mitochondrion. The matrix is very protein dense and contains the mitochondrial translation machinery as well as enzymes of the TCA cycle and other metabolic pathways. The matrix also contains two AAA proteases, Lon and ClpXP. Lon removes oxidized proteins in the matrix, particularly iron-sulfur containing proteins (Bota and Davies, 2002). Knockdown of Lon expression using RNAi in human lung fibroblasts leads to abnormal mitochondrial function and morphology, as well as activation of apoptosis (Bota et al., 2005). Human ClpXP is an ATP-dependent protease which plays a role in the unfolded protein response and is composed of a double-stack of ClpP subunits flanked on each end by a ClpX subunit (Figure 1.1) (Haynes et al., 2010; Kang et al., 2005). In *c. elegans*, nascent polypeptides unbound by chaperones are degraded by ClpP (Haynes et al., 2010). These degradation products are then transported into the cytosol via HAF-1, a mitochondria-localized peptide transporter. These peptides activate the transcription factor ZC376.7, which induces transcription of mitochondrial chaperone proteins and ClpP. In the ClpP-deficient mouse hearts, levels of mitochondrial chaperones are increased, respiratory supercomplexes are decreased, and there is an approximate 4-fold increase in the accumulation of mtDNA (Gispert et al., 2013).

Peptides from numerous matrix and inner membrane proteins are exported from mitochondria in an ATP-dependent manner (Augustin et al., 2005). Most likely, these peptides are generated by proteases such as Lon and ClpXP, and then transported to the cytosol where are they are ubiquitinated and subsequently degraded by the proteasome. There is also evidence that the UPS participates in the normal turnover of intra-mitochondrial proteins and that these proteins do not have to be cleaved by

proteases prior to export and degradation. In addition, inhibition of the proteasome results in increased oxidation, diminished intramitochondrial protein translation, increased glycolysis, and overall mitochondrial dysfunction in neurons (Sullivan et al., 2004). These findings propose an interesting system which enables proteasome degradation of proteins that are otherwise untouchable by the UPS.

1.2.2 Mitochondrial Derived Vesicles

When damage to mitochondria occurs on a larger scale, the refolding or degradation by chaperones and proteases are inadequate. However, when the damage is not enough to require removal of the entire mitochondrion via mitophagy, portions of mitochondria may be pinched off instead and segregated for degradation (Figure 1.2). These small vesicles, termed mitochondrial derived vesicles (MDVs), bud off functionally respiring mitochondria at a steady rate under baseline conditions (Soubannier et al., 2012a), and fuse with Lamp1-positive late endosomes/lysosomes via Stx17 and the SNARE complexes (McLelland and Lee, 2016). The formation of the MDVs is significantly increased during oxidative stress (Soubannier et al., 2012a). These vesicles transport oxidized proteins to the lysosomes for degradation, suggesting that this is another mechanism of mitochondrial quality control. Interestingly, these vesicles are formed independently of Drp1-mediated mitochondrial fission and autophagy (Neuspiel et al., 2008). Soubannier et al. have also reported that cardiac mitochondria form MDVs and that cargo of these MDVs is highly selective and depends on the type of oxidative stress (Soubannier et al., 2012b). In mouse hearts, MDVs form readily under baseline conditions and production is up-regulated in response to

doxorubicin-induced stress (Cadete et al., 2016). Intriguingly, it was also demonstrated that the formation of these MDVs in response to oxidative stress requires the presence of PINK1 and Parkin (McLelland et al., 2014). While PINK1 and Parkin have well established roles in mitophagy, it appears that this role in MDV formation is a separate, independent pathway, and is currently a subject under active investigation.

1.2.3 Autophagy and Mitophagy

1.2.3.1 Autophagy

There are three forms of autophagy: microautophagy, the direct delivery of substrates into lysosomes, chaperone-mediated autophagy (CMA), the delivery of substrates into lysosomes mediated through chaperone proteins, and macroautophagy, the delivery of substrates to the lysosomes via sequestration by double-membrane vesicles called autophagosomes. Macroautophagy, more commonly referred to as “autophagy”, is the most studied of these three forms and is a general mechanism by which the cell can degrade and recycle proteins and organelles (Mizushima et al., 2011; Youle and Narendra, 2011). After an autophagy-triggering stress, the Vps34-Beclin1-Vps15 complex can activate the autophagy pathway by initiating phagophore nucleation (Kubli and Gustafsson, 2012). This membrane can derive from numerous sources such as the plasma membrane, the golgi complex, the endoplasmic retirculum, or mitochondria (Cook et al., 2014). Autophagy proteins (Atg) Atg5, Atg12, and Atg16L form a complex that coordinates to elongate the phagophore into a cup-shaped membrane that is capable of sequestering cargo. Cytosolic microtubule-associated protein 1 light chain 3 (LC3-I) conjugates with phosphatidylethanolamine to form

autophagosomal-membrane bound LC3-II, which can be used as a marker for the formation of autophagosomes (Kubli and Gustafsson, 2012). Once the phagophore engulfs the cargo to be degraded, it matures into a fully-formed double membrane vesicle called the autophagosome. This vesicle can then fuse with an endosome to form an amphisome, or bypass this step and directly fuse with a lysosome, whose acid hydrolases and peptidases degrade the contents of the vesicle.

It was long thought that autophagy was a non-selective process (Seglen et al., 1990), but diligent research has proved this not to be the case. For instance, ubiquitination is often used to mark proteins for degradations by the UPS, but it can also direct substrates to the autophagy pathway (Kirkin et al., 2009). Autophagy can also degrade specific organelles such as peroxisomes (Dunn et al., 2005) or mitochondria (Wang and Klionsky, 2011).

Much of our understanding of autophagy comes from a variety of mouse models in which autophagy is perturbed. At birth, autophagy is upregulated during a period of starvation which is crucial to survival (Kuma et al., 2004). Mice deficient for Atg5, a gene critical for autophagosome formation, die within one day of delivery and display diminished amino acid concentrations in their bodies, as well as signs of energy depletion (Kuma et al., 2004). Inducible heart-specific knockouts of Atg5 show different effects depending on when the gene is ablated. Deletion in the adult mouse results in rapid heart failure (Nakai et al., 2007). These hearts also have disorganized sarcomeres and aberrant mitochondrial morphology. Conversely, embryonic deletion results in the normal development of the heart, which only displays dysfunction after pressure overload (Nakai et al., 2007). Interestingly, these mice begin to die at six months of age

and exhibit ventricular dilation, mitochondrial abnormalities, and declining heart function (Taneike et al., 2010).

1.2.3.2 Mitophagy Receptors

Autophagy plays a major role in the removal of damaged mitochondria, in a process called mitophagy. In mitophagy, damaged mitochondria are segregated from the mitochondrial network and then sequestered by autophagosomes. There are several mechanisms by which mitochondria can be recognized by autophagosomes. Studies have discovered that there are proteins and lipids present in the outer mitochondrial membrane that can directly function as mitophagy receptors, thus eliminating the need for ubiquitination and adaptor proteins (Figure 1.3 b). For instance, Nix/BNIP3L and BNIP3 are pro-apoptotic BH3-only proteins that are located on the OMM in cells (Hanna et al., 2012; Novak et al., 2010). Although they are both known to induce mitochondrial dysfunction and cell death, they can also direct mitochondria to autophagosomes by directly binding to LC3 or gamma-aminobutyric acid receptor-associated protein (GABARAP) on the autophagosome (Hanna et al., 2012; Novak et al., 2010; Schwarten et al., 2009).

1.2.3.3 PINK1/Parkin

The best studied mechanism of mitophagy is the PINK1-Parkin pathway (Figure 1.3 a). In a healthy cell, the serine-threonine kinase PINK1 is imported into mitochondria by the TOM complex and then actively degraded by MPP and PARL (Jin et al., 2010). However, upon loss of mitochondrial membrane potential, PINK1 is no longer imported and it accumulates on the OMM (Jin et al., 2010). PINK1 accumulation results in recruitment of the E3 ubiquitin ligase Parkin (Jin et al., 2010; Narendra et al., 2008).

Once recruited, Parkin initiates ubiquitination of several OMM proteins such as Hexokinase I, VDAC1, Mitofusin (Mfn)1/2, and Miro (Geisler et al., 2010; Okatsu et al., 2012; Tanaka et al., 2010; Wang et al., 2011). The addition of ubiquitin to mitochondrial substrates serves as signal for autophagic degradation. For instance, the adaptor protein p62 can bind to both ubiquitinated substrates via its ubiquitin associated domain (UBA) and to LC3 on the autophagosomal membrane (Pankiv et al., 2007). Hence, it physically links ubiquitin-tagged mitochondria to autophagosomes for engulfment by binding both LC3 and ubiquitin simultaneously.

The importance of the PINK1/Parkin pathway in clearing dysfunctional mitochondria in the heart has been demonstrated by several studies. For instance, Parkin deficient mice have hampered recovery of cardiac contractility after sepsis activation (Piquereau et al., 2013b), and impaired mitophagy after myocardial infarction, resulting in reduced survival and larger infarct sizes relative to controls (Kubli et al., 2013b). Parkin-mediated mitophagy also plays an important role in the preconditioning process (Huang et al., 2011). More recently, it was found that Parkin also plays a key role in the maturation of mitochondria in the neonatal heart, directing the metabolic shift from carbohydrate to fatty acid oxidation after birth (Gong et al., 2015). PINK1-deficient hearts are more susceptible to *ex vivo* I/R injury compared to wild type (Siddall et al., 2013), and overexpression of PINK1 in HL-1 cardiac cells protects against simulated I/R-mediated cell death (Siddall et al., 2013). Billia et al. found that PINK1 deficiency leads to ventricular dysfunction and hypertrophy at 2 months of age (Billia et al., 2011). These hearts have increased fibrosis, apoptosis, oxidative stress, and reduced mitochondrial respiration (Billia et al., 2011; Siddall et al., 2013). This is in contrast to

Parkin$^{-/-}$ mice which have normal mitochondrial and cardiac function at this age (Kubli et al., 2013b). Collectively, this suggests that the PINK1/Parkin pathway plays an important role in clearing damaged mitochondria after stress and that PINK1 might have additional functions in myocytes.

1.2.3.4 Fission/Fusion

To aid in the selective removal of damaged mitochondria from the mitochondrial network, these organelles can undergo asymmetric fission. In this process, a mitochondrion that has accumulated significant damage can segregate damaged proteins to only one daughter mitochondrion (Twig et al., 2008). The second, healthy, daughter has a higher membrane potential and may fuse back into the mitochondrial network, while the damaged daughter can be cleared from the cell. Mitochondrial fission is mediated by cytosolic Drp1 which forms a ring around the mitochondrion's exterior and pinches it into two daughters (Smirnova et al., 2001). Conditional, cardiac-specific ablation of Drp1 in the mouse results in enlarged mitochondria, cardiac myocyte death, and lethal dilated cardiomyopathy (Song et al., 2015).

On the other side of the coin of mitochondrial fission is mitochondrial fusion. Mitochondrial fusion prevents mitophagy and can therefore protect cells against excessive degradation of mitochondria (Gomes et al., 2011). Fusion can also help to rescue damaged mitochondria, by diluting out the damaged proteins or allowing wild type mtDNA to compensate for defects (Chan, 2012), at the cost of reducing the health of the overall network (Bhandari et al., 2014). Fusion of mitochondria involves two components to form a functional mitochondrion: fusion of the outer membranes, as well as fusion of the inner membranes. Outer membrane fusion is dependent on Mfn1 and

Mfn2 in mammals (Chen et al., 2003). Cardiac specific deletion of Mfn1/2 is embryonic lethal and conditional deletion in the adult heart leads to mitochondrial dysfunction, mitochondrial fragmentation, and a rapid progression to lethal dilated cardiomyopathy despite no cardiac myocyte death (Chen et al., 2011; Song et al., 2015). Fusion of the inner mitochondrial membranes is driven by the GTPase Opa1 (Chan, 2012). Knockout of Opa1 is embryonic lethal, though heterozygotes display reduced mtDNA levels and develop both cardiac and mitochondrial dysfunction by 12 months of age (Chen et al., 2012). Cardiac-specific deletion of the protease Yme1l results in stress-induced processing of Opa1 (Wai et al., 2015). This processed, short form of Opa1 is impaired in its mitochondrial fusion ability. As a result, these mice display fragmented mitochondria, fibrosis, necrotic cell death, a metabolic switch to glucose oxidation, and ultimately develop dilated cardiomyopathy.

1.3 Compromised Mitochondrial Quality Control in Aging and Disease

The mechanisms underlying the development of heart failure are very complex and not fully understood. However, recent studies have provided evidence that mitochondrial dysfunction is an important contributor to both development of heart failure and the aging process. For instance, mutations in genes that disrupt mitochondrial function are associated with cardiac dysfunction in both mice (Thomas et al., 2013) and humans (Marin-Garcia and Goldenthal, 2002). Also, mtDNA accumulates mutations with age which leads to impaired mitochondrial respiration, increased ROS production, and development of age-related cardiomyopathy (Kujoth et al., 2005).

Multiple lines of evidence indicate that the accumulation of dysfunctional mitochondria in diseased or aged tissues might, in part, be due to reduced mitochondrial quality control. Several studies have reported that chronic stress and/or aging affects proteins that are involved in the mitochondrial quality control pathways (at all levels). Impairment of mitochondrial protein quality control processes that leads to mitochondrial dysfunction and reduced mitophagy will result in accumulation of dysfunctional mitochondria in the cell. First, the UPS system is important in the quality control of mitochondrial proteins, particularly those on the OMM, and studies have found that inadequate proteasomal degradation exists in animal models of heart disease and in a large subset of human failing hearts (Wang and Robbins, 2014). Other studies have reported that reduced activity of mitochondrial proteases can contribute to heart disease and aging. For instance, mice that carry a mutation in HtrA2 that inactivates its protease activity in non-neuronal tissues exhibit a phenotype of premature aging with weight loss, osteoporosis, curvature of the spine, muscle atrophy, and cardiac hypertrophy (Plun-Favreau et al., 2012). Moreover, studies have found that aging is associated with reduced Lon protease activity in various tissues. For instance, Lon levels and activity in skeletal muscle mitochondria from old mice is significantly decreased compared to young mice, which correlates with increased levels of oxidized mitochondrial proteins (Bota et al., 2002). This study also found that increased chronic oxidative stress in MnSOD heterozygous mice exacerbates the effects of aging on reduced Lon activity. Interestingly, Deval et al. found that Lon protein levels increases with age in rat hearts while overall Lon activity remains unchanged, suggesting that there is an accumulation of inactive Lon (Delaval et al., 2004). Furthermore, Hoshino et al. reported that Lon is

subject to oxidative modifications which attenuate its protease activity in failing mouse hearts (Hoshino et al., 2014). Thus, these studies demonstrate that chronic stress and aging negatively affect proteins that are involved in mitochondrial quality control.

In addition, multiple studies indicate that autophagy diminishes with aging and it has been proposed that the reduced autophagic response contributes directly to the aging phenotype (Cuervo, 2008). For instance, tissue-specific knockouts of essential autophagy genes results in the appearance of many age-associated problems, such as the accumulation of inclusion bodies containing ubiquitinated proteins, accumulation of lipofusin-containing lysosomes, disorganized mitochondria, and increased oxidative stress (Hartleben et al., 2010; Komatsu et al., 2007; Nakai et al., 2007; Singh et al., 2009). In contrast, increased autophagy delays aging and extends longevity. For instance, caloric restriction is a potent physiological inducer of autophagy and is well known to extend life span in animals. It reduces the incidence of diabetes, cardiovascular disease, cancer, and brain atrophy (Colman et al., 2009; Omodei and Fontana, 2011). Interestingly, selective activation of mitophagy by Parkin delays the aging process. Cardiac specific Parkin transgenic mice are resistant to aging and aged mice exhibit fewer dysfunctional mitochondria compared to age-matched wild type controls (Hoshino et al., 2013). Similarly, Parkin overexpression extends life span and improves mitochondrial function in *Drosophila melanogaster* (Rana et al., 2013). In contrast, Parkin deficiency results in the accrual of abnormal mitochondria in aged myocytes (Kubli et al., 2013a). This suggests that specifically activating Parkin-mediated mitophagy might be cardioprotective. Balance between mitochondrial

biogenesis and mitophagy is critical as excessive mitophagy can overtax the remaining mitochondria, induce damage, and even initiate apoptosis.

1.4 The Endosomal-Lysosomal Pathway

The endosomal pathway is involved in the endocytosis of extracellular content and plasma membrane receptors, and the subsequent shuttling of these endosomes either back to the cell surface, through a recycling pathway, or degradation of endosomal content through fusion with lysosomes (Huotari and Helenius, 2011). The endosomal pathway has a large variety of roles, from receptor internalization and degradation, transport of enzymes, and release of neurotransmitters, to bacterial and viral pathogenesis (Huotari and Helenius, 2011; Sudhof, 2004). Disruption of the endosomal pathway has been implicated in several neuropathologies including Alzheimer's Disease (Xu et al., 2016), Down Syndrome (Xu et al., 2016), and Parkinson's Disease (Perrett et al., 2015). Both the brain and the heart are highly metabolic organs and several studies suggest a link in pathologies between the two (Finsterer and Wahbi, 2014; Kubli et al., 2013b; Mielcarek et al., 2014; Sun et al., 2015; van Buchem et al., 2014). Thus, it is very likely that the endosomal pathway has an important role in heart health and function. In fact, one study has shown that the EHD3 pathway, involved in endosomal trafficking in non-excitable and heterologous cells, has a role in cardiac contractility by affecting expression and localization of ion exchangers and calcium channels (Curran et al., 2014). However, more studies investigating endosomal dysfunction and potential CVDs that could arise from such defects are needed.

The endosomal pathway is governed by Rab GTPase proteins. These GTPases cycle between an active GTP-bound form and an inactive GDP-bound form (Stenmark, 2009). Particular Rab proteins can not only be used as markers for the different types of endosomes, such as early endosomes (EEs), late endosomes (LEs), and recycling endosomes, but they also impart specific functionalities. For instance, early endosomes are marked by the GTPase Rab5. Rab5 enables early endosomes to fuse with one another to form larger vesicles. As the vesicles mature, Rab5 is replaced by Rab7, which enables fusion with lysosomes. Alternatively, EEs can become recycling endosomes, in which case they are marked by Rab11 and Rab35 (slow recycling) or by Rab4 (fast recycling). As EEs mature into LEs, they undergo a variety of changes. In addition to the Rab5 to Rab7 switch, the endosomes enlarge, acidify, and form intraluminal vesicles (ILVs). These ILVs are invaginations of the endosomal membrane that form small vesicles within the endosome which contain ubiquitinated proteins. Endosomes with ILVs are also called multivesicular bodies (MVBs).

ILVs are formed by the endosomal sorting complex required for transport (ESCRT) complexes. These complexes (ESCRT-0, -I, -II, and –III) are responsible for the recognition, sequestration, and sorting of ubiquitinated proteins into ILVs (Henne et al., 2011). ESCRT-0, composed of Hrs and Stam1/2 proteins, is responsible for recognition of ubiquitinated proteins to be sorted into the ILV (Williams and Urbe, 2007). SiRNA depletion of Hrs reduces the number of ILVs found within EEs (Razi and Futter, 2006). Recruitment of the ESCRT-I complex is dependent on ESCRT-0 (Henne et al., 2011). In mammalian systems, ESCRT-I is composed of Tsg101, Vps28, Vps37, and hMvb12 (Henne et al., 2011; Williams and Urbe, 2007). Of this complex, Tsg101 is

required for vacuolar morphology of endosomes. Depletion of this subunit impairs receptor degradation and alters endosomal morphology (Doyotte et al., 2005; Razi and Futter, 2006). Snf8, Eap20, and Eap45 together form the ESCRT-II complex. This complex recruits ESCRT-III proteins to the endosome, and depletion of ESCRT-II subunits results in missorting of vacuolar hydrolases (Williams and Urbe, 2007). ESCRT-III is made up of the proteins CHMP1 through CHMP7. ESCRT-III is responsible for vesicle budding of the ILV. This complex is disassembled by the Vps4-Vta1 complex, which is required for the complete formation of ILVs (Henne et al., 2011; Williams and Urbe, 2007).

Due to the endosomal pathway's ability to recognize and sequester ubiquitinated cargo and its ability to fuse with lysosomes, it is possible that this pathway is involved in the degradation of damaged proteins and organelles of the cell.

1.5 Rationale and Specific Aims of the Thesis

Heart disease places a large burden on our society: it is the leading cause of death, claiming 1 out of every 3 lives, and costs us approximately $312.6 billion annually (Go et al., 2013). Functional mitochondria are an integral component of cardiac health, and are responsible for supplying the heart with vast amounts of energy in the form of ATP. Mitochondria accumulate damage with age and through genetic and environmental stressors (Kotiadis et al., 2014; Kujoth et al., 2005). These damaged mitochondria can cause myocyte death and have been implicated in the development of heart failure (Edgar et al., 2009; Hammerling and Gustafsson, 2014). The clearance of

damaged mitochondria is thus important for myocytes survival and effective function of the heart.

To date, the only known mechanism of whole-organelle mitochondrial clearance is via the autophagy pathway. One mediator of mitophagy, Parkin, is recruited to depolarized mitochondria membranes by the serine-threonine kinase PINK1 (Narendra et al., 2008). Parkin ubiquitinates outer mitochondrial membrane proteins, marking the organelle for degradation. Our lab has previously shown that in the absence of Parkin, mitophagy in the heart is impaired under stress conditions, and leads to heart failure and increased mortality after MI (Kubli et al., 2013b). However, we have recently discovered that Parkin still efficiently clears dysfunctional mitochondria in autophagy-deficient *Atg5*$^{-/-}$ mouse embryonic fibroblasts (MEFs), *suggesting that a novel mechanism of mitochondrial clearance exists in cells*. Therefore, I hypothesize **Parkin-mediated clearance of damaged mitochondria via the endosomal-lysosomal pathway plays a critical role in maintaining a healthy network of mitochondria in cells.**

Aim 1: To characterize the role of endosomal clearance of mitochondria. *Hypothesis: The endosomal pathway significantly contributes to the clearance of damaged mitochondria in cells to ensure cellular survival.*

Aim 2: To determine the mechanism through which damaged mitochondria are targeted to the endosomal pathway. *Hypothesis: Parkin-mediated ubiquitination of*

mitochondrial substrates results in the sequestration of mitochondria by ESCRT complexes.

Parts of Chapter 1 were originally published in *the Journal of Molecular and Cellular Cardiology.* Hammerling, B. C., & Gustafsson, A. B. Mitochondrial quality control in the myocardium: cooperation between protein degradation and mitophagy. *Journal of Molecular and Cellular Cardiology.* 75: 122-130, 2014. © 2014 Elsevier Inc. The dissertation author was the primary investigator and author of this paper.

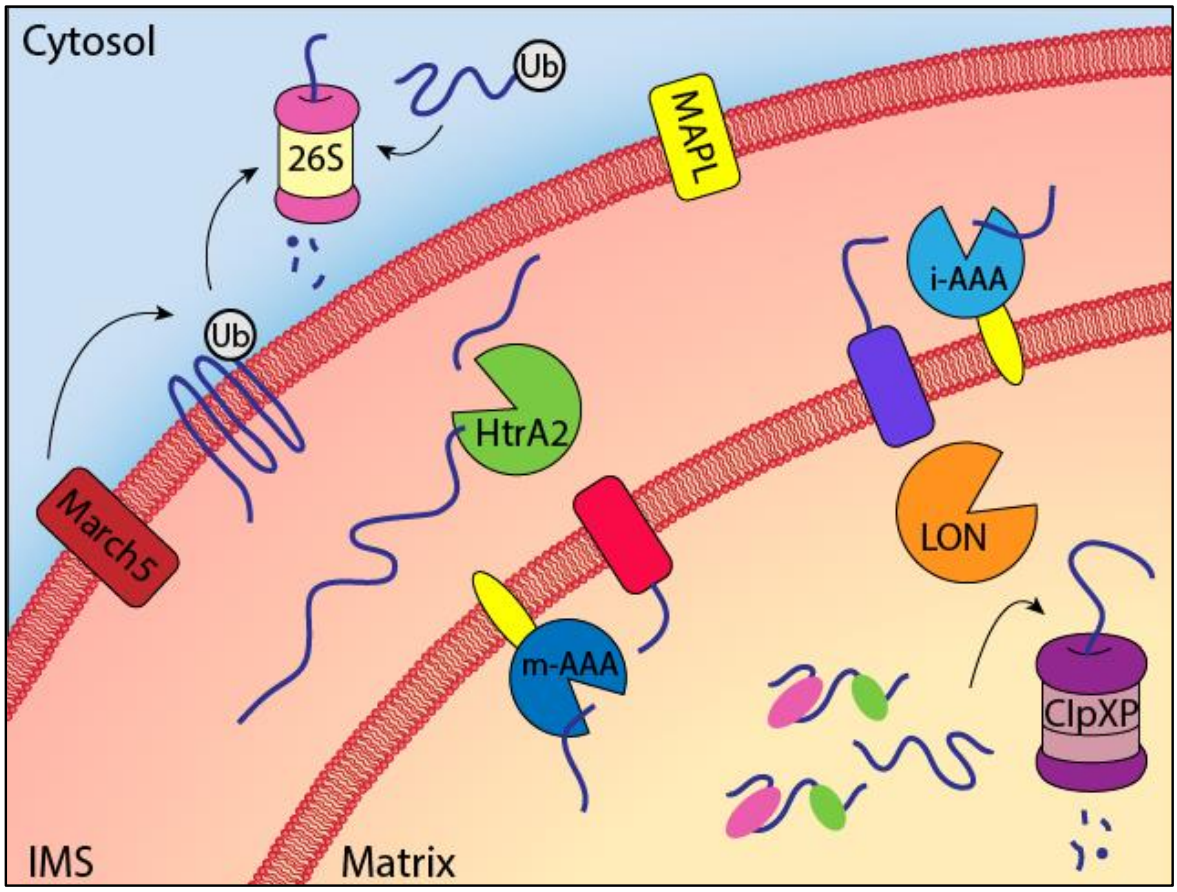

Figure 1.1 The mitochondrion contains many protein quality control proteins. Outer mitochondrial membrane (OMM) E3 ubiquitin ligases such as March5 and MAPL tag proteins for degradation by the 26S proteasome, which is also responsible for the breakdown of the majority of ubiquitinated cytosolic proteins. Within the intermembrane space (IMS), HtrA2 is the chief protease in charge of protein degradation. Two ATPases Associated with diverse cellular Activity proteases, the matrix (m-) and the intermembrane (i-) AAA, identify misfolded polypeptides on their respective side of the IMM for degradation. Lon and ClpXP are the two most important QC proteases in the mitochondrial matrix. Lon is primarily responsible for the removal of oxidized proteins. ClpXP, composed of two ClpP subunits flanked by ClpX, plays a role in the unfolded protein response, degrading proteins unbound by chaperones (pink and green).

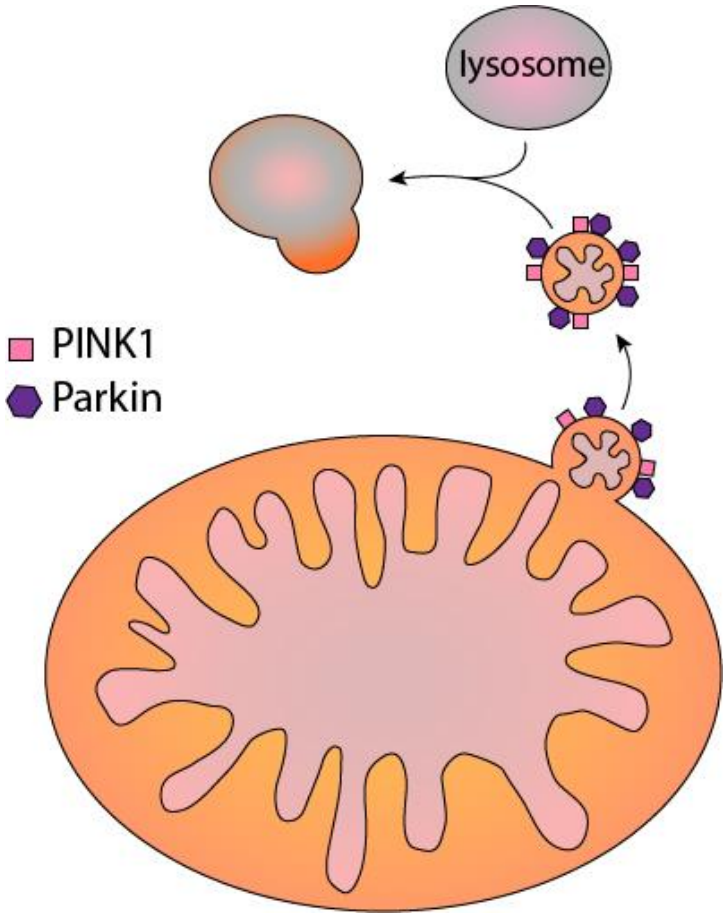

Figure 1.2. Mitochondrial-derived vesicles bud off and fuse with lysosomes for degradation.
Small vesicles containing mitochondrial proteins and lipids bud off from mitochondria under baseline conditions and under oxidative stress. Formation of these vesicles requires the presence of PINK1 and Parkin. After budding off from the mitochondria, these vesicles fuse with lysosomes for degradation.

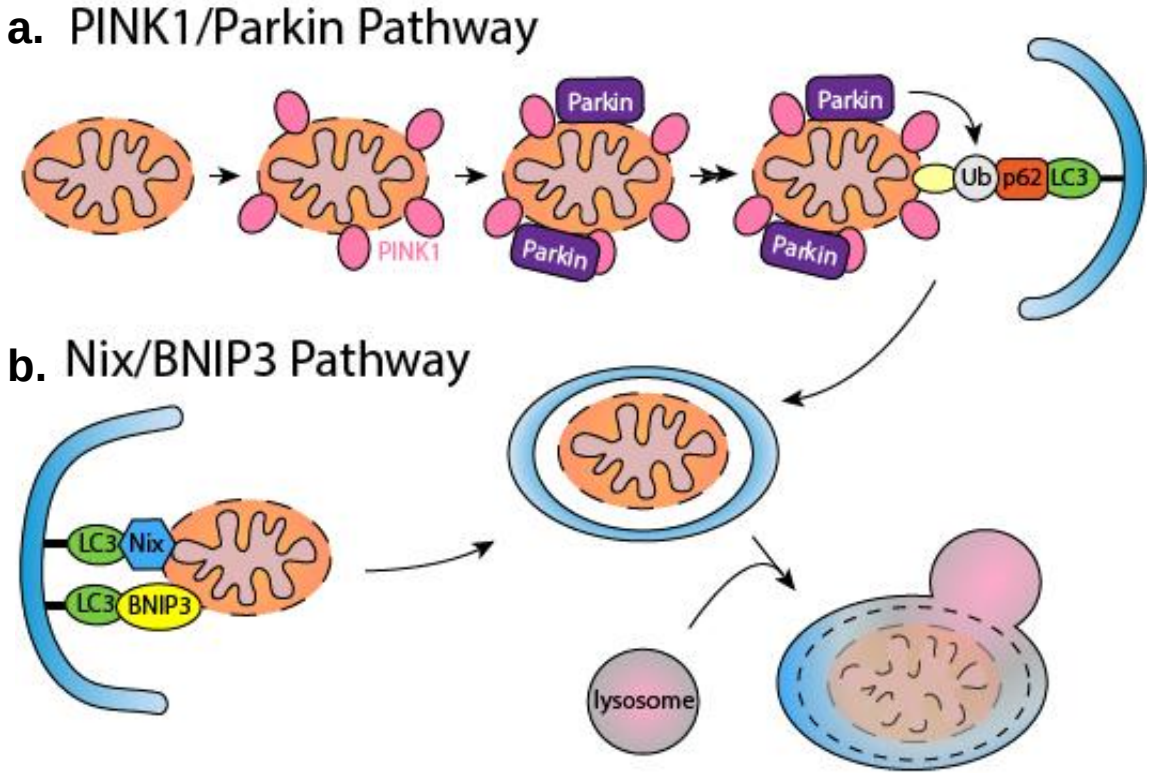

Figure 1.3. Mitochondrial autophagy (mitophagy) can proceed through the PINK1/Parkin or the Nix/BNIP3 pathways.
(a) Upon loss of mitochondrial membrane potential, PINK1 accumulates on the OMM surface. PINK1 recruits Parkin, which ubiquitinates OMM proteins, thus inducing engulfment of the mitochondrion by the autophagosome through p62 and LC3. **(b)** Nix and BNIP3 function as autophagy receptors on mitochondria by binding to LC3 on the autophagosome. Both pathways result in the autophagic sequestration of the mitochondrion, fusion with a lysosome, and degradation of the organelle.

CHAPTER 2: EXPERIMENTAL METHODS AND MATERIALS

Antibodies

The following antibodies were used for immunofluorescence (IF) and Western blotting (WB) experiments: Actin (WB 1:2000; Sigma; no. A4700), Beclin1 (WB 1:1000; Santa Cruz; no. sc-11427), Chmp3 (IF 1:100; WB 1:1000; Santa Cruz; no. sc-67228), Eea1 (WB 1:1000; Cell Signaling; no. 3288), Gapdh (WB 1:2000, Genetex; GTX627408), Hgs (IF 1:100; WB 1:1000; Abcam; no. ab155539), Lamp2 (IF 1:100; Abcam; ab13524), Lamp2 (WB 1:1000; Santa Cruz; sc-18822), LC3 (WB 1:1000; Cell Signaling; no. 4108), OxPhos Complex IV subunit 1 (IF 1:100; Life Technologies; no. 459600), p62 (WB 1:1000; ARP; no. 03-GP62-C), Rab5 (IF 1:100; WB 1:1000; Cell Signaling; no. 3547), Rab7 (WB 1:1000; Cell Signaling; no. 9367), Snf8 (IF 1:100; WB 1:1000; Santa Cruz; no. sc-390747), Tim23 (IF 1:100; WB 1:1000; BD Biosciences; no. 611222), Tom20 (IF 1:200; WB 1:1000; Santa Cruz; sc-11415), Tsg101 (IF 1:100; WB 1:1000; Abcam; no. ab83), and tubulin (WB 1:2000; Sigma; no. T6074). Secondary antibodies used were goat anti-mouse or goat anti-rabbit HRP, Alexa Fluor 488 or 594 (Life Technologies).

Animals

All experimental procedures were performed in accordance with institutional guidelines and approved by the Institutional Animal Care and Use Committee of the University of California San Diego. αMHC-Cre mice were obtained from Jackson Labs (Stock no. 011038). $Atg7^{flox/flox}$ mice were obtained from Dr. Tomoki Chiba, Metropolitan

Institute of Medical Science, Japan (Komatsu et al., 2005). Sprague Dawley rats were obtained from Harlan Laboratories.

Myocardial Infarction

Mice were subjected to myocardial infarction by permanently ligating the left anterior descending coronary artery as described previously (Huang et al., 2010). Briefly, 8 to 12 week old WT or *Atg7* cKO mice were anesthetized with isoflurane, intubated, and ventilated. Pressure-controlled ventilation (Harvard Apparatus) was maintained at 9 cm H_2O. A 7-0 silk suture was placed around the LAD coronary artery and then tightened. The suture was left in place, and the incision was immediately closed.

Echocardiography

Echocardiography was performed as previously described (Kubli et al., 2013b) using a Vevo770 In Vivo Micro-Imaging System with an RMV707B 15-45 MHz imaging transducer (VisualSonics Inc.). Mice were maintained under light anesthesia through a nose cone (1.5% isoflurane, 98.5% O_2). Mice were placed in a supine position on a recirculating water warming pad maintained at 42°C while acquiring measurements. Cardiac parameters were quantified using the VisualSonics software.

Mitochondrial Isolation and Extracellular Flux Analysis

To obtain intact mitochondria, 8 to 12 week old hearts were minced in 70 mM sucrose, 210 mM mannitol, 5 mM HEPES, 1 mM EGTA, 0.5% fatty acid-free BSA, pH

7.2. Samples were then homogenized with a Polytron tissue grinder at 11,000 rpm for 3 seconds and then with a Potter-Elvehjem PTFE at 2000 rpm with 4 strokes of the pestle before centrifugation three times at 600 x g for 5 mins at 4°C to remove debris. Mitochondria were pelleted from the supernatant by centrifugation at 6000 x g for 10 mins at 4°C. Mitochondrial protein concentrations were determined using Bradford assay.

Mitochondria respiration was measured using the Seahorse XF96 Analyzer (Seahorse Bioscience – Agilent Technologies). Mitochondria were plated on to 8-well Seahorse microplates at a density of 0.5 µg per well. Assay media (70 mM sucrose, 220 mM mannitol, 10 mM KH_2PO_4, 5 mM $MgCl_2$, 2 mM HEPES, 1 mM EGTA, 0.2% fatty acid-free BSA, and 4 mM ADP) containing different substrates were used to assess glucose metabolism (10 mM pyruvate and 1 mM malate), fatty acid oxidation (40 µM palmitoyl-L-carnitine and 1 mM malate), and Complex II-dependent oxygen consumption (10 mM succinate and 2 µM rotenone). Oligomycin (2 µM) was added to inhibit ATP synthase followed by three successive additions of 1.5 µM FCCP to obtain maximal respiration rate and confirm mitochondria were functional. Data were analyzed using Wave for Desktop (Seahorse Bioscience – Agilent Technologies).

Cells and Culture Conditions

Mouse embryonic fibroblasts (MEFs) were maintained in MEF culture media (DMEM (Life Technologies) supplemented with 10% FBS (Life Technologies), 100 U/mL penicillin (Gemini) and 100 µg/mL streptomycin (Gemini)) and cultured in a 5% CO_2 atmosphere at 37 °C. WT and *Atg5*$^{-/-}$ MEFs were generously provided by Dr. Noboru

Mizushima (The University of Tokyo, Japan); Primary WT and *Atg7*$^{-/-}$ MEFs were kindly provided by Dr. Toren Finkel (NIH, USA) (Lee et al., 2012); WT and *Ulk1*$^{-/-}$ MEFs were generously provided by Dr. Mondira Kundu (St. Jude Children's Research Hospital , USA)(Kundu et al., 2008); *Ulk2*$^{-/-}$ and *Ulk1/2*$^{-/-}$ MEFs were obtained from Cancer Research Technology Ltd. None of these cell lines are listed in the database of commonly misidentified cell lines maintained by ICLAC. Neonatal cardiac myocytes were prepared from 1-2 day old Sprague Dawley rats by enzymatic digestion of the hearts (Karwatowska-Prokopczuk et al., 1998) and subsequent plating on gelatin-coated Nunc™ Lab-Tek™ Chamber Slides (Thermo Scientific) in a 4:1 ratio DMEM (Life Technologies) to M199 (Life Technologies) plus 10% FBS (Life Technologies), 100 U/mL penicillin (Gemini), 100 µg/mL streptomycin (Gemini), and 100 µM BrdU (Sigma). Myocytes were cultured in serum-free media at 37^{o}C with 5% CO_2. Cell lines have not been tested for mycoplasma contamination. Simulated ischemia/reperfusion was initiated by incubating myocytes in ischemic buffer (125 mM NaCl, 8 mM KCl, 1.2 mM KH_2PO_4, 1.25 mM $MgSO_4$, 1.2 mM $CaCl_2$, 6.25 mM $NaHCO_3$, 20 mM 2-deoxyglucose, 5 mM Na-lactate, 20 mM HEPES, pH 6.6) and placing the dishes in hypoxic pouches (GasPak™EZ, BD Biosciences), equilibrated to 95% N_2, 5% CO_2. Reperfusion was initiated by changing to Krebs-Henseleit buffer (110 mM NaCl, 4.7 mM KCl, 1.2 mM KH_2PO_4, 1.25 mM $MgSO_4$, 1.2 mM $CaCl_2$, 25 mM $NaHCO_3$, 15 mM glucose, 20 mM HEPES, pH 7.4). Normoxic control cells were maintained in Krebs-Henseleit buffer throughout the experiment. Hypoxia experiments were performed by placing cells in hypoxic buffer (MEF culture media as described above, plus 20 mM HEPES, pH 7.4 (Gibco) and placing the dishes in a 5% CO_2 atmosphere at 37 °C for normoxic controls,

or in hypoxic pouches (GasPak^{TM}EZ, BD Biosciences), equilibrated to 95% N_2, 5% CO_2 for hypoxic experimental conditions.

Transient Transfections, Plasmids, and siRNA Knockdown

Cells were transiently transfected with DNA using Fugene 6 Transfection Reagent (Promega) according to the manufacturer's instructions. Generation of BNIP3W18A was prepared using site directed mutagenesis by PCR with BNIP3 wild type as a template (Hanna et al., 2012). Myc vector and myc-BNIP3 were previously described (Kubli et al., 2008). Cells transfected with BNIP3 constructs were rescued with 50 μM ZVAD (Millipore, 627610) to inhibit apoptosis. YFP-Parkin was a gift from Richard Youle (Addgene plasmid #23955)(Narendra et al., 2008); Myc-Parkin and HA-Parkin were gifts from Ted Dawson (Addgene plasmids #17612, #17613) (Zhang et al., 2000); EGFP-Rab5Q79L and EGFP-Rab5S34N were a gift from Qing Zhong (Addgene plasmids #28046, #28045) (Sun et al., 2010); p40PX-EGFP was a gift from Michael Yaffe (Addgene plasmid #19010) (Kanai et al., 2001); GFP-Rab9 and GFP-Rab9S21N were gifts from Richard Pagano (Addgene plasmids #12663, #12664)(Choudhury et al., 2002); mPlum-Mito-3 was a gift from Michael Davidson (Addgene plasmid #55988)(Day and Davidson, 2009); and GFP-Rab5 and GFP-Rab7 were gifts from JoAnn Trejo (UCSD, USA). Beclin1 knockdown experiments were performed by transfecting 20 nM AllStars Negative Control (Qiagen, no. SI03650318; seq: CAGGGTATCGACGATTACAAA) or Beclin 1 siRNA (Sigma, siRNA ID: SASI_Mm01_00048143; seq: CUGAGAAUGAAUGUCAGAA) with HiPerFect Transfection Reagent (Qiagen) for 96 h, according to the manufacturer's instructions.

Rab7 knockdown experiments were performed by transfecting 20 nM Rab7 siRNA SMARTpool (Dharmacon, no. L-040859-02-0005; seqs: CAGCUGGAGAGACGAGUUU, CGACAGACUUGUUACCAUG, GAGCGGACUUUCUGACCAA, and CAGAAGUGGAACUGUACAA) or AllStars Negative Control siRNA with Dharmafect 4 Transfection Reagent (Dharmacon) for 96 h, according to the manufacturer's instructions. Knockdown of ESCRT proteins was performed by transfecting 20 nM AllStars Negative Control, 80 nM Hgs siRNA SMARTpool (Dharmacon, no. L-055516-01-0005, seqs: CAAGAUACCUCAACCGGAA, AAGCAUCACUGCCGAGCAU, CGUACAAUAUGCAGAAUCU, AGACAGACUCUCAGCCCAU), 40 nM Tsg101 siRNA (Sigma, siRNA ID: SASI_Mm01_00065312; seq: GGUACAAUCCCAGUGCGUU), 80 nM Snf8 siRNA SMARTpool (Dharmacon, no. L-049190-01-0005; seqs: UCGGAAUGGAGGUCUGAUA, GACUGAGUGUGGAGGGGUA, CAAGAGAUCCGGAAGAAUC, CUACAUCAGCAGGUGUUAA), or 100 nM Chmp3 siRNA SMARTpool (Dharmacon, no. L-062411-01-0005; seqs: GUGAAAUGCAGGACAGUUA, GGGUUAACGUGCUGUGUUG, UGAGAAGAGUAGAUUGAAU, GUACAGAAUGGCUUUGUUA), with HiPerFect Transfection Reagent (Qiagen) for 96 h, according to the manufacturer's instructions

Adenoviral Infections and shRNA Knockdown

Cells were infected with adenoviruses in DMEM + 2% heat inactivated serum for 3 h and rescued with growth media. Experiments were performed 20 h later. Generation of adenoviruses encoding mCherry-Parkin, mCherry-ParkinR42P, and mCherry-ParkinG430D were previously described (Kubli et al., 2013b). The BNIP3 adenovirus

was previously described (Hanna et al., 2012). The myc-Parkin, p40PX-EGFP, and Drp1K38E adenoviruses were generated using the pENTR directional TOPO cloning kit (Invitrogen) followed by recombination into the pAd/CMV/V5-DEST Gateway vector (Invitrogen). Ad-GFP-Rab5S34N was a gift from Pyong Woo Park (Boston Children's Hospital, USA)(Hayashida et al., 2008); Mfn2WT and Mfn2EE viruses were provided by Gerald W. Dorn II(Chen and Dorn, 2013). Ad-Beclin1 shRNA was provided by Dr. Junichi Sadoshima (Hariharan et al., 2013). Knockdown experiments were performed by infecting cells with Ad-U6-scramble-RNAi control (Vector Biolabs, #1122) or Ad-Beclin1 shRNA and experiments were performed 96 h later.

Cell Death Assays

Cells transfected with empty myc vector myc-BNIP3, empty pEGFP-C1 (Clontech, 6084-1), or GFP-Rab5S34N (generously donated by JoAnn Trejo, UCSD) were stained with BOBO-3 Iodide (1:1000, Thermo Fisher Scientific, B3586) plus Hoechst 33342 for 20 minutes. Cell death was assessed as the number of BOBO-3 positive cells divided by total number of Hoechst 33342 positive cells as described (Rubinsztein et al., 2012). Cells infected with β-gal or myc-Parkin (MOI: 150) were treated with vehicle or 5 mM 3-methyladenine (Sigma) for 30 min prior to DMSO (Sigma) or 25 μM FCCP (Sigma) exposure. Cells with Rab7 knockdown were infected with mCherry-Parkin (MOI: 150) and then re-transfected with control or Rab7 siRNA. Cells overexpressing Ad-GFP or Ad-GFP-Rab5S34N (MOI: 75) plus Ad-myc-Parkin (MOI: 150) were treated with DMSO or 25 μM FCCP for 24 h. Cells with ESCRT protein knockdowns were infected with mCherry-Parkin (MOI: 75) and then re-transfected with

control or ESCRT-specific siRNA for another 48 h. Cells were then treated with DMSO or 25 μM FCCP for 24 h. In hypoxia cell death experiments, cells were infected with mCherry-Parkin (MOI: 75) and Ad-GFP or Ad-GFP-Rab5S34N (MOI:40), placed in hypoxic buffer, and kept at normoxia or hypoxia for 34 h as described above. To assess viability, cells were stained with Yo-Pro-1 (1:1000; Life Technologies), propidium iodide (1:3000; Life Technologies), or with Po-Pro-3 (1:1000; Life Technologies) plus Hoechst 33342 for 20 minutes. Cell death was assessed as the number of Yo-Pro-1, propidium iodide, or Po-Pro-3 positive cells divided by total number of Hoechst 33342 positive cells as described (Kubli et al., 2007).

Immunofluorescence

Cells were fixed with 4% paraformaldehyde (Ted Pella Inc.) in Dulbecco's Phosphate Buffered Saline without calcium chloride and without magnesium chloride (PBS) (Gibco, no. 14200-075), permeabilized with 0.2% Triton X-100 or 0.1% saponin (for Lamp2 staining) in PBS, and blocked in 5% normal goat serum. Myocytes were blocked with 5% normal goat serum plus 0.2% Tween20 in PBS (PST). Cells were incubated with primary antibodies (4^{o}C, overnight) in PBS (MEFs) or PST (myocytes), rinsed with PBS, incubated with secondary antibodies (37^{o}C, 1 h), and counter-stained for nuclei with Hoechst 33342 (Invitrogen). Fluorescence images were captured using a Carl Zeiss Axio Observer Z1 fitted with a motorized Z-stage with a 63X Plan-Apochromat (oil immersion) objective. Z stacks of red and green fluorescence separated by 0.6 μm along the *z*-axis were acquired with an ApoTome using a high-resolution AxioCam MRm digital camera and Zeiss AxioVision 4.8 software (Carl Zeiss).

Mitochondrial clearance was scored on a per cell basis. Mitochondrial clearance progresses through a well-documented series of steps including nuclear aggregation prior to complete removal (Yoshii et al., 2011), thus cells displaying nuclear aggregation or lack of mitochondria were scored as “cleared.” Endosomal and autophagic vesicles in cells were quantified by counting the number of distinct, visible puncta in a maximal projection image of each cell. Co-localization was determined by manually scoring the number of puncta on single Z-stack slices that had clear signal in both red and green image channels. All scoring of morphology and puncta counts were scored un-blinded with respect to sample identity. Confocal images were captured on a Leica SPE II (Leica) inverted confocal microscope equipped with 405, 488, 561, and 637 nm lasers, with 0.25 µm step size between optical sections. Assessment of mitochondrial depolarization was performed by transfecting cells with HA-Parkin and GFP-Rab5, treating with DMSO or 25 µM FCCP for 4h, and adding MitoTracker Red CMXROS (Thermo Fisher Scientific, no. M7512) at a final concentration of 250 nM for 20 min prior to fixation and subsequent staining.

Western Blot Analysis

Samples were lysed in 50 mM Tris-HCl, 150 mM NaCl, 1 mM EGTA, 1 mM EDTA, 1% Triton X-100, and Complete protease inhibitor cocktail (Roche). Tissues were homogenized with a Polytron tissue grinder at 22,000 rpm for 3 seconds. Lysates were cleared by centrifugation at 20,000 x g for 20 min at 4°C. Proteins were separated on NuPAGE Bis-Tris gels (Life Technologies) and transferred to nitrocellulose membranes. Membranes were incubated with the indicated antibodies and imaged with

a Bio-Rad ChemiDoc XRS+ imager. Band densitometry quantification was performed using the software Quantity One (Bio-Rad).

Isolation of the Heavy Membrane Fraction

Atg5$^{-/-}$ MEFs were infected with mCherry-Parkin virus (MOI: 75) and were treated with DMSO or 25 µM FCCP for 4 h. Cells were collected using a cell scraper and incubated isolation buffer (220 mM mannitol, 70 mM sucrose, 1 mM EDTA, and 10 mM HEPES at 7.4 pH) for 45 min on ice. Cells were homogenized using an Eppendorf pestle and centrifuged for 10 min at 1000 x g to pellet unbroken cells. The supernatant was collected and centrifuged for 15 min at 14000 x g to collect the heavy membrane fraction. After removal of the supernatant, the remaining pellet was resuspended in isolation buffer and separated by SDS-PAGE.

Endosome Pull Down and Mass Spectrometry

GFP-Rab5Q79L-positive endosomes were isolated from *Atg5*$^{-/-}$ MEFs using a protocol adapted from Hanna *et. al. 2012* (Hanna et al., 2012). Briefly, MEFs were infected with mCherry-Parkin (MOI: 75) plus GFP or GFP-Rab5Q79L (MOI: 50) for 12 h. After treatment with DMSO or 25 µM FCCP for 4 h, MEFs were homogenized in ice-cold buffer (0.25 M sucrose, 20 mM Tris-HCl, pH 7.0) supplemented with protease inhibitors (Roche) and then centrifuged for 5 min at 600 x g. The supernatants were incubated with a monoclonal mouse GFP antibody coupled to MACS magnetic beads (Miltenyl Biotech, 130-091-125) overnight before being applied to a MACS MS separation column (Miltenyl Biotech, 130-042-201). Proteins were eluted in a buffer containing 50 mM Tris-

HCl (pH 6.8), 120 mM DTT, 1% SDS, 1 mM EDTA, 0.005% bromophenol blue, and 10% glycerol. The proteins were separated on SDS-PAGE, subjected to in-gel trypsin digestion, and analyzed by LC-MS/MS as described (Wu et al., 2014). The proteomics analysis was done at the Rutgers University Neuroproteomics Core Facility (New Jersey). Heat map was generated as a ratio of the spectra counts for a given condition over the spectra counts for GFP DMSO for each protein. A value of 2 was added to each spectra count in order to generate ratios.

Real Time quantitative PCR

RNA was extracted using the RNeasy Mini Kit (Qiagen) and reverse transcribed to cDNA with the QuantiTect Reverse Transcription Kit (Qiagen) according to the manufacturer's instructions. qPCR was performed with standard TaqMan primers and TaqMan Universal Mastermix II (Applied Biosystems) on a 7500 Fast RealTime PCR system (Applied Biosystems). Fold difference was calculated by the comparative C_T($2^{-\Delta\Delta C}$T) method against Gapdh or 18s (Schmittgen and Livak, 2008). Primers used targeted mouse Rab5a (Integrated DNA Technologies; assay ID: Mm.PT.56a.10093885), Rab5b (Integrated DNA Technologies; assay ID: Mm.PT.56a.29871709), Rab5c (Integrated DNA Technologies; assay ID: Mm.PT.56a.28760014), and Rab7 (Integrated DNA Technologies, assay ID Mm.PT.58.10841588). Male and female mice, age 8-12 weeks, were used for qPCR of hearts.

Electron Microscopy

For the correlated light and electron microscopy, cells were plated on gridded MatTek dishes (MatTek Corporation) and transfected with GFP-Rab5, nanobody against GFP (VHH)-APEX2 (Kirchhofer et al., 2010), HA-Parkin, and mPlum-mito-3 using Fugene6 (Promega Inc.) according to the manufacturer's instructions. Cells were treated with 25 µM FCCP or DMSO for 4 hours, then fixed in 2.5% glutaraldehyde in 0.1M cacodylate buffer pH 7.4 for 1 hour on ice, and imaged on a Leica SPE II (Leica) inverted confocal microscope. For VHH-APEX2, the DAB staining was performed as previously described (Lam et al., 2015). Cells were post-fixed in 1% osmium tetroxide for 30 minutes on ice. After several washes in cold double distilled water, cells were dehydrated in a cold graded ethanol series (20%, 50%, 70%, 90%, 100%) 3 minutes each on ice, then washed in room temperature 100% ethanol, and embedded in Durcupan ACM resin (Electron Microscopy Sciences, Hatfield, PA). Sections were cut using a diamond knife (Diatome) at a thickness between 200nm and 300nm for electron tomography and collected on LuxFilm grids (Luxel Corporation). Colloidal gold particles (5 and 10nm diameter) were deposited on each side of the sections to serve as fiducial markers. EM data were obtained using FEI Titan high base microscope operated at 300kV; micrographs were produced using a 4k x 4k Gatan CCD camera (US4000). For each section, montages of the cell of interest were acquired using the SerialEM software package. The set of 2D EM maps of the cell under scrutiny was correlated with the 3D light microscopy (LM) stack allowing a global registration of the two modalities. This enabled the EM tracking of puncta representing the colocalization of the Rab5-GFP and the mitochondrial signal in the LM volume. This was accomplished using an in-house software allowing side-by-side comparison of multiple views across different

microscopy modalities, and establishing an optimal 3D registration. For tomography, double-tilt series were collected using the SerialEM package. For each series the sample was tilted from -60 to +60 degrees, every 0.5 degree. Tomograms were generated using iterative reconstruction procedure (Phan et al., 2017). To analyze larger volumes consecutive sections were reconstructed serially. 3D reconstruction modeling was done with the IMOD tomography software package (Kremer et al., 1996).

Statistical Analysis

All experiments were independently repeated in the laboratory. Data were collected from experiments performed in at least triplicate, and expressed as mean ± s.e.m. No statistical method was used to predetermine sample size. Differences between groups were assayed using repeated-measure ANOVA tests with Tukey or Dunnett's post hoc test or by Student's t-test, as determined by the data type. The data meet the assumptions of this test, and variances are similar between the groups that are being compared. Differences were considered to be significant when $p < 0.05$. Analyses were done un-blinded with respect to sample identity. Data were excluded if transfection efficiency was less than 40%, or if cells appeared unhealthy in control conditions.

Parts of Chapter 2 were originally published in *Nature Communications*. Hammerling, B. C., Najor, R. H., Cortez, M. Q., Shires, S. E., Leon, L. J., Gonzalez, E. R., Boassa, D., Phan, S., Thor, A., Jimenez, R. E., Li, H., Kitsis, R. N., Dorn II, G. W., Sadoshima, J., Ellisman, M. H., Gustafsson, A. G. A Rab5 Endosomal Pathway

Mediates Parkin-Dependent Mitochondrial Clearance. *Nature Communications*. 8: 14050, 2017; doi:10.1038/ncomms14050 © 2017 Nature Publishing Group. The dissertation author was the primary investigator and author of this paper.

Parts of Chapter 2 were originally published in *Small GTPases*. Hammerling, B. C., Shires, S. E., Leon, L. J., Cortez, M. Q., Gustafsson, A. G. Isolation of Rab5-Positive Endosomes Reveals a New Mitochondrial Degradation Pathway Utilized by BINP3 and Parkin. *Small GTPases*. 1-8, 2017; doi: doi:10.1080/21541248.2017.1342749. © 2017 Taylor & Francis Online. The dissertation author was the primary investigator and author of this paper.

CHAPTER 3: PARKIN DIRECTS AUTOPHAGY-INDEPENDENT MITOCHONDRIAL CLEARANCE

3.1 Introduction

Despite autophagy's importance under basal and stress conditions, autophagy-deficient mice and cells are nonetheless viable (Kuma et al., 2004). Deletion of Atg5 in the heart during early embryogenesis results in the development of mice that are phenotypically normal (Nakai et al., 2007). However, when subjected to a pressure overload model, these mice rapidly develop cardiac dysfunction and heart failure. Similarly, adulthood ablation of this gene under baseline conditions induces heart failure. This indicates that a lack of autophagy in the heart during development can be compensated by other, unknown mechanisms. However in the adult heart, a sudden loss of autophagy results in drastic, deleterious effects.

Recent studies indicate that pathways alternative to traditional autophagy exist that can clear unwanted entire organelles including mitochondria. For instance, autophagy-deficient erythrocytes are still able to eliminate all their organelles including mitochondria during maturation through a process called alternative autophagy (Nishida et al., 2009). This pathway derives its double-membrane autophagosomes from the trans-golgi network and these vesicles are positive for Rab9. Moreover, similar to autophagy, this pathway is dependent on the upstream regulator Ulk1 (Honda et al., 2014). However, the extent to which alternative autophagy is employed is unknown. In addition to alternative autophagy, there may yet be other pathways that can compensate for impaired autophagy.

An important regulator of selective autophagy, and specifically mitophagy, is the E3 ubiquitin ligase Parkin. Depolarization of mitochondria results in the accumulation of the serine-threonine kinase PINK1 on the outer mitochondrial membrane. PINK1 then recruits Parkin, which in turn labels proteins on the outer mitochondrial membrane with ubiquitin. The ubiquitin then acts as a signal for degradation through the autophagy pathway. Specifically, ubiquitin can be bound by adaptor proteins such as p62, and by LC3 on the autophagosome. In this chapter, I investigate whether Parkin can promote clearance of depolarized mitochondria in autophagy-deficient cells. We have performed experiments to determine whether mitochondrial fission or fusion is required for this process, and whether alternative Rab9-mediated autophagy is involved.

3.2 Results

3.2.1 Autophagy-Deficient Cells Clear Mitochondria After FCCP Treatment

To investigate whether Parkin-mediated mitochondrial clearance was altered in autophagy-deficient cells, we utilized embryonic fibroblasts from *Atg5* knockout mice (*Atg5*$^{-/-}$ MEFs) and their control littermates (wild-type (WT) MEFs) (Kuma et al., 2004). *Atg5* is part of the Atg5/12/16 complex which is required for elongation of the autophagosomal membrane; consequently, autophagosomes cannot form in absence of *Atg5* (Kuma et al., 2004). Consistent with previous studies, treatment of cells with the mitochondrial uncoupler FCCP, led to formation of autophagosomes in WT but not *Atg5*$^{-/-}$ MEFs (Figure 3.1). LC3-I is a cytosolic protein that becomes lipidated and incorporated into autophagosomal membranes as LC3-II, which can be visualized as puncta when using the GFP-LC3 reporter (Kabeya et al., 2000). We found that under

baseline conditions, neither WT nor *Atg5*$^{-/-}$ MEFs formed LC3-positive puncta (Figure 3.1 a). After treatment with FCCP, WT but not *Atg5*$^{-/-}$ cells, had increased the formation of LC3-puncta, indicating the generation of autophagosomes. Western blots for LC3 confirmed these results (Figure 3.1 b) as well as verified the accumulation of p62 in autophagy-deficient cells. The autophagy adaptor p62/Sqstm1 binds to ubiquitinated mitochondria and is degraded by autophagy along with the mitochondria (Okatsu et al., 2010). Interestingly, p62 levels decreased when *Atg5*$^{-/-}$ MEFs were treated with FCCP, indicating that p62 is being degraded even in the absence of autophagy. Next, we tested whether organelles such as mitochondria are also being degraded in addition to the protein p62. Thus, we assessed changes in mitochondrial content in response to FCCP treatment in WT and *Atg5*$^{-/-}$ MEFs overexpressing YFP-Parkin. FCCP is a potent inducer of Parkin-mediated mitochondrial autophagy (Chen and Dorn, 2013). In both WT and *Atg5*$^{-/-}$ MEFs, FCCP treatment led to Parkin translocation to mitochondria by 12 hours post-treatment (Figure 3.2 a). By 48 hours, mitochondria were cleared from both cell types. Intriguingly, the rate of mitochondrial clearance, as assessed by immunfluorescent staining and Western blotting for the mitochondrial protein Tom20, were similar in WT and autophagy-deficient cells (Figure 3.2 a-c).

I then tested primary MEFs isolated from *Atg7*$^{-/-}$ embryos to confirm that our observations were not specific to *Atg5*$^{-/-}$ MEFs. Specifically, I wanted to verify that knockout of another core autophagy gene, *Atg7*, would produce the same results. Also, because the *Atg5*$^{-/-}$ MEFs are transformed with the SV40 virus, some compensatory pathways may have developed in these cells. Indeed, I verified that FCCP-mediated mitochondrial clearance also occurred in primary MEFs deficient for the autophagy-

related gene *Atg7* (Figure 3.3). *Atg7*$^{-/-}$ MEFs showed mitochondrial clearance at the same rate as their WT counterparts by immunofluorescence and Western blotting for the mitochondrial proteins Tim23 and Tom20. These results indicate that the traditional *Atg5/7*-dependent autophagy pathway is not required for mitochondrial clearance.

3.2.2 Functional Parkin is Required for FCCP-Mediated Mitochondrial Clearance

Mitochondria are large organelles that cannot be degraded through the ubiquitin-proteasome system. As a result, they need to be sequestered by vesicles to be eliminated from the cytosol. The best studied mechanism of mitochondria removal is via Parkin-mediated mitophagy. Parkin mediates ubiquitination of depolarized or damaged mitochondria. This results in engulfment by autophagosomes and degradation through the autophagy pathway. Next, we wanted to test whether Parkin was required for clearance of depolarized mitochondria in *Atg5*$^{-/-}$ MEFs. MEFs lack detectable levels of Parkin (Ding et al., 2010), and overexpression of Parkin in *Atg5*$^{-/-}$ MEFs resulted in both p62/Sqstm1 and Tom20 degradation after FCCP exposure, even though these cells are defective in autophagy (Figure 3.4 a-c). This degradation only occurred in the presence of Parkin, as overexpression of βgal instead did not result in mitochondrial clearance with FCCP. This indicates that Parkin is required for the clearance of mitochondria and the adaptor protein p62 in autophagy-deficient cells.

Parkin is a ubiquitin ligase and there are known nonfunctional Parkinson's disease associate mutants, ParkinR42P or ParkinG430D, which are defective in ubiquitin-like and RING2 domains, respectively (Sriram et al., 2005). As a result, these mutants are impaired in their ability to ubiquitinate substrates such as mitochondria. I

found that ParkinR42P or ParkinG430D were unable to efficiently clear their mitochondria in response to FCCP when overexpressed in MEFs (Figure 3.4 d,e). Thus, these findings indicate that Parkin-mediated ubiquitination is a prerequisite for degradation of depolarized mitochondria in autophagy-deficient cells.

3.2.3 Membrane-Ion Permeabilization, but not DNA Damage, Induces Mitochondrial Clearance

I wanted to test whether mitochondrial clearance was driven by any variety of cellular stress, or if it was only specifically triggered by mitochondrial depolarization. In addition to using FCCP, which depolarizes mitochondria by increasing membrane permeability to H^+, I tested whether valinomycin, which depolarizes mitochondria by permeabilizing the membrane to K^+, would also promote mitochondrial clearance in the absence of autophagy. Indeed, I found that valinomycin treatment resulted in clearance of mitochondria in both WT and *Atg5*$^{-/-}$ MEFs in the presence of Parkin (Figure 3.5 a,b). In contrast, DNA damage by Actinomycin D, an inhibitor for RNA synthesis which induces apoptosis (Martin et al., 1990), did not promote mitochondrial clearance in WT and *Atg5*$^{-/-}$ MEFS (Figure 3.5 c,d). These results indicate that mitochondrial stress, but not DNA damage, induces mitochondrial clearance in *Atg5*$^{-/-}$ MEFs.

3.2.4 Mitochondrial Fission and Fusion Proteins are not Required for Mitochondrial Clearance

Mitochondria are highly dynamic organelles and undergo fission or fusion to adapt to changes in the cellular environment. Fission occurs in response to

mitochondrial stress and has been linked to mitophagy. To investigate whether mitochondrial fission is a prerequisite for clearance, I decided to manipulate proteins involved in the regulation of fission and fusion. The mitochondrial fission protein, Drp1, mediates asymmetrical fission allowing for segregation and selective removal of depolarized mitochondrial fragments by autophagy (Twig et al., 2008). However, inhibiting Drp1-mediated mitochondrial fission by overexpressing the dominant negative Drp1K38E did not affect Parkin-mediated mitochondrial clearance in *Atg5*$^{-/-}$ MEFs (Figure 3.6). In opposition to the process of mitochondrial fission is fusion. The proteins Mfn1/2 are responsible for fusion of the outer mitochondrial membrane (van der Bliek et al., 2013). Promoting mitochondrial fusion by overexpression of Mfn2 or Mfn2(T111E/S442E), which lacks mitochondrial fusion activity but is a constitutive Parkin receptor (Chen and Dorn, 2013; Gong et al., 2015), did not affect Parkin-mediated mitochondrial clearance in response to FCCP treatment in *Atg5*$^{-/-}$ MEFs (Figure 3.7). Thus, our data suggest that mitochondrial clearance can still occur in the absence of Drp1-mediated mitochondrial fission or in the presence of excess mitochondrial fusion proteins. This is in agreement with the fact that Drp1-deficient mice do not have defective mitochondrial clearance (Song et al., 2015), suggesting that mitochondria clearance can occur independently of mitochondria fission.

3.2.5 Mitochondrial Clearance is not Dependent on Alternative Autophagy

There are reports of an alternative form of autophagy that occur in *Atg5/7*-deficient cells that derive their membranes from the trans-golgi network. These vesicles are also double-membraned and are Rab9 positive (Nishida et al., 2009). To examine

whether *Atg5/7*-independent alternative autophagy contributes to mitochondrial clearance, we examined *Atg5*$^{-/-}$ MEFs for the presence of Rab9-positive vesicles. Although the number of Rab9-positive vesicles significantly increased after FCCP treatment, there was little colocalization between Rab9 and mitochondria in these cells by immunofluorescent analysis (Figure 3.8 a-c). This suggests that mitochondria are not being sequestered by these vesicles. Also, overexpression of Rab9S21N, a dominant negative mutant of Rab9 (Choudhury et al., 2002), failed to reduce Parkin-mediated mitochondrial clearance in *Atg5*$^{-/-}$ MEFs by 24 hours (Figure 3.8 d,e).

Both alternative autophagy and traditional mitophagy pathways require the upstream Unc-51 Like Autophagy Activating Kinase 1 (Ulk1) (Kundu et al., 2008; Nishida et al., 2009). We confirmed that neither Ulk1 nor its homologue Ulk2 is required for Parkin-mediated clearance in response to FCCP treatment. In fact, we observed similar levels of mitochondrial clearance in WT, *Ulk1*$^{-/-}$, *Ulk2*$^{-/-}$, and *Ulk1/2*$^{-/-}$ MEFs overexpressing Parkin (Figure 3.9). Thus, these results confirm that neither traditional nor alternative autophagy is required for Parkin-mediated mitochondrial clearance in *Atg5*$^{-/-}$ MEFs.

3.3 Discussion

In this chapter, I report that autophagy-deficient *Atg5*$^{-/-}$ or *Atg7*$^{-/-}$ MEFs are capable of clearing damaged mitochondria upon FCCP treatment. Moreover, this clearance is induced by mitochondrial membrane depolarization, but not by other stressors such as DNA damage. This highlights the fact that mitochondrial quality control is a distinct and regulated process independent of general protein and organelle

homeostasis. It is already known that mitochondrial depolarization can trigger PINK1/Parkin-mediated mitophagy (Matsuda et al., 2010; Narendra et al., 2008). Other stressors that affect mitochondria, such as hypoxia, oxidative stress, and cytosolic calcium overload, are also capable of inducing mitophagy (Kubli and Gustafsson, 2012; Saelens et al., 2004). Our data suggest that mitochondrial depolarization can also induce mitochondrial clearance independent of traditional *Atg5/7*-mediated autophagy.

Interestingly, I also found that mitochondrial clearance in autophagy-deficient cells is dependent on functional Parkin. This suggests that a new downstream pathway for mitochondrial clearance is reliant on Parkin-mediated ubiquitination. Again, such redundancies point to the importance of having functional mitochondrial clearance. However, this raises an intriguing possibility that patients harboring disease-associated mutants of Parkin not only have defects in traditional Parkin-mediated mitophagy but also defects in this alternative, potentially compensatory, pathway.

Mitochondria are thought to undergo asymmetric fission in order to segregate oxidized and otherwise damaged proteins within the mitochondrion from the healthy components (Dorn and Kitsis, 2015). This separation then allows for the damaged mitochondrion to be preferentially cleared from the cell. The data here demonstrate that mitochondrial clearance can occur independently of the fission protein Drp1. This is perhaps due to the fact that all the mitochondria are simultaneously depolarized, and asymmetrical fission is not possible. This is confirmed by the fact that Drp1-deficient mice are still able to clear mitochondria (Song et al., 2015). Interestingly, Drp1-deficiency leads to excessive mitophagy confirming the importance of Drp1 in mediating asymmetrical fission

It has been shown that alternative autophagy can be stimulated in cells with deficient-autophagy. This pathway still forms double-membrane autophagosomes, however their source material is different. Membranes are derived from the trans-golgi network and have been implicated in the clearance of mitochondria from erythrocytes (Honda et al., 2014; Nishida et al., 2009). Also, HeLa cells undergoing starvation or hypoxia have also been reported to clear a portion of their mitochondria through the alternative autophagy pathway, and most significantly, this pathway is required for a metabolic switch and pluripotency in iPSC reprogramming (Hirota et al., 2015; Ma et al., 2015). While alternative autophagy is clearly an important pathway, our data here preclude both traditional and alternative autophagy, suggesting that an additional pathway for mitochondrial quality control might exist in cells. Given that the cell already has several pathways for protein and organelle quality control, including the UPS, traditional-, and alternative-autophagy pathways, the discovery of yet another pathway highlights the importance of such cellular homeostasis. Thus, if any one of these pathways is impaired, there are still several backup mechanisms in place to ensure removal of toxic protein aggregates and organelles. In the next chapter, I test the hypothesis that the endosomal pathway is involved in mitochondrial clearance in these cells.

Parts of Chapter 3 were originally published in *Nature Communications*. Hammerling, B. C., Najor, R. H., Cortez, M. Q., Shires, S. E., Leon, L. J., Gonzalez, E. R., Boassa, D., Phan, S., Thor, A., Jimenez, R. E., Li, H., Kitsis, R. N., Dorn II, G. W., Sadoshima, J., Ellisman, M. H., Gustafsson, A. G. A Rab5 Endosomal Pathway

Mediates Parkin-Dependent Mitochondrial Clearance. *Nature Communications*. 8: 14050, 2017; doi:10.1038/ncomms14050 © 2017 Nature Publishing Group. The dissertation author was the primary investigator and author of this paper.

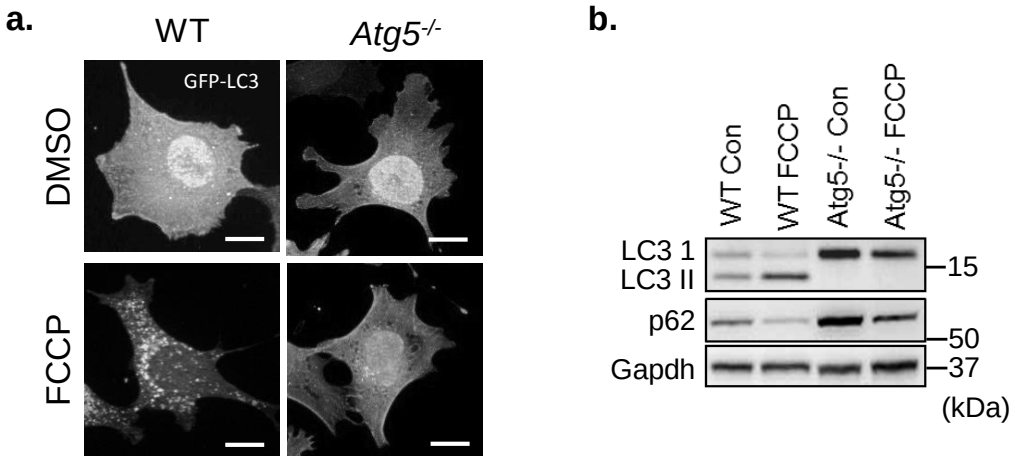

Figure 3.1. *Atg5*$^{-/-}$ MEFs are autophagy deficient.
(a) Representative images of WT and *Atg5*$^{-/-}$ MEFs overexpressing GFP-LC3. Scale bars=20 µm. **(b)** Western blot for LC3, p62, and Gapdh in WT and *Atg5*$^{-/-}$ MEFs overexpressing Parkin after treatment with 25 µM FCCP for 9 h.

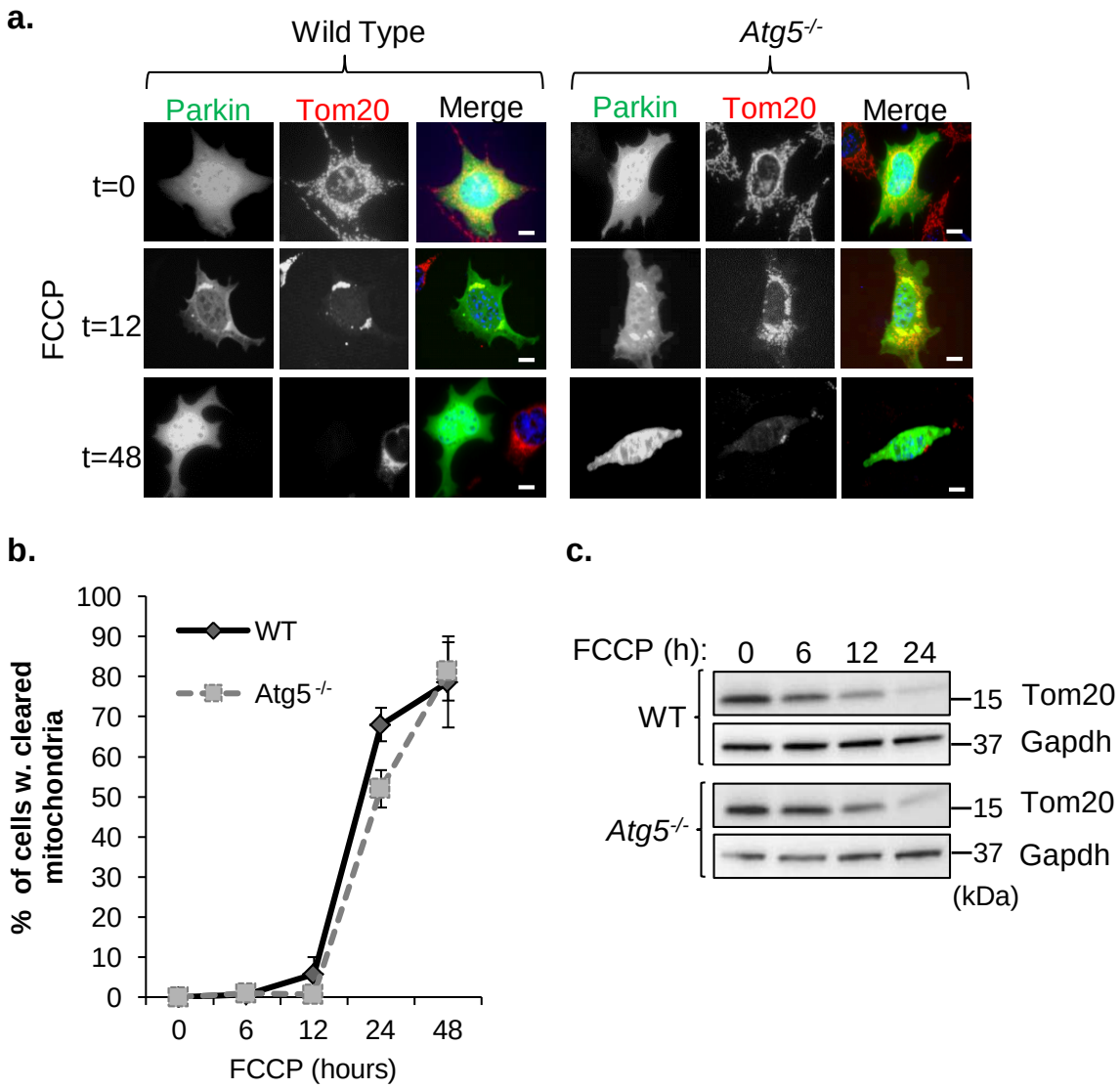

Figure 3.2. FCCP mediates mitochondrial clearance in *Atg5*$^{-/-}$ MEFs.
(a) Representative images of WT and *Atg5*$^{-/-}$ MEFs overexpressing YFP-Parkin. Cells were fixed at the indicated time points (in hours) after treatment with FCCP (25 µM) and stained with anti-Tom20 to label mitochondria. Scale bars=20 µm. **(b)** Quantification of WT and *Atg5*$^{-/-}$ MEFs with cleared mitochondria by Tom20 staining after FCCP treatment (n=100 cells screened for mitochondria in 3 independent experiments). **(c)** Western blot time course of Tom20 protein levels in WT and *Atg5*$^{-/-}$ MEFs overexpressing Parkin after FCCP treatment (25 µM). Nuclei were counterstained with Hoechst 33342 (blue). All values are means±s.e.m from independent experiments. Statistical significance was calculated using ANOVA followed by Dunnett's test for multiple comparison.

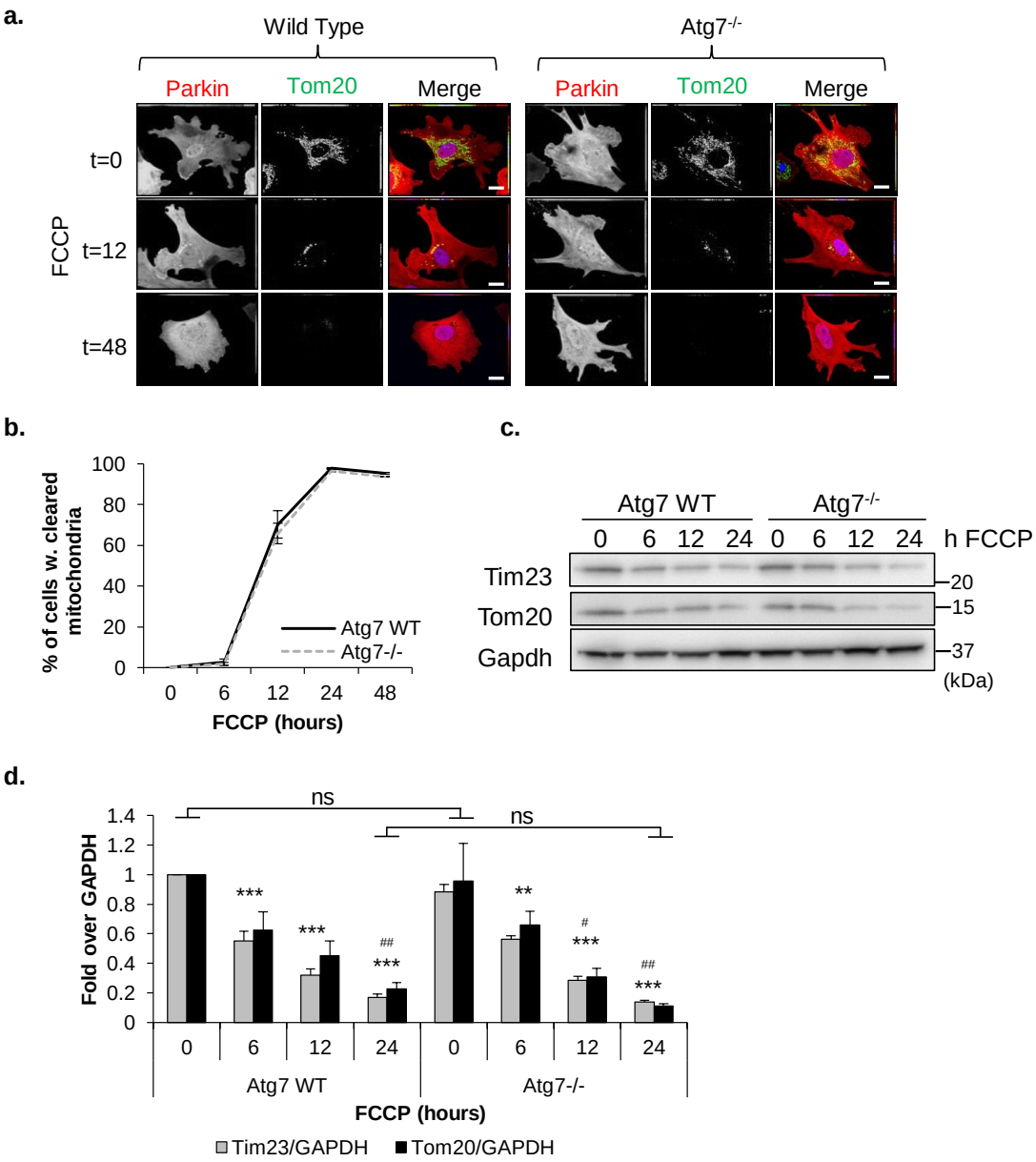

Figure 3.3. Autophagy machinery is not required for mitochondrial clearance. **(a)** Representative images of primary WT and *Atg7*$^{-/-}$ MEFs infected with mCherry-Parkin and treated with DMSO or 25 µM FCCP. Cells were fixed at the indicated time points (in hours) and stained with anti-Tom20 to label mitochondria. Scale bars=20 µm. Nuclei were counterstained with Hoechst 33342 (blue). **(b)** Quantification of WT and *Atg7*$^{-/-}$ MEFs with cleared mitochondria by Tom20 staining after 25 µM FCCP treatment (n=150 cells screened for mitochondria in 3 independent experiments). **(c)** Representative Western blot time course of Tim23 and Tom20 protein levels in WT and *Atg7*$^{-/-}$ MEFs overexpressing Parkin after FCCP treatment (25 µM). **(d)** Band densitometry of Tim23 and Tom20 protein levels from panel **c** (n=3, **p<0.01, ***p<0.001 vs 0 h Tim23; #p<0.05, ##p<0.01 vs 0 h Tom20). All values are means±s.e.m from independent experiments. Statistical significance was calculated using ANOVA followed by Dunnett's test for multiple comparison.

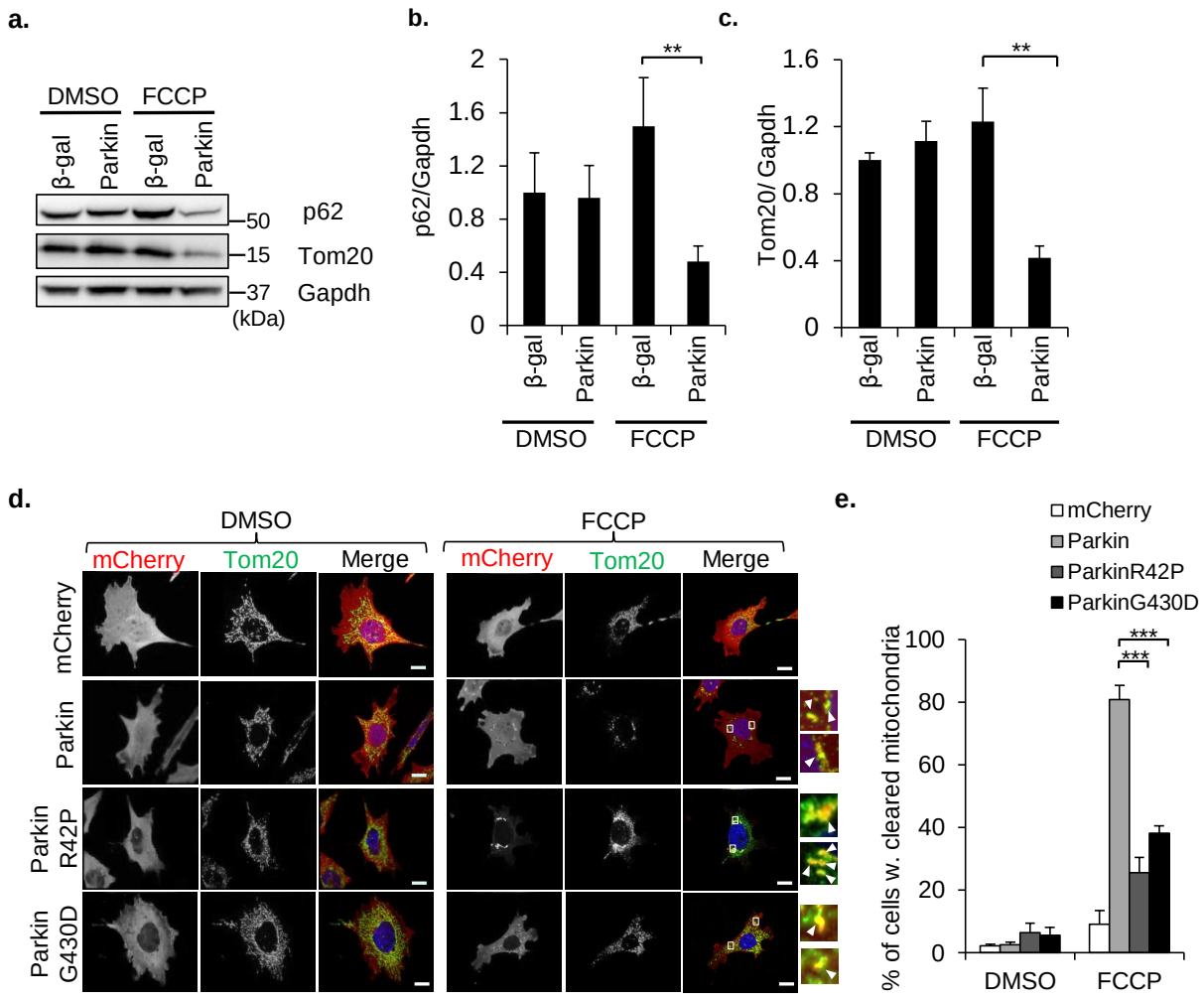

Figure 3.4. Mitochondrial clearance is dependent on Parkin.
(a) Western blot for p62 and Tom20 in *Atg5*$^{-/-}$ MEFs overexpressing Ad-βgal or Ad-Parkin after treatment with DMSO or FCCP (25 μM) for 24 h. **(b,c)** Band densitometry of p62 **(b)** and Tom20 **(c)** protein levels from panel a (n=3, **p<0.01). **(d)** Representative images of *Atg5*$^{-/-}$ MEFs infected with mCherry, mCherry-Parkin, mCherry-ParkinR42P, or mCherry-ParkinG430D were treated with DMSO or 25 μM FCCP for 24 h. Cells were fixed and stained with anti-Tom20 to label mitochondria. Arrowheads show colocalizing puncta. Scale bars=20 μm. **(e)** Quantification of Tom20-positive cells after FCCP treatment (n=300 cells screened for mitochondria in 3 independent experiments, ***p<0.001). Nuclei were counterstained with Hoechst 33342 (blue). All values are means±s.e.m from independent experiments. Statistical significance was calculated using ANOVA followed by Dunnett's test for multiple comparison.

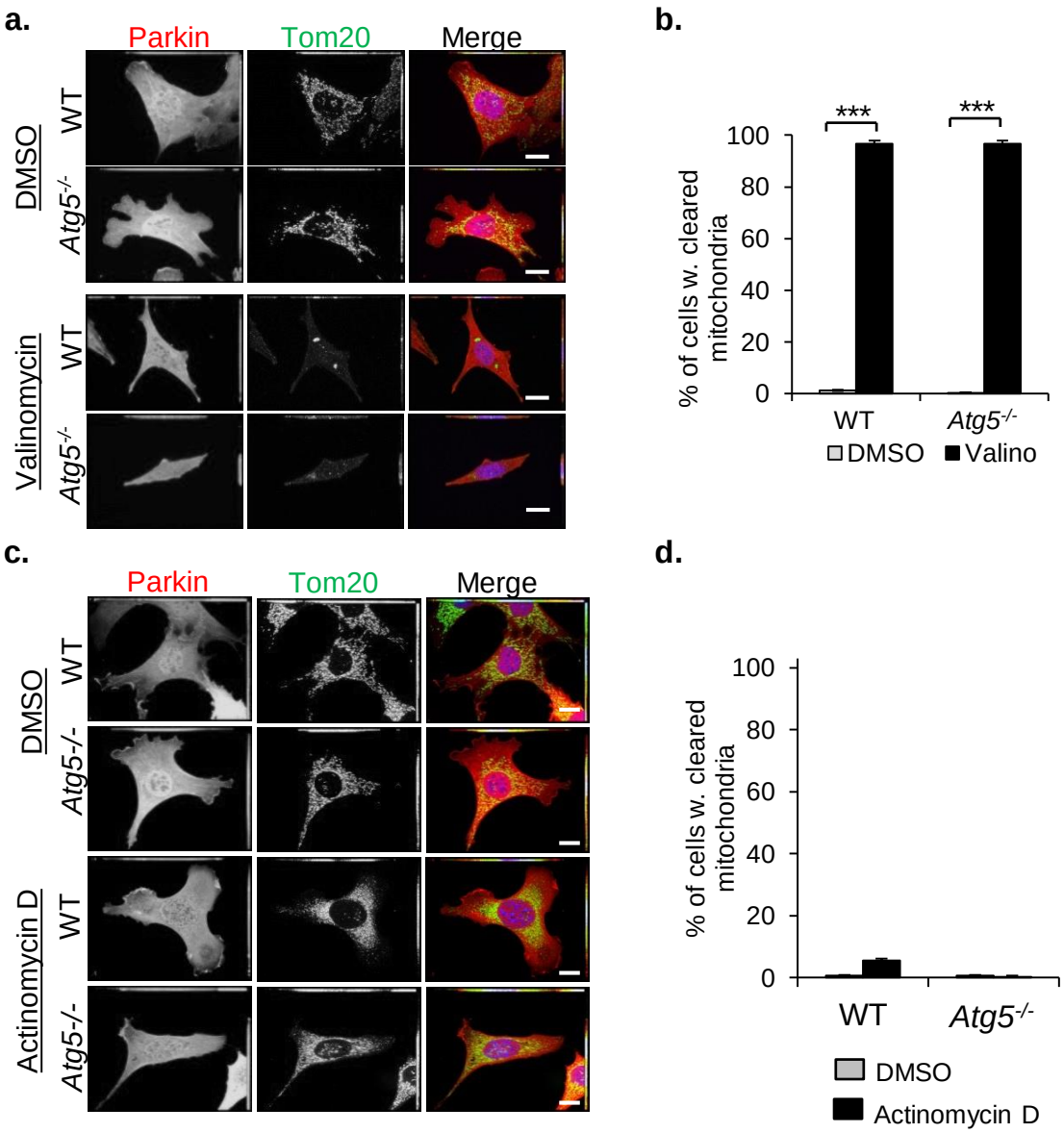

Figure 3.5. Membrane depolarization, but not DNA damage, can trigger mitochondrial clearance.

(a) Representative images of WT and *Atg5*$^{-/-}$ MEFs infected with mCherry-Parkin and treated with DMSO or 10 µM valinomycin for 24 h. After treatment, cells were fixed and stained with anti-Tom20. Scale bars=20 µm. **(b)** Quantification of mitochondrial clearance in response to valinomycin (n=200 cells screened for mitochondria in 3 independent experiments, ***p<0.001 vs DMSO).). **(c)** Representative images of WT and *Atg5*$^{-/-}$ MEFs overexpressing mCherry-Parkin and treated with DMSO or actinomycin D (0.05 µg/mL) for 24 h. Cells were stained with anti-Tom20. **(d)** Quantification of mitochondrial clearance (n=200 cells screened for mitochondria in 3 independent experiments) in response to actinomycin D. Scale bars=20 µm. Nuclei were counterstained with Hoechst 33342 (blue). All values are means±s.e.m from independent experiments. Statistical significance was calculated using ANOVA followed by Dunnett's test for multiple comparison.

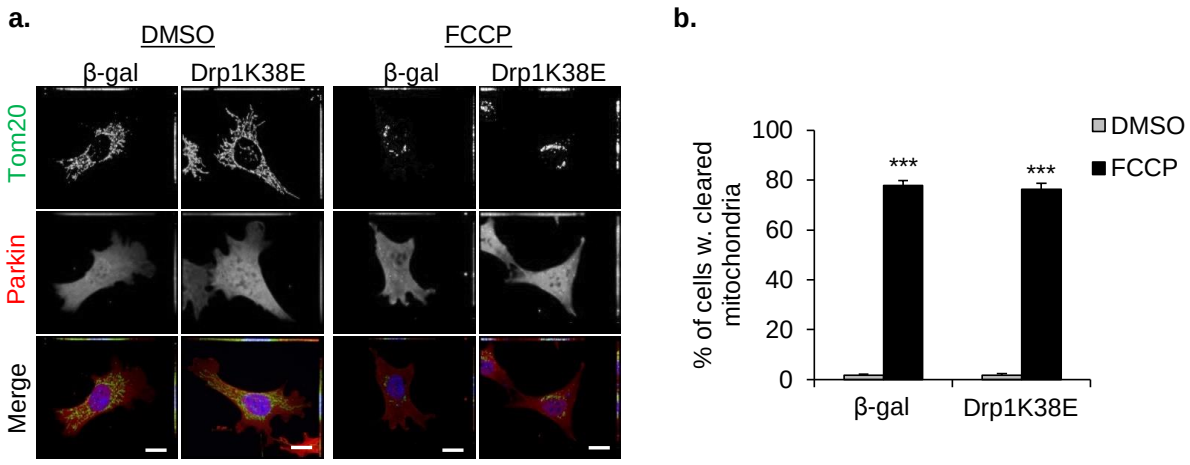

Figure 3.6. Drp1-mediated mitochondrial fission is not required for FCCP-mediated mitochondrial clearance.
(a) Representative images of *Atg5*$^{-/-}$ MEFs overexpressing Parkin and β-gal or Drp1K38E. After 25 μM FCCP treatment (24 h), cells were fixed and stained with anti-Tom20. Scale bars=20 μm. **(b)** Quantification of cells undergoing mitochondria clearance (n=200 cells screened for mitochondria in 3 independent experiments, ***p<0.001 vs DMSO). All values are means±s.e.m from independent experiments. Statistical significance was calculated using ANOVA followed by Dunnett's test for multiple comparison.

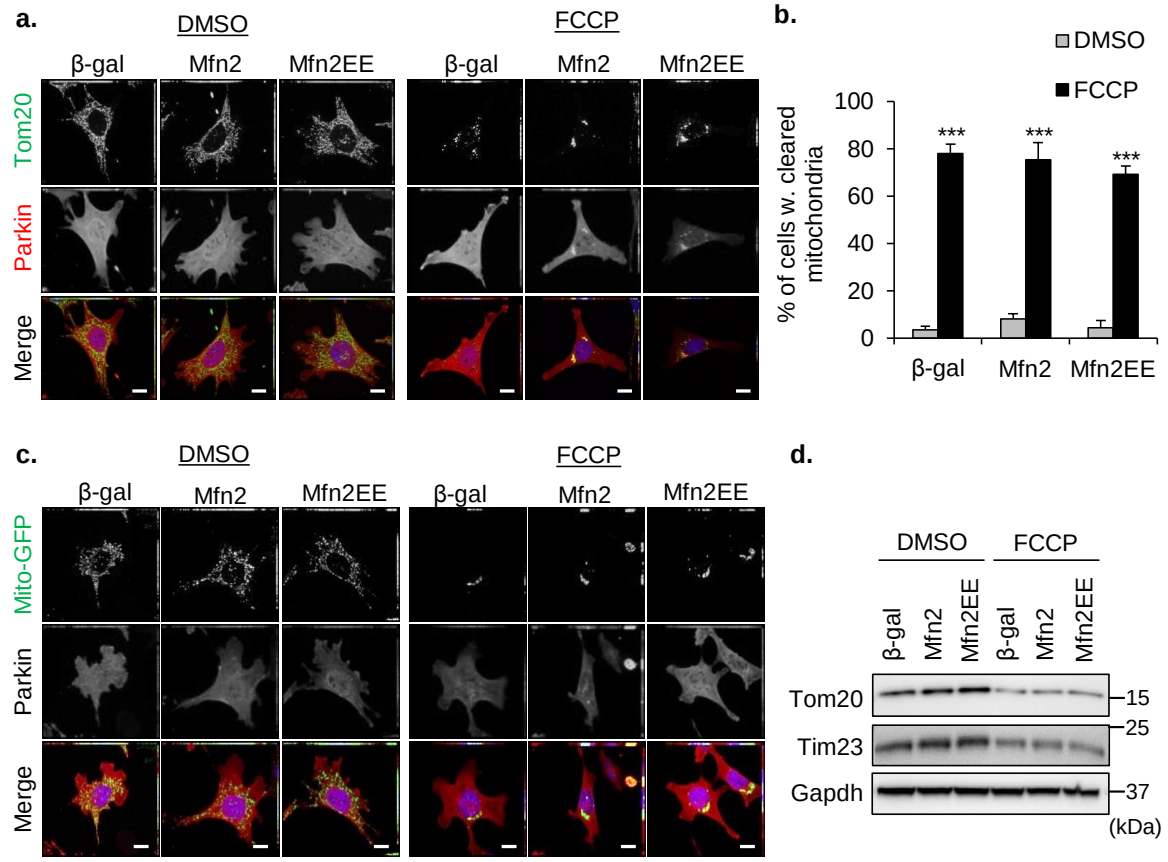

Figure 3.7. Affecting mitochondrial fusion does not alter FCCP-mediated mitochondrial clearance.

(a) Representative images of *Atg5*$^{-/-}$ MEFs overexpressing mCherry-Parkin plus βgal, Mfn2 or Mfn2EE. After treatment with 25 µM FCCP for 24 h, cells were fixed and stained with anti-Tom20. Scale bars=20 µm. **(b)** Quantification of cells undergoing mitochondria clearance (n=150 cells screened for mitochondria in 3 independent experiments, ***p<0.001 vs DMSO). **(c)** Representative images of *Atg5*$^{-/-}$ MEFs overexpressing mCherry-Parkin and Mito-GFP (localizes to mitochondrial matrix) plus Mfn2 or Mfn2EE. Scale bars=20 µm. **(d)** Western blot for Tom20, Tim23, and GAPDH in *Atg5*$^{-/-}$ MEFs overexpressing Parkin plus Ad-β-gal, Ad-Mfn2, or Ad-Mfn2EE. Nuclei were counterstained with Hoechst 33342 (blue). All values are means±s.e.m from independent experiments. Statistical significance was calculated using ANOVA followed by Dunnett's test for multiple comparison.

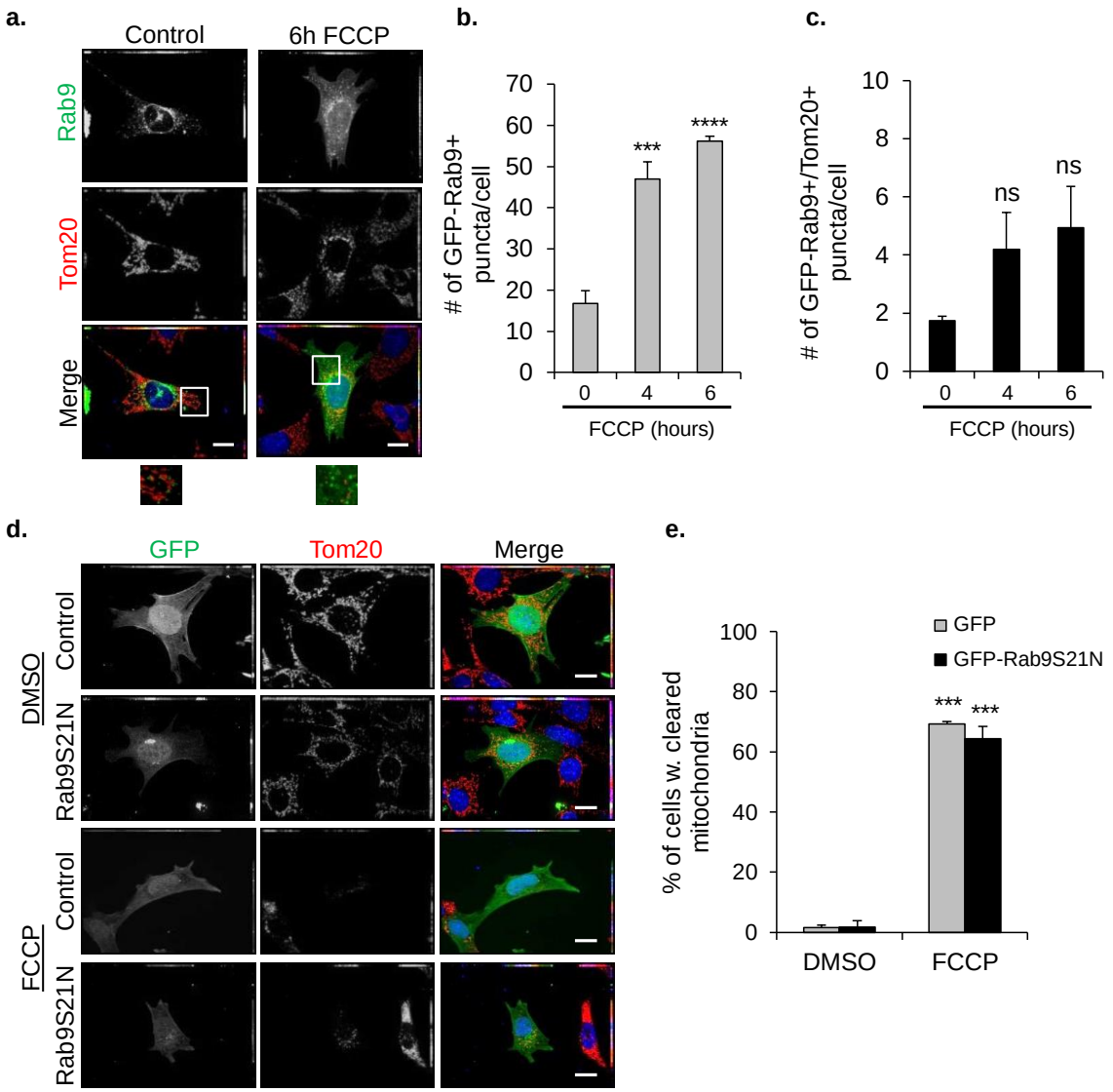

Figure 3.8. Rab9-mediated alternative autophagy does not contribute to Parkin-mediated clearance in *Atg5*$^{-/-}$ MEFs.

(a) Representative images of *Atg5*$^{-/-}$ MEFs transfected with GFP-Rab9 and HA-Parkin. After 25 µM FCCP treatment, cells were fixed and stained with anti-Tom20 to label mitochondria. Scale bars=20 µm. **(b,c)** Quantification of GFP-Rab9 positive puncta **(b)** and their colocalization **(c)** with Tom20 labeled mitochondria in *Atg5*$^{-/-}$ MEFs (n=45 cells scored for number of puncta in 3 independent experiments, ***p<0.001, ****P<0.0001 vs 0 h, ns=not significant). **(d)** Representative images of *Atg5*$^{-/-}$ MEFs transfected with HA-Parkin plus GFP or GFP-Rab9S21N. After treatment with FCCP for 24 h, cells were fixed and stained with anti-Tom20. Scale bars=20 µm. **(d)** Quantification of mitochondrial clearance in response to 25 µM FCCP (n=200 cells screened for mitochondria in 3 independent experiments, ***p<0.001 vs GFP+DMSO) cells. Nuclei were counterstained with Hoechst 33342 (blue). All values are means±s.e.m from independent experiments. Statistical significance was calculated using ANOVA followed by Dunnett's test for multiple comparison.

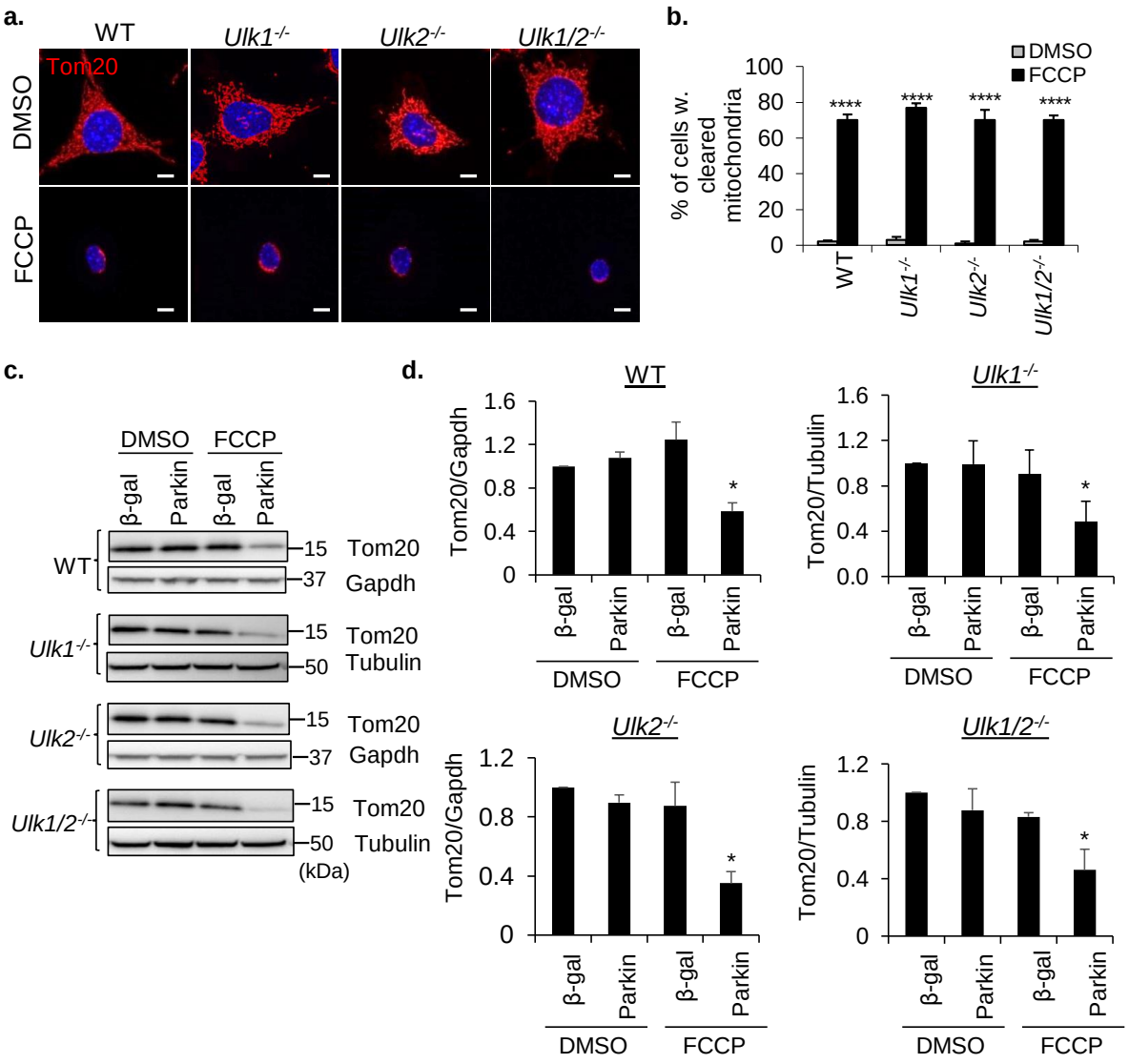

Figure 3.9. Ulk1/2 are not required for Parkin-mediated clearance of damaged mitochondria.

(a) Representative images of WT, *Ulk1*$^{-/-}$, *Ulk2*$^{-/-}$, and *Ulk1/2*$^{-/-}$ MEFs transfected with HA-Parkin, treated with 25 μM FCCP (24 h), and stained with anti-Tom20 to label mitochondria. Scale bars=20 μm. **(b)** Quantification of cells undergoing mitochondrial clearance (n=550 cells screened for mitochondria in 3 independent experiments, ****p<0.0001 vs DMSO). **(c)** Representative Western blots for Tom20, Tubulin, and GAPDH in WT, *Ulk1*$^{-/-}$, *Ulk2*$^{-/-}$, and *Ulk1/2*$^{-/-}$ MEFs infected with Ad-βgal or Ad-Parkin after treatment with DMSO or FCCP (25 μm) for 24 h. **(d)** Band densitometry of Tom20 levels (n=3, *p<0.05 vs β-gal + FCCP). Nuclei were counterstained with Hoechst 33342 (blue). All values are means±s.e.m from independent experiments. Statistical significance was calculated using ANOVA followed by Dunnett's test for multiple comparison.

CHAPTER 4: EARLY ENDOSOMES SEQUESTER MITOCHONDRIA VIA ESCRT COMPLEXES, MATURE, AND ARE DEGRADED

4.1 Introduction

Endosomes, though primarily known for their role in receptor recycling and degradation, have several aspects in common with the autophagy pathway. First, they can recognize ubiquitinated proteins, such as plasma membrane receptors that are marked for internalization and for delivery to endosomes. Second, these vesicles are involved in sequestration and transport, and third, they fuse with lysosomes to degrade their cargo. The endocytic vesicles of this pathway are regulated and can be identified by their Rab GTPases. Early endosomes are marked by the small GTPase Rab5, which is a critical regulator of their biogenesis and function (Zeigerer et al., 2012). Rab5 also mediates endocytosis and enables homotypic fusion between early endosomes into larger vesicles (Stenmark, 2009). As these early vesicles mature, they become more acidic, develop intraluminal vesicles (ILVs), and Rab5 is replaced by the GTPase Rab7, which marks late endosomes (Huotari and Helenius, 2011). Rab7 also enables endosomal fusion with lysosomes.

Endosomes can recognize and sequester ubiquitinated proteins through the ESCRT complexes. These complexes, ESCRT-0, -I, -II, and –III, can be found on the endosome surface where they bind ubiquitinated proteins and pull them into the endosome through a process of invagination and scission (Campsteijn et al., 2016). Each complex, except for ESCRT-III, can directly bind ubiquitinated proteins and assist in the recruitment of subsequent complex. ESCRT-III promotes inward vesicle budding,

and the ESCRT complexes are disassembled by Vps4-Vta1. Together, the ESCRTs produce intraluminal vesicles within the endosomes. While these vesicles are reported to be approximately 40-100 nm in size (Williams and Urbe, 2007), it is possible that they can grow in size to accommodate larger cargo. In the previous chapter, I showed that depolarized mitochondria can be cleared from autophagy-deficient cells, and this process is dependent on the E3 ubiquitin ligase Parkin. Thus in this chapter, I investigate whether the endosomal pathway is involved in their clearance.

4.2 Results:

4.2.1 Endosomes Sequester Damaged Mitochondria and Activation Requires Beclin1

Our findings in chapter 3 demonstrate clearly that depolarized mitochondria are able to be cleared from autophagy-deficient cells. Therefore, we sought to test the hypothesis that mitochondria are being sequestered into endosomes that ultimately fuse with lysosomes for degradation. The endosomal-lysosomal degradation pathway plays a role in cellular quality control by degrading ubiquitinated plasma membrane proteins (Marchese et al., 2008). However, it is currently unknown if this pathway also participates in the degradation of entire organelles such as mitochondria. We discovered that mitochondrial depolarization with FCCP led to a rapid increase in the number of Rab5 positive early endosomes in WT and *Atg5*$^{-/-}$ MEFs and that a significant number of these endosomes colocalized with mitochondria after treatment (Figure 4.1 a-f). We confirmed that these colocalizing mitochondria are depolarized by lack of mitotracker Red staining (Figure 4.1 g). Moreover, at these early time points, within 8

hours, there is negligible cell death in response to the FCCP exposure (Figure 4.1 h). Therefore, it is unlikely that these mitochondria within early endosomes are a result of endocytosis from neighboring, dead cells. I also confirmed that treatment with the K+ protonophore valinomycin, but not the DNA-damaging agent Actinomycin D, caused an increase in the number of Rab5-positive vesicles in both WT and *Atg5*$^{-/-}$ MEFs (Figures 4.2), consistent with their respective ability to trigger mitochondrial clearance (Figures 3.4). Another defining characteristic of early endosomes is the generation of the lipid phosphatidylinositol 3-phosphate (PI(3)P) at the membrane by the Vps34 PI3K complex (Maxfield and McGraw, 2004). Several critical Rab5 interacting proteins, such as Eea1, Rabenosyn-5, and Rabankyrin-5, bind to PI(3)P at the endosome (Stenmark, 2009). To monitor activity of the Vps34 PI3K complex on Rab5-positive endosomes, we overexpressed a GFP conjugated PX domain from p40, which specifically binds PI(3)P at the early endosomes (Kanai et al., 2001). We observed an increase in the colocalization between p40PX-EGFP and Rab5 in both WT and *Atg5*$^{-/-}$ MEFs after FCCP treatment (Figure 4.3). These findings suggest that endosomal activity and sequestration of dysfunctional mitochondria into endosomes occur even in cells with intact autophagy.

There is cross talk between the various degradation pathways and it is possible that some of the autophagy molecules might also function to regulate the endosome-lysosomal degradation pathway. Beclin1 is a known component of the Vps34 PI3K complex. Therefore, we examined whether Beclin1 was found on the “activated” early endosomes. We found that there is increased colocalization between p40PX-EGFP and Beclin1 in both WT and *Atg5*$^{-/-}$ MEFs after FCCP treatment (Figure 4.4 a-c). We also

observed a significant increase in Beclin1 and Rab5 colocalization in *Atg5*$^{-/-}$ MEFs in response to FCCP treatment (Figure 4.4 d-f), confirming that Beclin1 is found on the early endosomes. Furthermore, silencing of Beclin1 with siRNA suppressed the increase in the number of Rab5-positive endosomes and the colocalization between Rab5 and mitochondria in *Atg5*$^{-/-}$ MEFs upon FCCP treatment (Figure 4.5). *Ulk1* is an upstream regulator of both traditional and alternative autophagy (Kundu et al., 2008; Nishida et al., 2009). However, it is possible that *Ulk2* can compensate for *Ulk1* activity. Therefore we examined cells deficient for both *Ulk1/2* and found no defect on early endosomal activity in response to FCCP treatment (Figure 4.6). This is consistent with the fact that these knockout lines still display mitochondrial clearance (Figure 3.9). Thus, our data indicate that early endosome formation and Rab5-mediated mitochondrial clearance requires the presence of Beclin1, but not Ulk1/2.

4.2.2 Mitochondria Accumulate in Constitutively Active Rab5Q79L-Positive Endosomes

The small GTPase Rab5 functions in the biogenesis and homotypic fusion of early endosomes (Zeigerer et al., 2012). Mutating the glutamine to leucine at amino acid residue 79 in the GTPase domain results in a constitutively active Rab5 that is unable to hydrolyze bound GTP. Thus, overexpression of Rab5Q79L in cells leads to fusion of early endosomes resulting in oversized endosomes with an average size of 2 - 5 µm that are unable to mature into late endosomes (Stenmark et al., 1994a; Stenmark et al., 1994b). Here, I confirmed that overexpression of Rab5Q79L led to formation of enlarged early endosomes (EEE) in both wild type (WT) and the autophagy-deficient

Atg5$^{-/-}$ MEFs overexpressing Parkin (Figure 4.7 a,b). I also observed the presence of a significant number of mitochondria inside the EEEs after treatment with FCCP (Figure 4.7 b,c). This suggests that depolarized mitochondria accumulate inside the EEEs in both WT and *Atg5*$^{-/-}$ MEFs. We usually observe approximately 6-10 mitochondria per cell, where each colocalizes with a single Rab5-positive early endosomes after FCCP treatment. In contrast, each enlarged Rab5Q79L-positive endosome usually contains several mitochondria inside of them (Figure 4.7 c). This is likely due to the fact that Rab5Q79L-positive endosomes accumulate fragmented mitochondria through homotypic fusion and that these vesicles are unable to mature.

Next, we aimed to perform proteomics analysis of isolated Rab5-positive endosomes to confirm mitochondrial content. The conversion from Rab5-positive early endosomes to Rab7-posititve late endosomes occurs very rapidly, on the timescale of a few minutes (Rink et al., 2005). Due to the transient number of early endosomes containing mitochondria present in cells at any given time, it was challenging to isolate a sufficient number of Rab5-positive vesicles for proteomics analysis. Thus, we took advantage of cells overexpressing Rab5Q79L which accumulate the EEEs containing mitochondria. We have previously isolated intact GFP-positive autophagosomes using antibody against GFP conjugated to magnetic beads (Hanna et al., 2012). Here, we adapted this protocol to isolate Rab5-positive endosomes. We used anti-GFP conjugated to magnetic beads to capture the enlarged Rab5-positive vesicles from *Atg5*$^{-/-}$ MEFs (Figure 4.8 a). After confirming that we successfully pulled down endosomes by blotting for the markers Rab5 and Eea1 (Figure 4.8 b), but not lysosomal protein Lamp2, the purified endosomes were resolved on one-dimensional SDS-PAGE,

subjected to in-gel tryptic digestion and analysis by LC MS/MS. The mass spectrometry confirmed the presence of mitochondrial proteins in GFP-Rab5Q79L labeled endosomes. The number of mitochondrial proteins was also increased after FCCP treatment (Figure 4.8 c). Furthermore, GFP-Rab5Q79L-labeled endosomes contained higher levels of proteins related to endosomal cargo and mitophagy than controls after FCCP treatment (Figure 4.8 c). These results confirm the presence of mitochondria within Rab5-positive early endosomes.

4.2.3 Correlated Light and Electron Microscopy Confirms Mitochondria inside Rab5-Positive Early Endosomes

To further confirm that mitochondria were internalized into Rab5-positive endosomes, we performed correlated light and 3D electron tomography. Using this technique, we are able to identify colocalization events by immunofluorescence and then perform 3D electron tomography of these same events. This allows us to confirm that the colocalization truly represents mitochondria inside early endosomes and not that they are merely adjacent to one another. We observed labeled mitochondria (mPlum-mito) colocalizing with GFP-Rab5 positive early endosomes after FCCP treatment by confocal microscopy. These colocalization events were confirmed at high resolution by correlated electron microscopy using a nanobody against GFP fused to an EM-compatible probe APEX2 (Lam et al., 2015), which can oxidize diaminobenzidine (DAB) into an EM contrasting agent for easier identification (Figure 4.9), and subsequent tomographic analysis (Figure 4.10). The electron tomographic volumes

confirmed the presence of entire mitochondria contained within intraluminal vesicles, which themselves were inside single membrane Rab5 positive endosomes.

4.2.4 Mitochondria are Sequestered into Endosomes via ESCRT Complexes

I then wanted to investigate the mechanism by which mitochondria are sequestered by early endosomes. The endosomal ESCRT complexes, ESCRT-0, -I, -II, and –III, bind ubiquitinated cargo and pull them into the endosome through a process of invagination and scission (Campsteijn et al., 2016). Each complex is composed of a variety of proteins, and knockdown of key subunits impairs function of the whole complex (Williams and Urbe, 2007). I found colocalization between mitochondria and key proteins in the various ESCRT complexes, Hgs (ESCRT-0), Tsg101 (ESCRT-I), Snf8 (ESCRT-II) and Chmp3 (ESCRT-III) after treatment with FCCP in *Atg5*$^{-/-}$ MEFs (Figure 4.11 a). Next, we isolated the heavy membrane fraction, which is enriched in mitochondria, by density-dependent centrifugation. This confirmed a significant increase in several of these ESCRT proteins and Rab5 after FCCP treatment (Figure 4.11 b,c). Because the centrifugation force used to pellet the heavy membrane fraction is too low to spin down isolated early endosomes (Goldman et al., 1998), this suggests the ESCRT proteins and Rab5 are associated with mitochondria. We were also able to identify a mitochondrion in the process of being engulfed by an early endosome in an electron tomographic volume (Figure 4.11 d), which morphologically supports the ESCRT model of membrane invagination and subsequent scission. These data suggest that ESCRT complexes are involved in mitochondrial sequestration into endosomes.

In addition, knockdown of Hgs, Tsg101, and Snf8 proteins led to decreased mitochondrial clearance and increased cell death in response to FCCP (Figure 4.12). Damaged mitochondria, if not cleared, can cause cell death, through release of pro-death factors and excessive production of reactive oxygen species (Chen and Zweier, 2014; Kubli and Gustafsson, 2012). Thus, reduced removal of the mitochondria in cells with ESCRT protein knockdown might be contributing to the enhanced FCCP-mediated cell death. Interestingly, knockdown of Chmp3 (ESCRT-III) did not lead to reduced mitochondrial clearance or significantly enhance FCCP-mediated cell death. This may be due to incomplete knockdown of Chmp3 or compensation by other subunits in the ESCRT-III complex. These data further support the hypothesis that mitochondria are recognized and sequestered into endosomes by the ESCRT complexes.

4.2.5 Mitochondria-Containing Endosomes Mature and are Degraded

Finally, I wanted to confirm that mitochondria engulfed in Rab5-postive vesicles were delivered to lysosomes for degradation. Early endosomes mature into late endosomes before fusing with lysosomes and this maturation involves a switch from Rab5 to Rab7 (Rink et al., 2005). We found that there was a significant increase in the number of Rab7 positive endosomes and that a significant number of mitochondria colocalized with Rab7 in *Atg5*$^{-/-}$ MEFs after FCCP treatment (Figure 4.13 a-c). Late endosomes then fuse with lysosomes where the cargo is degraded. In agreement with this, we observed a significant increase in the number of LAMP2-positive lysosomes and their colocalization with mitochondria in *Atg5*$^{-/-}$ MEFs after FCCP treatment (Figure 4.13 d-f). Overall, these findings suggest that dysfunctional mitochondria are

sequestered inside early endosomes, which mature into late endosomes, and are subsequently delivered to lysosomes for degradation.

4.3 Discussion

Here, I report that damaged mitochondria are sequestered by Rab5-positive endosomes in both wild-type and *Atg5*$^{-/-}$ MEFs. Not only is this a novel role for endosomes, but it also suggests that this pathway can be utilized by WT cells with intact autophagy to clear damaged organelles. More studies are required to determine under what conditions and to what extent WT cells and tissues utilize this pathway for quality control degradation. For instance, while alternative autophagy is specifically utilized in erythrocyte maturation and iPS reprogramming (Honda et al., 2014; Ma et al., 2015), the endosomal pathway may have a specific role for mitochondrial clearance in some yet-to-be-identified process.

I also report here that the activation of the endosomal pathway is dependent on Beclin1, a known upstream regulator of both the traditional and alternative autophagy pathways (Funderburk et al., 2010). Beclin1 has also been implicated in the endosomal pathway as its binding partners UVRAG and Rubicon have been reported to interact with the early endosomal protein Eea1 (Funderburk et al., 2010). Our data further support the notion that Beclin1 is an upstream regulator of the endosomal pathway. What determines the preferential binding partners of Beclin1, and thus which downstream pathway is activated, is of interest. Not only would the answer to this question provide insight into the cellular mechanisms of protein and organelle quality control, but perhaps Beclin1's preferential binding partners can be swayed through

genetic or pharmacological intervention in order to promote or inhibit a particular downstream degradation pathway.

The experiments using Rab5Q79L, a constitutively active form of Rab5, more clearly demonstrate mitochondrial sequestration and accumulation within early endosomes. In fact, our correlated light and electron microscopy data show that several mitochondria can be found within a single endosome, even in the absence of Rab5Q79L overexpression (Figure 4.9 b,g). This further illustrates the point that endosomes are able to change in size, from the typically reported 20-50 nm (Hopkins and Trowbridge, 1983), to accommodate larger cargo such as mitochondria. Interestingly, the EM also confirms that the mitochondria are contained within single-membrane vesicles, which is in contrast to autophagy which generates a double membrane-vesicle. This further substantiates that this process is distinct from, and not another variant of, autophagy.

I also report here that ESCRT complexes are involved in the recognition and sequestration of damaged mitochondria into endosomes, and that knockdown of these complexes impairs mitochondrial clearance and increases FCCP-mediated cell death. Interestingly, it has been reported that knockdown of ESCRT complexes increases the number of autophagosomes, suggesting a connection between these two pathways (Raiborg and Stenmark, 2009). However, it appears that ESCRTs can mediate fusion between autophagosomes and lysosomes and may be involved in the final closure of the autophagosome. Thus in the absence of ESCRTs, autolysosomes cannot form. While this may explain the results in WT MEFs, it would not account for the clearance observed in autophagy-deficient MEFs. Here, the only explanation is that mitochondria

cannot be sequestered in endosomes in the absence of the ESCRT complexes. Furthermore, not only does this provide a mechanism by which endosomes can engulf mitochondria, but it fits with the earlier data in which we determined that Parkin-mediated ubiquitination is required for mitochondrial clearance. In this model, Parkin ubiquitinates damaged mitochondria, and this tag is recognized by the ESCRT complexes which results in the sequestration of mitochondria into the endosomes. Lastly, we have shown that once mitochondria are sequestered by endosomes, these vesicles mature into late endosomes and fuse with lysosomes for degradation. This confirms that the mitochondria are being eliminated through this pathway, and it is not an aberrant sequestration event with no resolution.

In conclusion, here I have provided evidence that the endosomal-lysosomal pathway is capable of sequestering and degrading damaged mitochondria in the presence of Parkin. To date, this is a novel role for the endosomal pathway. In the next chapter, I examine whether this pathway has functional significance, and whether it plays a role in cardiac myocytes. Cardiac myocytes are terminally differentiated and are sensitive to mitochondria-induced cell death (Kubli and Gustafsson, 2012). Thus, it is likely that these cells employ a variety of quality control mechanisms to ensure the health of the mitochondrial network.

Parts of Chapter 4 were originally published in *Nature Communications*. Hammerling, B. C., Najor, R. H., Cortez, M. Q., Shires, S. E., Leon, L. J., Gonzalez, E. R., Boassa, D., Phan, S., Thor, A., Jimenez, R. E., Li, H., Kitsis, R. N., Dorn II, G. W., Sadoshima, J., Ellisman, M. H., Gustafsson, A. G. A Rab5 Endosomal Pathway

Mediates Parkin-Dependent Mitochondrial Clearance. *Nature Communications*. 8: 14050, 2017; doi:10.1038/ncomms14050 © 2017 Nature Publishing Group. The dissertation author was the primary investigator and author of this paper.

Parts of Chapter 4 were originally published in *Small GTPases*. Hammerling, B. C., Shires, S. E., Leon, L. J., Cortez, M. Q., Gustafsson, A. G. Isolation of Rab5-Positive Endosomes Reveals a New Mitochondrial Degradation Pathway Utilized by BINP3 and Parkin. *Small GTPases*. 1-8, 2017; doi: doi:10.1080/21541248.2017.1342749. © 2017 Taylor & Francis Online. The dissertation author was the primary investigator and author of this paper.

Figure 4.1. Depolarized mitochondria are sequestered in Rab5-positive early endosomes in WT and *Atg5*$^{-/-}$ MEFs.
(a,b) Representative images of WT **(a)** and *Atg5*$^{-/-}$ **(b)** MEFs overexpressing GFP-Rab5, myc-Parkin, and stained with anti-COX IV to label mitochondria. Arrowheads show colocalizing puncta. Scale bars=20 µm. **(c,d)** Quantification of GFP-Rab5 positive puncta **(c)** and their colocalization **(d)** with COX IV labeled mitochondria in WT cells in response to 25 µM FCCP (n=45 cells scored for number of puncta in 3 independent experiments, *p<0.05,**p<0.01 vs 0 h). **(e,f)** Quantification of GFP-Rab5 positive puncta **(e)** and their colocalization **(f)** with COX IV labeled mitochondria in *Atg5*$^{-/-}$ cells in response to 25 µM FCCP (n=45 cells scored for number of puncta in 3 independent experiments, *p<0.05, **p<0.01, ***p<0.001 vs 0 h). **(g)** Representative images of WT and *Atg5*$^{-/-}$ MEFs transfected with GFP-Rab5 and HA-Parkin, treated with DMSO or 25 µM FCCP for 4 h, and stained with MitoTracker Red CMXRos (MT Red). After treatment, cells were fixed and stained with anti-Tom20. Scale bars=20 µm. Arrowheads show colocalizing puncta. **(h)** Quantification of cell death. WT or *Atg5*$^{-/-}$ cells overexpressing mCherry-Parkin were exposed to FCCP (25 µM) for 0, 4, or 8 h and stained with Yo-Pro-1 (n=100 cells screened for cell death in 3 independent experiments). Nuclei were counterstained with Hoechst 33342 (blue). All values are means±s.e.m from independent experiments. Statistical significance was calculated using ANOVA followed by Dunnett's test for multiple comparison.

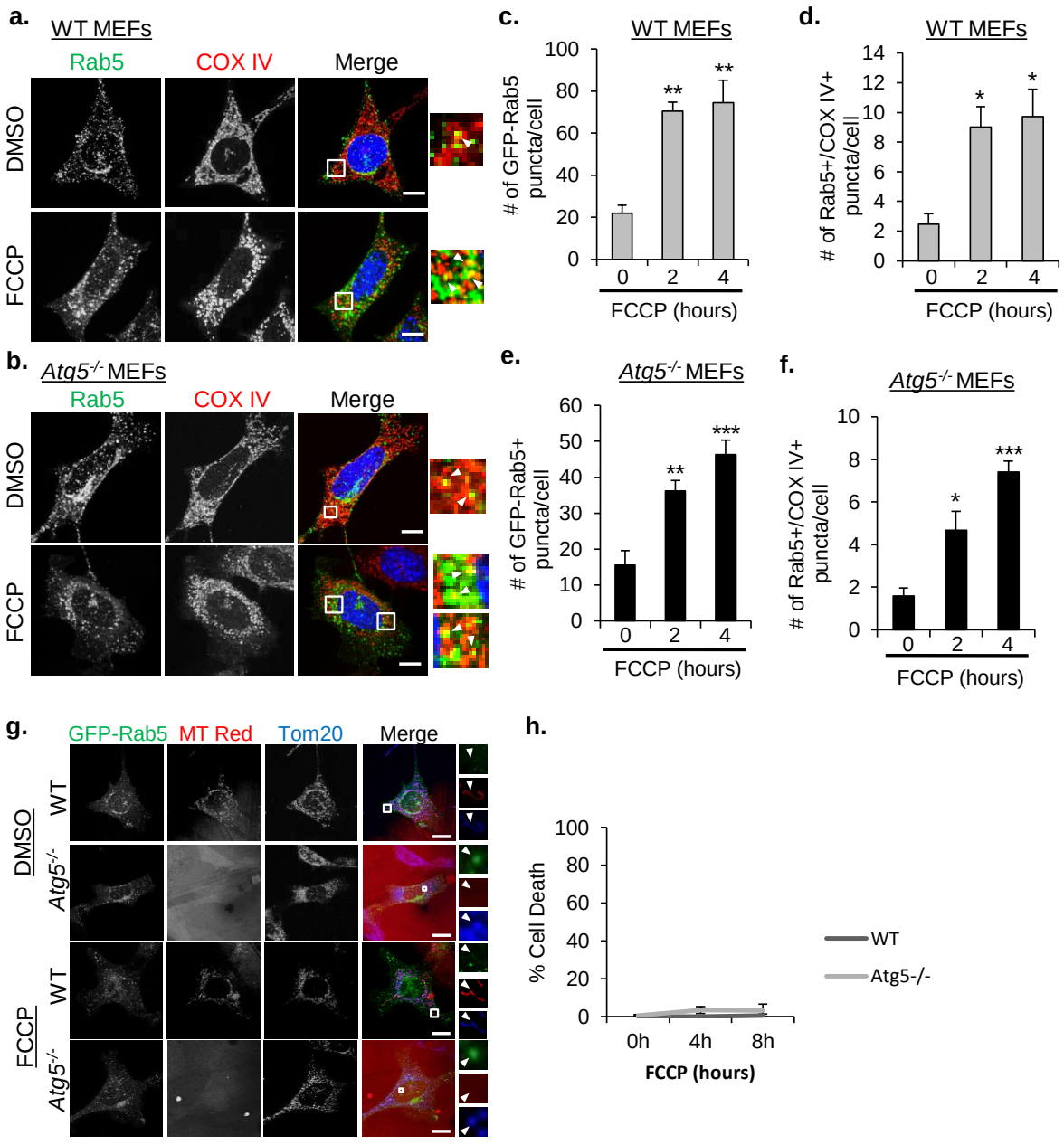
a.
WT MEFs
Rab5
COX IV
Merge
DMSO
FCCP
b.
Atg5-/- MEFs
c.
WT MEFs
# of GFP-Rab5 puncta/cell
FCCP (hours)
d.
WT MEFs
# of Rab5+/COX IV+ puncta/cell
FCCP (hours)
e.
Atg5-/- MEFs
# of GFP-Rab5+ puncta/cell
FCCP (hours)
f.
Atg5-/- MEFs
# of Rab5+/COX IV+ puncta/cell
FCCP (hours)
g.
GFP-Rab5
MT Red
Tom20
Merge
DMSO
FCCP
WT
Atg5-/-
h.
% Cell Death
FCCP (hours)
WT
Atg5-/-

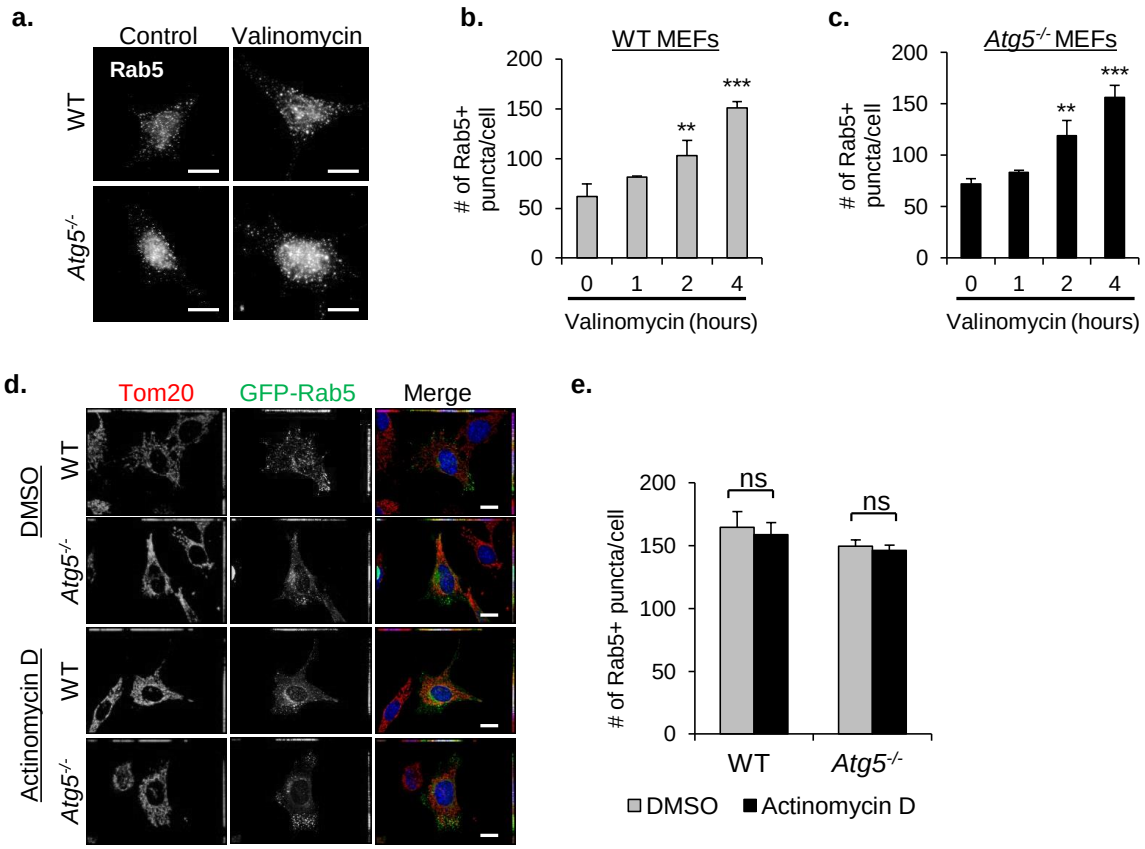

Figure 4.2. Rab5 is activated by mitochondrial depolarization, but not DNA damage.

(a) Representative images of WT and *Atg5*$^{-/-}$ MEFs infected with mCherry-Parkin and treated with DMSO or 10 μM valinomycin for 4 h. After treatment, cells were fixed and stained with anti-Rab5. Scale bars=20 μm. **(b,c)** Quantification of Rab5-positive vesicles in WT **(b)** and *Atg5*$^{-/-}$ **(c)** cells (n=30 cells scored for number of puncta in 3 independent experiments, **p<0.01, ***p<0.001). Nuclei were counterstained with Hoechst 33342 (blue). All values are means±s.e.m from independent experiments. Statistical significance was calculated using ANOVA followed by Dunnett's test for multiple comparison.

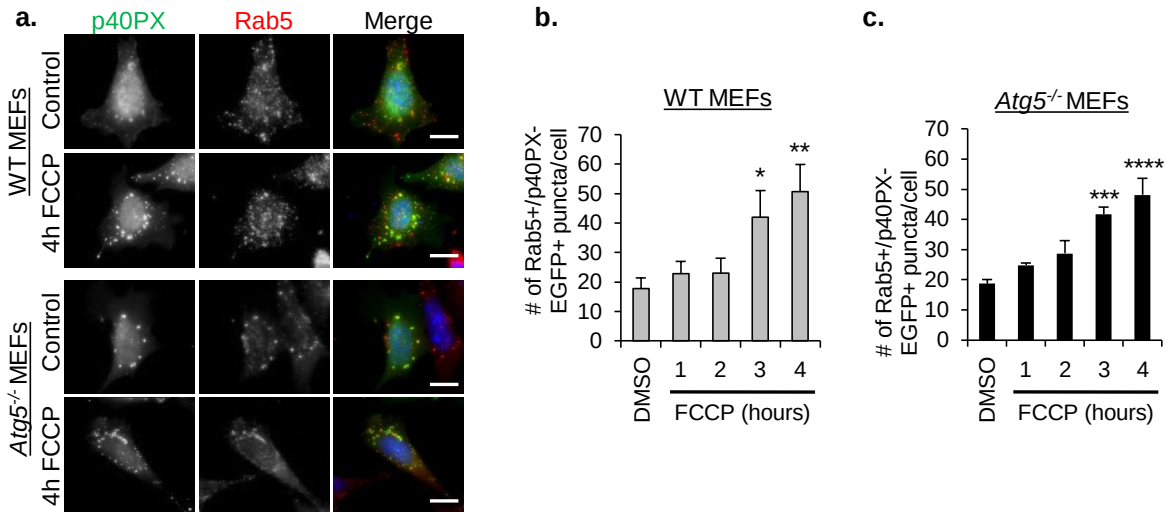

Figure 4.3. Rab5 colocalizes with active Vps34 in WT and *Atg5*$^{-/-}$ MEFs with FCCP. **(a)** Representative images of WT and *Atg5*$^{-/-}$ MEFs overexpressing p40PX-EGFP after DMSO or FCCP treatment (25 µM). Cells were stained with anti-Rab5 to label early endosomes. Scale bars=20 µm. **(b,c)** Quantification of puncta positive for p40PX-EGFP and Rab5 in WT (**b**, n=40 cells scored for number of puncta in 4 independent experiments, *p<0.05, **p<0.01, ***p<0.001, ****p<0.0001 vs DMSO) and *Atg5*$^{-/-}$ (**c**, n=40 cells scored for number of puncta in 3 independent experiments, *p<0.05 vs DMSO) cells. Nuclei were counterstained with Hoechst 33342 (blue). All values are means±s.e.m from independent experiments. Statistical significance was calculated using ANOVA followed by Dunnett's test for multiple comparison.

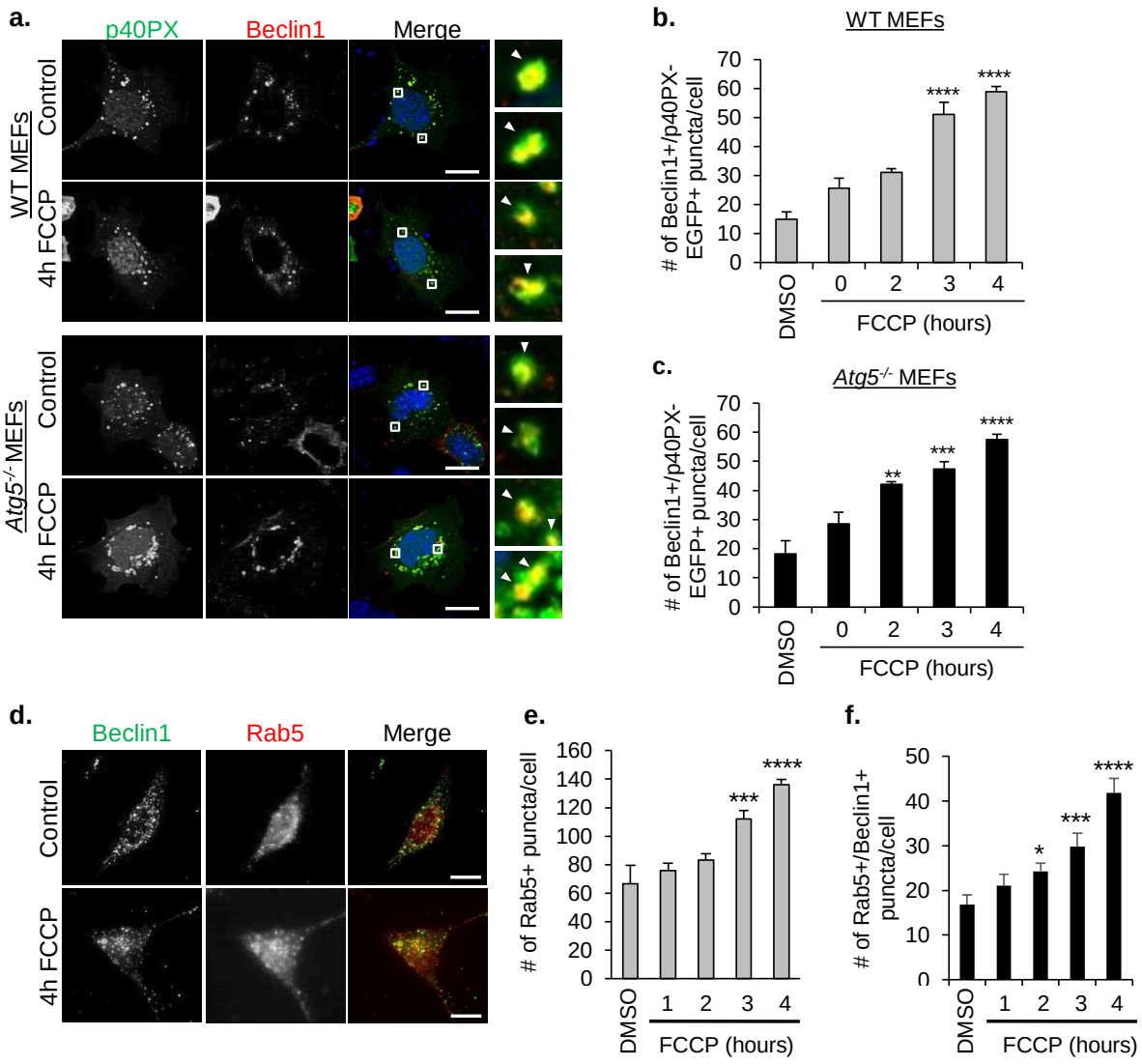

Figure 4.4. Beclin1 colocalizes with active Vps34 in WT and *Atg5*$^{-/-}$ MEFs after FCCP treatment.

(a) Representative images of WT and *Atg5*$^{-/-}$ MEFs overexpressing p40PX-EGFP, and HA-Beclin1. Cells were treated with DMSO or FCCP (25 µM) for 4 h. Arrowheads show colocalizing puncta. Scale bars=20 µm. **(b,c)** Quantification of puncta positive for p40PX-EGFP and HA-Beclin1 in WT **(b)** and *Atg5*$^{-/-}$ **(c)** cells (n=40 cells scored for number of puncta in 4 independent experiments, **p<0.01, ***p<0.001, ****p<0.0001 vs 0 h). **(d)** Representative images for *Atg5*$^{-/-}$ MEFs expressing HA-Beclin1, treated with DMSO or 25 µM FCCP and stained with anti-HA and anti-Rab5. Scale bars=20 µm. **(e,f)** Quantification of Rab5 positive puncta **(e)** and their colocalization **(f)** with Beclin1 in response to treatment (n=35 cells scored for number of puncta in 4 independent experiments, *p<0.05, ***p<0.001, ****p<0.0001 vs DMSO). Nuclei were counterstained with Hoechst 33342 (blue). All values are means±s.e.m from independent experiments. Statistical significance was calculated using ANOVA followed by Dunnett's test for multiple comparison.

Figure 4.5. Knockdown of Beclin1 impairs mitochondrial clearance.
(a) Western blot for Beclin1 and Actin in *Atg5*$^{-/-}$ MEFs transfected with 20 or 40 nM Beclin1 siRNA for 96 h. **(b)** Representative images of Parkin-expressing *Atg5*$^{-/-}$ MEFs transfected with control or Beclin1 siRNA, treated with DMSO or FCCP (25 µM) for 4 h. Fixed cells were stained with anti-Rab5 and anti-COX IV. Scale bars=20 µm. **(c,d)** Quantification of Rab5 positive puncta **(c)** and their colocalization **(d)** with COX IV labeled mitochondria in untransfected (un), control (con), or 20 nM Beclin1 siRNA transfected *Atg5*$^{-/-}$ cells expressing Parkin in response to DMSO or 25 µM FCCP (n=30 cells scored for number of puncta in 4 independent experiments, ***p<0.001). Nuclei were counterstained with Hoechst 33342 (blue). All values are means±s.e.m from independent experiments. Statistical significance was calculated using ANOVA followed by Dunnett's test for multiple comparison.

a.

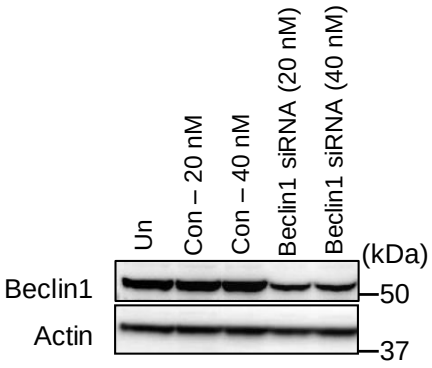
Un
Con – 20 nM
Con – 40 nM
Beclin1 siRNA (20 nM)
Beclin1 siRNA (40 nM)
(kDa)
Beclin1
Actin
50
37

b.

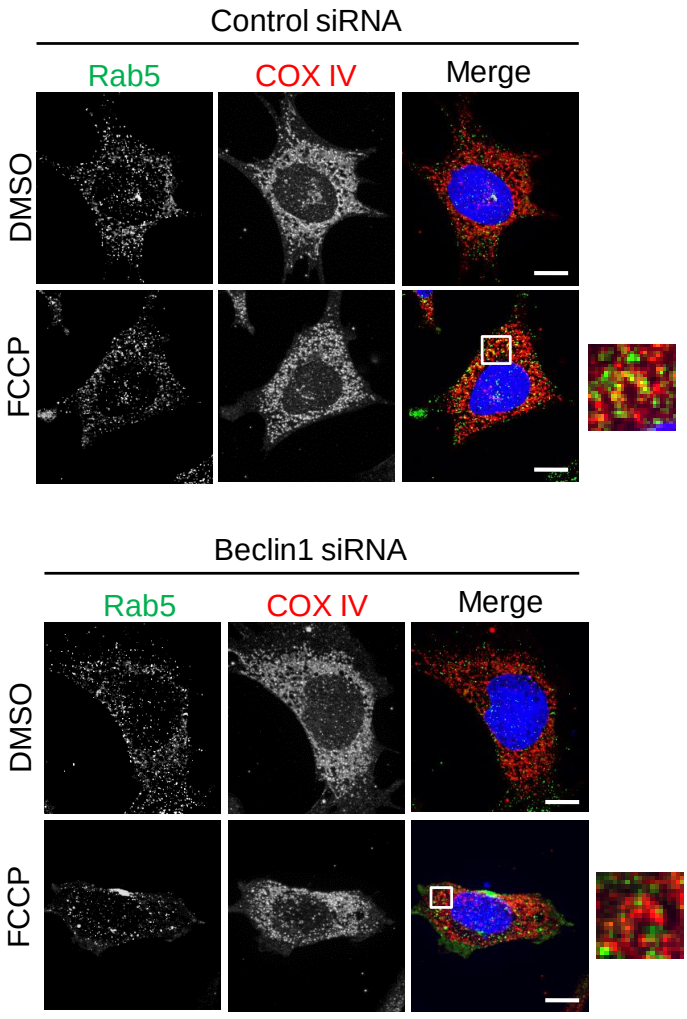
Control siRNA
Rab5
COX IV
Merge
DMSO
FCCP
Beclin1 siRNA
Rab5
COX IV
Merge
DMSO
FCCP

c.

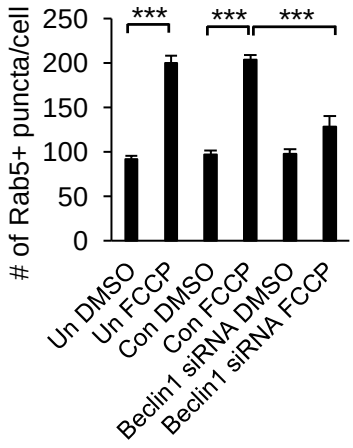
# of Rab5+ puncta/cell
250
200
150
100
50
0
***
***
***
Un DMSO
Un FCCP
Con DMSO
Con FCCP
Beclin1 siRNA DMSO
Beclin1 siRNA FCCP

d.

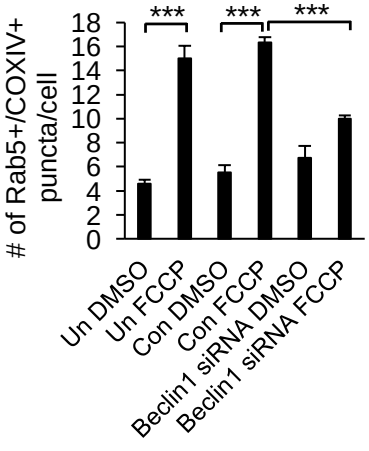
# of Rab5+/COXIV+ puncta/cell
18
16
14
12
10
8
6
4
2
0
***
***
***
Un DMSO
Un FCCP
Con DMSO
Con FCCP
Beclin1 siRNA DMSO
Beclin1 siRNA FCCP

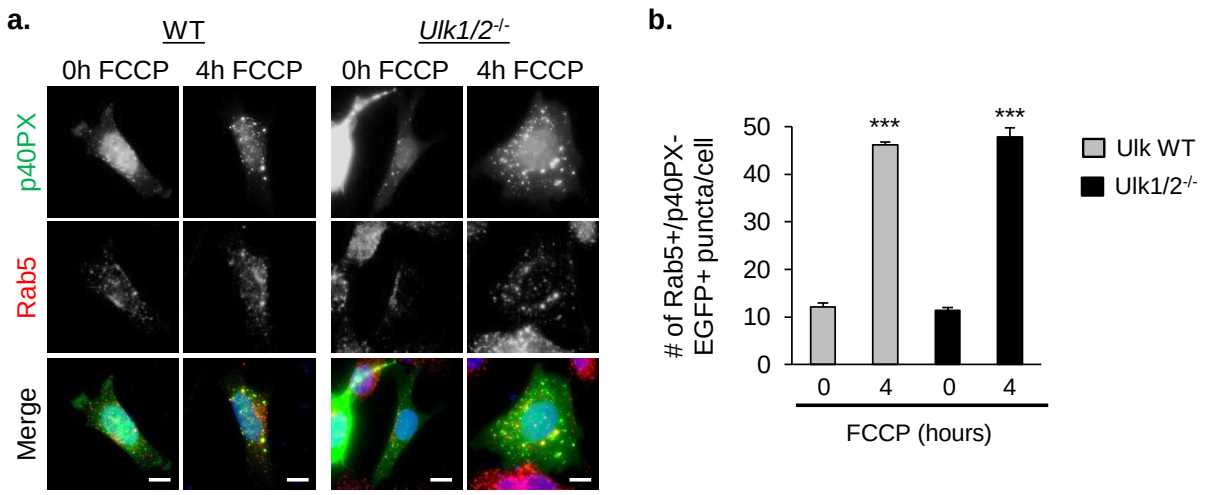

Figure 4.6. Ulk1/2-deficiency has no effect on early endosomal activity in response to FCCP treatment.
(a) Representative images of WT or *Ulk1/2*$^{-/-}$ transfected with p40PX-EGFP and treated with 25 µM FCCP for 0 or 4 h. After treatment, cells were fixed and stained with anti-Rab5. Scale bars=20 µm. **(b)** Quantification of colocalization between Rab5 and p40PX-EGFP positive puncta (n=30 cells scored for number of puncta in 3 independent experiments, ***p<0.001). Nuclei were counterstained with Hoechst 33342 (blue). All values are means±s.e.m from independent experiments. Statistical significance was calculated using ANOVA followed by Dunnett's test for multiple comparison.

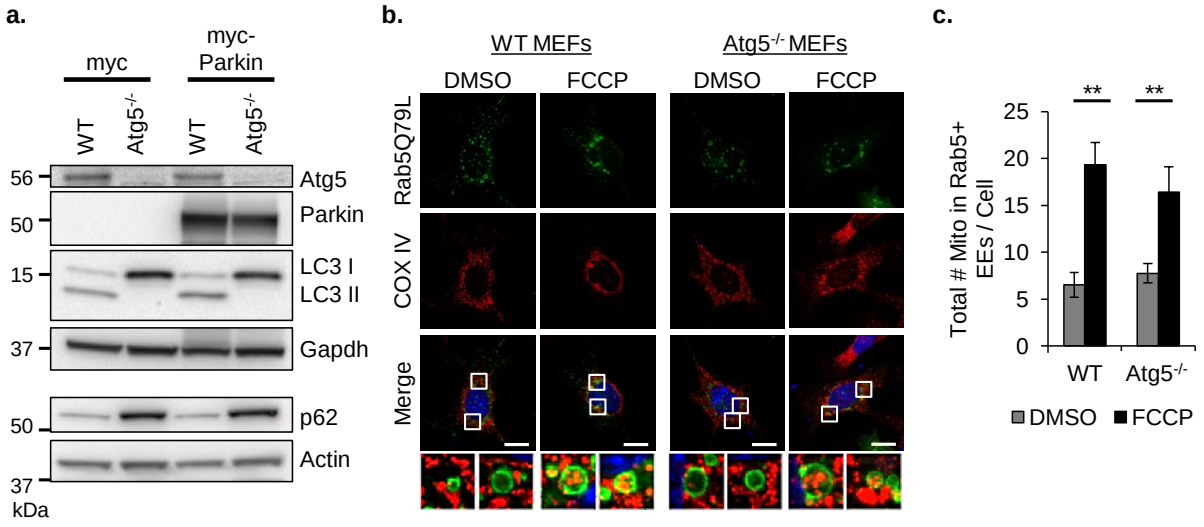

Figure 4.7. Mitochondria accumulate in enlarged Rab5Q79L-positive early endosomes.

(a) Western blot for Atg5, Parkin, LC3, and p62 levels in WT and *Atg5*$^{-/-}$ MEFs overexpressing myc or myc-Parkin. **(b)** Representative images of WT and *Atg5*$^{-/-}$ MEFs overexpressing GFP-Rab5Q79L plus myc-Parkin. Cells were treated with DMSO or 25 μM FCCP for 4 h, and then fixed and stained with anti-COX IV to visualize mitochondria. Nuclei were counterstained with Hoechst 33342 (blue). Scale bars=20 μm. **(c)** Quantification of mitochondria inside GFP-Rab5Q79L positive vesicles (n=3, **p<0.01 vs DMSO). EE=enlarged endosomes. Nuclei were counterstained with Hoechst 33342 (blue). All values are means±s.e.m from independent experiments. Statistical significance was calculated using ANOVA followed by Dunnett's test for multiple comparison.

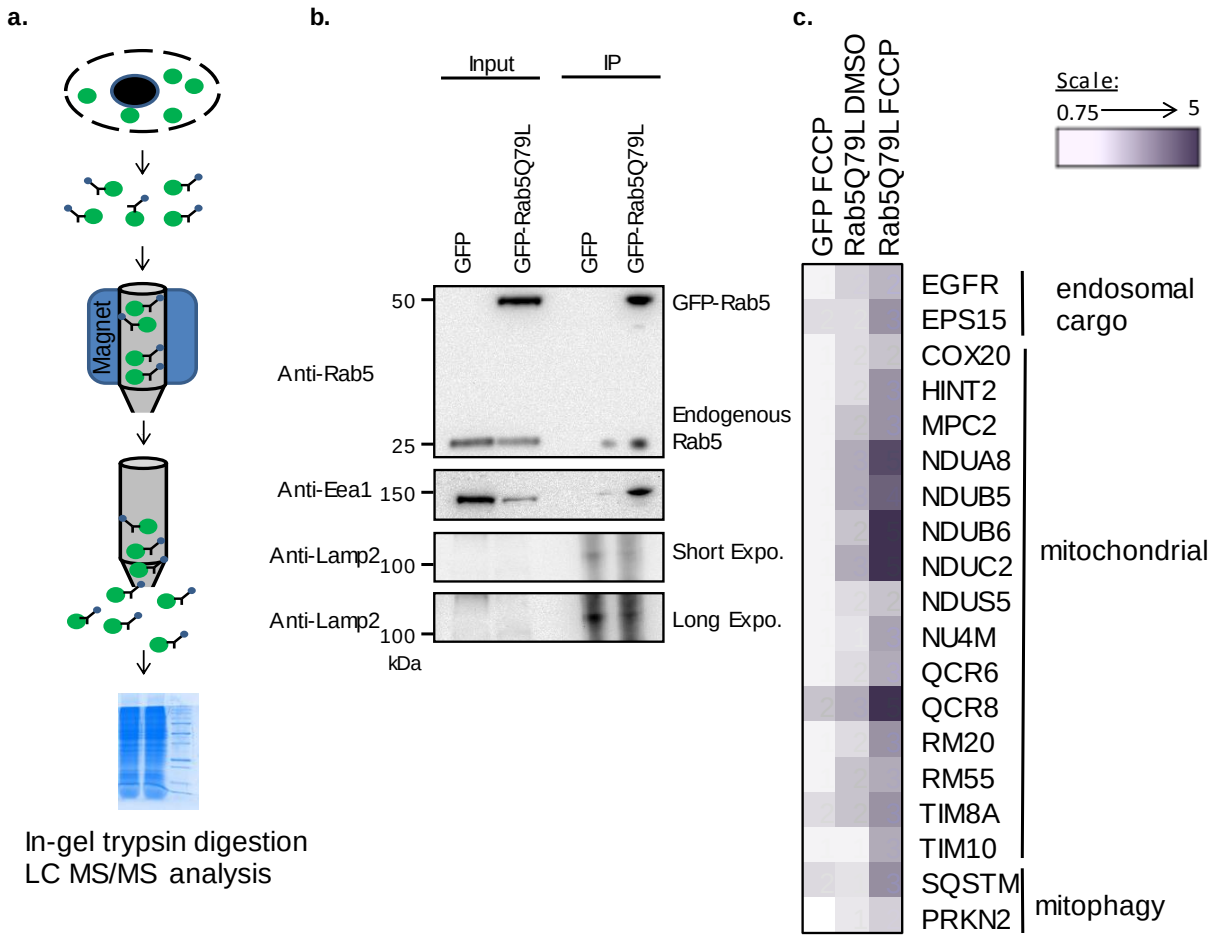

Figure 4.8. Pulldown of Rab5Q79L-positive endosomes enriches for mitochondrial markers.
(a) Scheme for isolation of GFP-labeled vesicles. **(b)** Immunoprecipitation (IP) of GFP (GFP) or GFP-Rab5Q79L (Rab5) with anti-GFP coupled to magnetic beads confirms enrichment for GFP-Rab5Q79L as well as endogenous Rab5. Pulldown also enriches for the early endosome marker Eea1. The lysosomal protein Lamp2 was undetectable unless blot was subjected to a long (10 min) exposure. **(c)** Heatmap of proteins from endosome isolation identified by mass spectrometry. Values were generated using a ratio of each sample to the GFP DMSO control. Scale is in fold change over GFP DMSO control.

Figure 4.9. Mitochondria are found inside Rab5-positive early endosomes by correlated light and electron microscopy.
(a) Confocal microscopy of WT **(a)** and *Atg5*$^{-/-}$ **(b)** MEFs transfected with GFP-Rab5, VHH-APEX2, mPlum-mito3, and HA-Parkin and treated with DMSO or FCCP (25 µM) for 4 h. Scale bars=20 µm. Overlay of confocal inset with electron microscopy of the same cell. Confocal images and electron micrographs of colocalizing puncta (boxes) are shown enlarged and indicated with arrowheads. Note: first inset in **(a)** is found adjacent to the nuclear envelope, but within the cytosol. Scale bar=200 nm. **(c-j)** Arrowheads mark instances of colocalization between mPlum-mito tagged mitochondria (red) and GFP-Rab5 endosomes (green) in WT **(c-f)** and *Atg5*$^{-/-}$ **(g-j)** MEFs after FCCP (25 µM, 4 h) treatment (colored images). Correlated electron microscopy of these puncta show mitochondria inside the lumen of single-membrane vesicles. EM Scale bars= 200 nm.

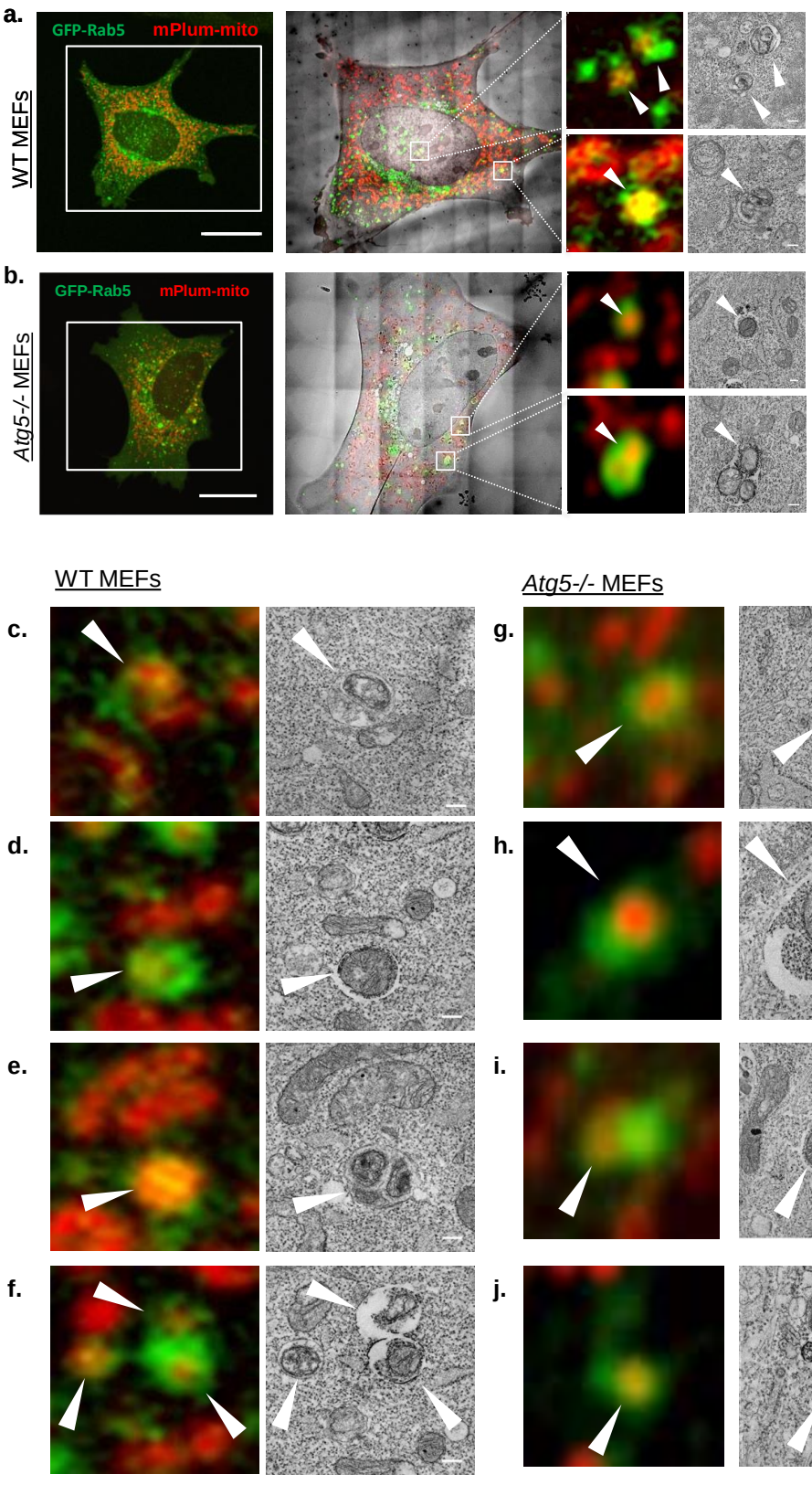
a.
GFP-Rab5
mPlum-mito
WT MEFs
b.
GFP-Rab5
mPlum-mito
Atg5-/- MEFs
WT MEFs
Atg5-/- MEFs
c.
d.
e.
f.
g.
h.
i.
j.

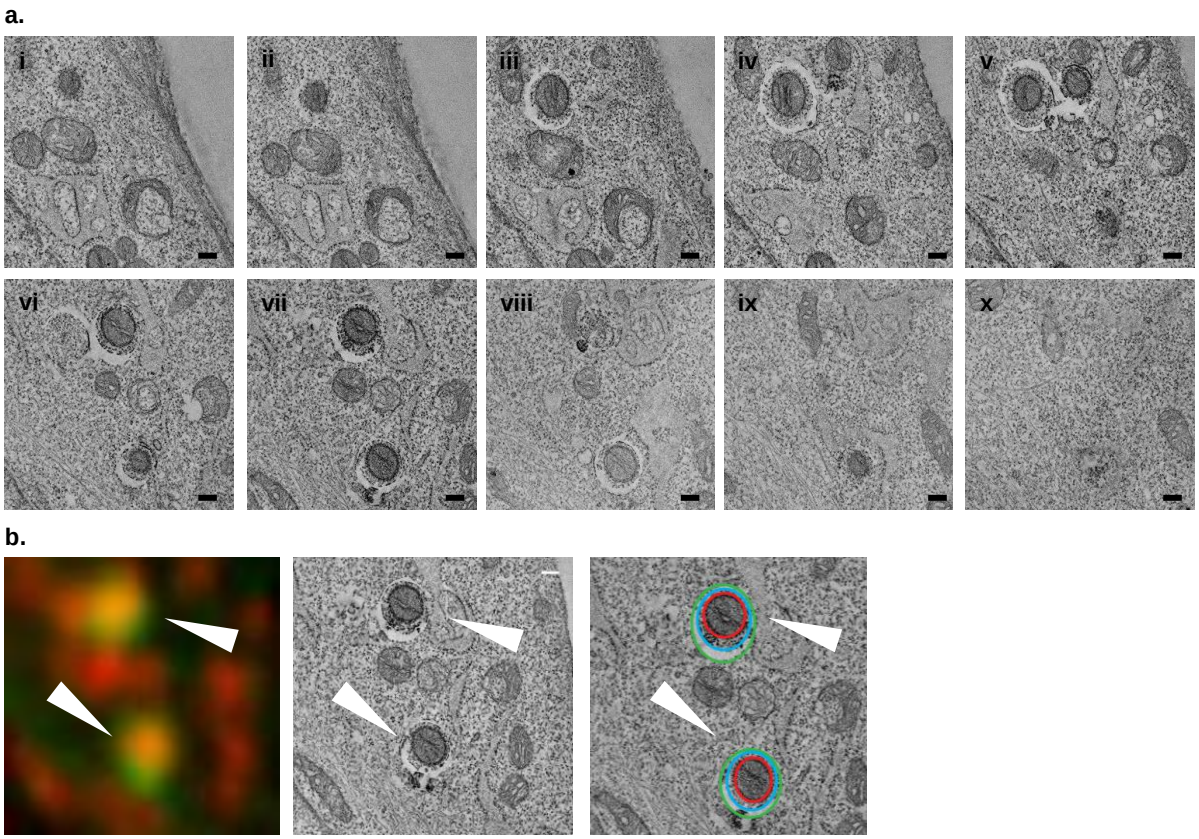

Figure 4.10. Tomographic Analysis Confirms Mitochondria Within Early Endosomes.

(a) Serial panels of tomographic analysis shows three mitochondria within early endosomes, surrounded by cytoplasmic material. **(b)** The identity of the mitochondria and the endosomes were confirmed by correlated confocal microscopy. Red= outline of mitochondria, blue= outline of engulfed cytoplasm surrounding the mitochondria, green= outline of the early endosome. Scale bars= 200 nm.

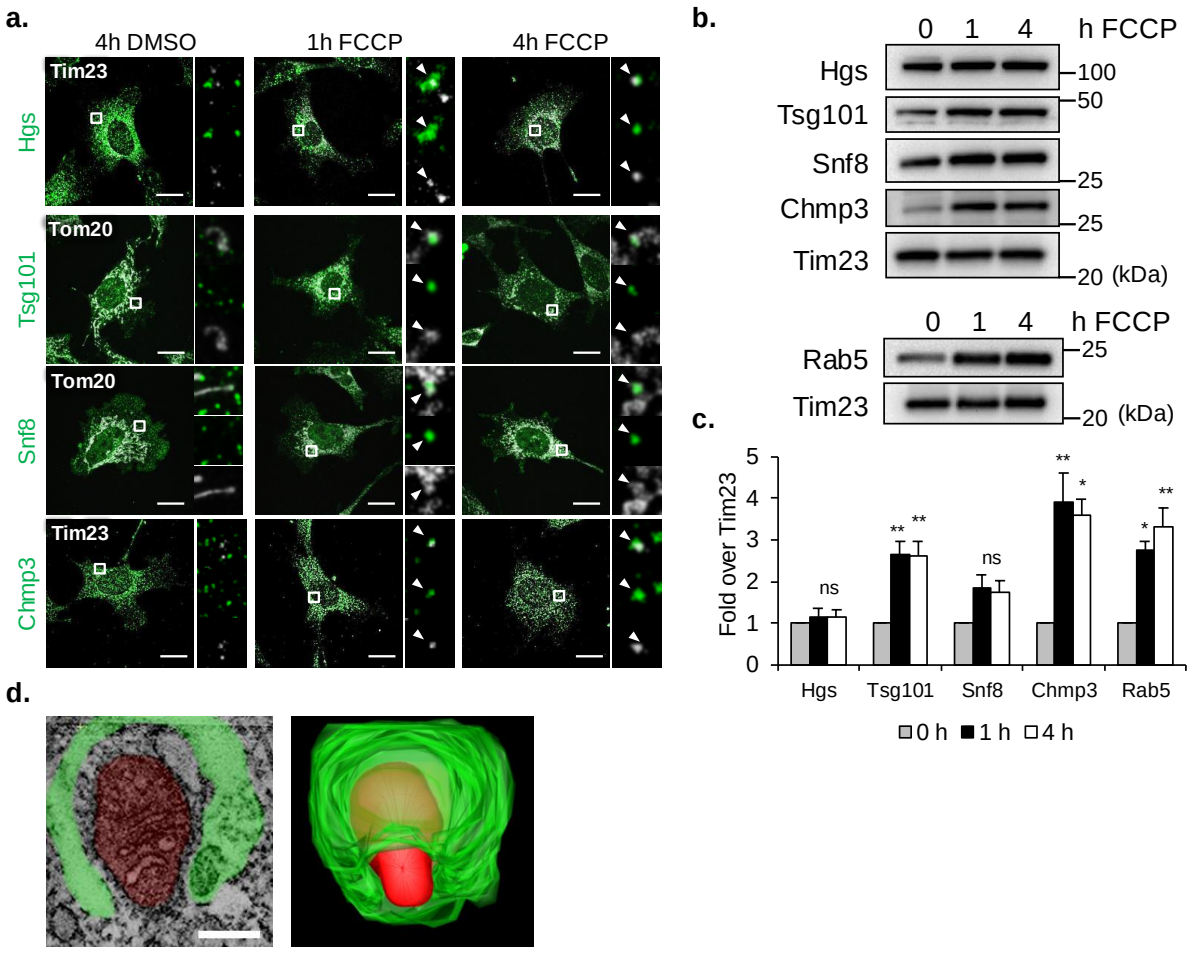

Figure 4.11. ESCRT complexes participate in sequestration of mitochondria.
(a) Confocal maximal image projections of *Atg5*$^{-/-}$ MEFs infected with mCherry-Parkin and treated with DMSO or 25 µM FCCP for the indicated time. Cells were stained with anti-Tim23 or anti-Tom20 (white) to label mitochondria, and for the indicated ESCRT protein (green). Enlarged boxes are single optical slices with arrowheads showing colocalization. Scale bars=20 µm. **(b)** Representative Western blot of isolation of the mitochondrial enriched heavy membrane fraction after 0, 1, or 4 h of 25 µM FCCP treatment in *Atg5*$^{-/-}$ MEFs overexpressing Parkin. Tim23 is shown as a mitochondrial loading control. **(c)** Band densitometry of protein levels from panel **b** (n=3, *p<0.05, **p<0.01, ns= not significant vs 0 h FCCP). **(d)** Single slice of an electron tomogram showing mitochondria (red) partially sequestered by an early endosome (green) in *Atg5*$^{-/-}$ MEFs (left). Scale bar = 200 nm. 3D reconstructed model of mitochondria (red) and endosome (green, right). All values are means±s.e.m from independent experiments. Statistical significance was calculated using ANOVA followed by Dunnett's test for multiple comparison.

Figure 4.12. Confirmation of ESCRT knockdown and the effect on mitochondria clearance.

(a) Western blots confirming siRNA knockdown of Hgs, Tsg101, Snf8, and Chmp3 by siRNA after 96 h. Un= untransfected, con= control siRNA transfected. **(b)** Images showing mitochondrial clearance after ESCRT protein knockdown. After ESCRT protein knockdown, *Atg5*$^{-/-}$ cells were infected with mCherry-Parkin, and treated with DMSO or 25 µM FCCP for 12 h. Fixed cells were stained with anti-Tom20 to label mitochondria. **(c)** Quantification of cell death. *Atg5*$^{-/-}$ MEFs were exposed to DMSO or FCCP (25 µM) for 24 h after siRNA knockdown and then stained with Po-Pro-3. (n= 200 screened for cell death in 3 independent experiments, *p<0.05, **p<0.01, ***p<0.001 ns= not significant). Nuclei were counterstained with Hoechst 33342 (blue). Arrowheads indicate individual cells. Scale bars=20 µm. All values are means±s.e.m from independent experiments. Statistical significance was calculated using ANOVA followed by Dunnett's test for multiple comparison.

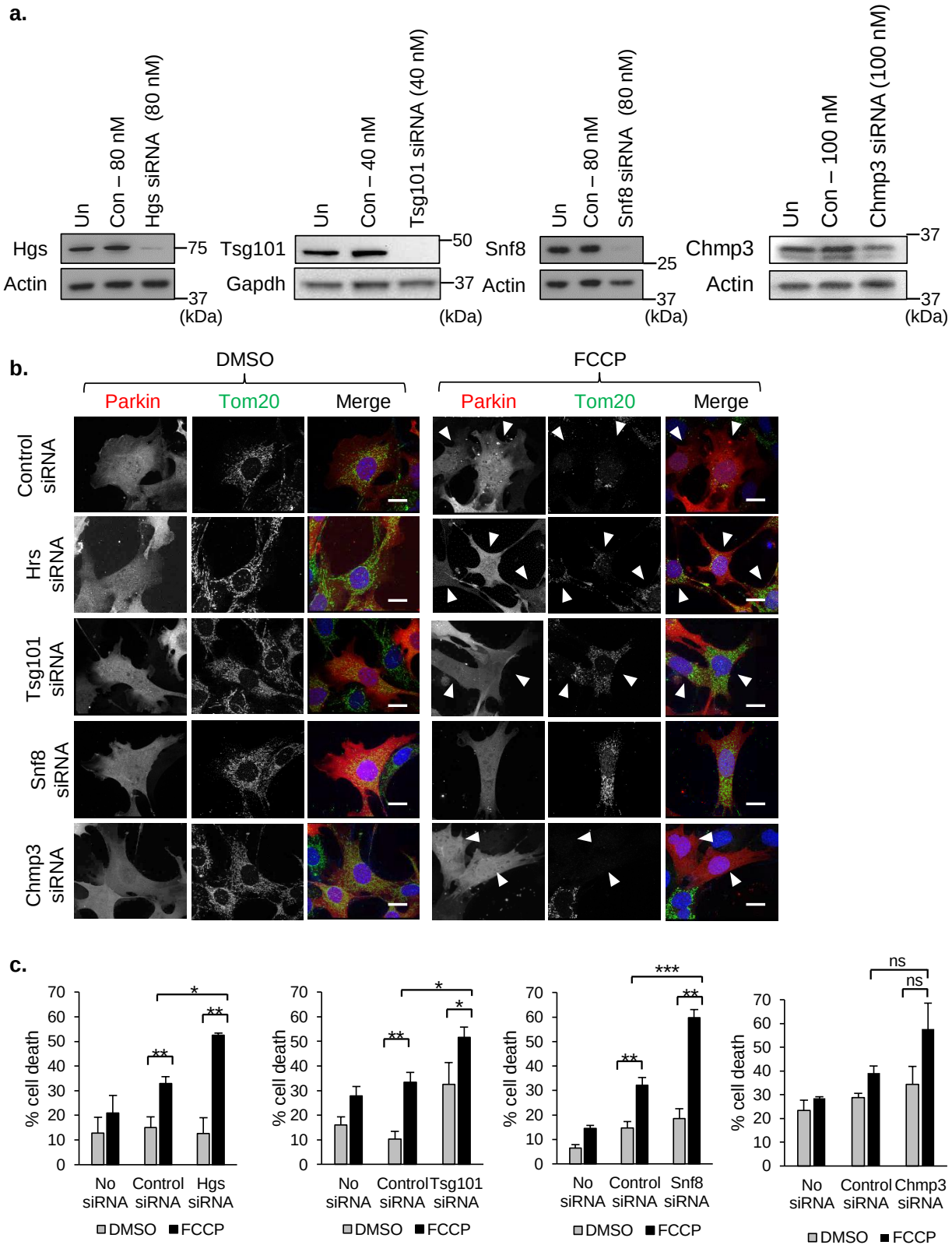
a.
Un
Con – 80 nM
Hgs siRNA (80 nM)
Hgs
Actin
75
37
(kDa)
Un
Con – 40 nM
Tsg101 siRNA (40 nM)
Tsg101
Gapdh
50
37
(kDa)
Un
Con – 80 nM
Snf8 siRNA (80 nM)
Snf8
Actin
25
37
(kDa)
Un
Con – 100 nM
Chmp3 siRNA (100 nM)
Chmp3
Actin
37
37
(kDa)
b.
DMSO
FCCP
Parkin
Tom20
Merge
Control siRNA
Hrs siRNA
Tsg101 siRNA
Snf8 siRNA
Chmp3 siRNA
c.
% cell death
No siRNA
Control siRNA
Hgs siRNA
Tsg101 siRNA
Snf8 siRNA
Chmp3 siRNA
DMSO
FCCP
ns

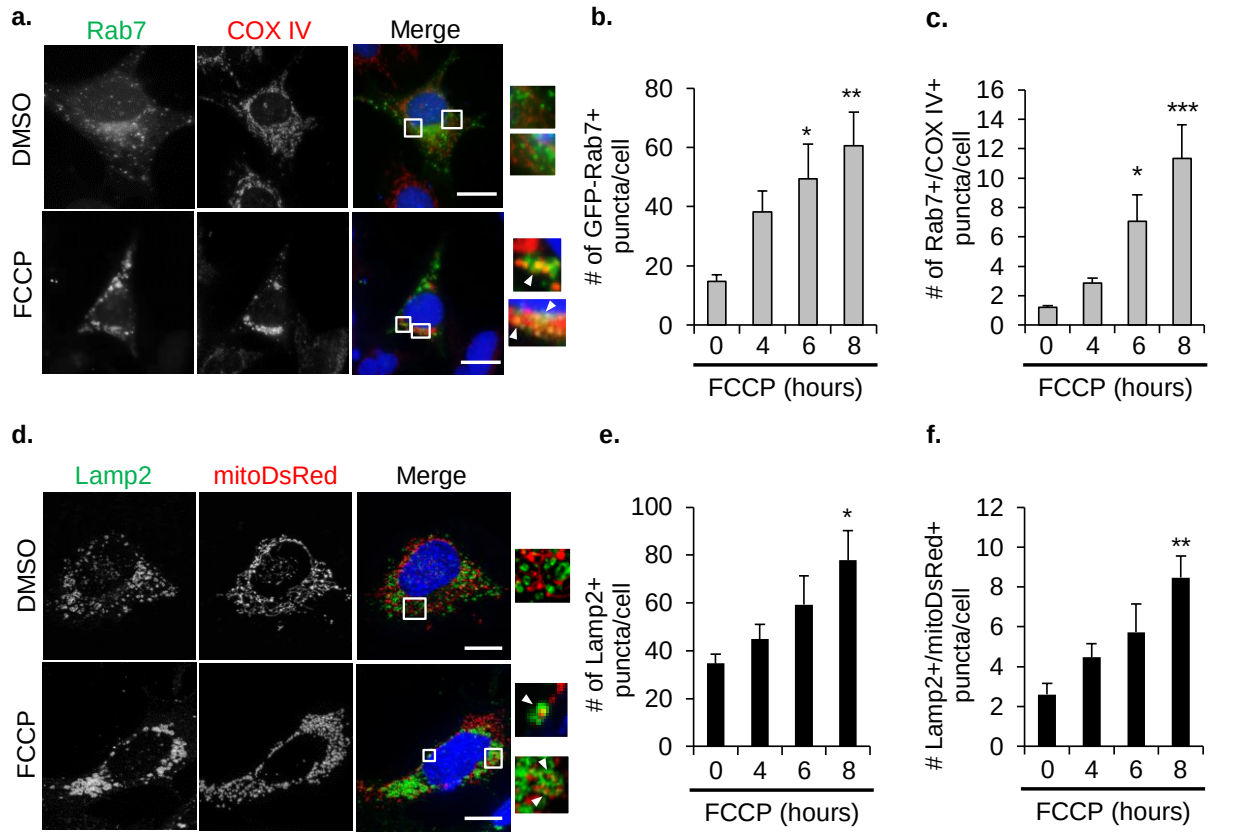

Figure 4.13. Mitochondria in late endosomes are delivered to lysosomes.
(a) Representative images of *Atg5*$^{-/-}$ MEFs overexpressing GFP-Rab7, HA-Parkin, and stained with anti-COX IV to label mitochondria. Arrowheads show colocalizing puncta. Scale bars=20 µm. **(b,c)** Quantification of GFP-Rab7 positive puncta **(b)** and their colocalization **(c)** with COX IV labeled mitochondria in *Atg5*$^{-/-}$ MEFs in response to 25 µM FCCP (n=45 cells scored for number of puncta in 3 independent experiments, *p<0.05,**p<0.01, ***p<0.001 vs 0 h). **(d)** Representative images of cells overexpressing MitoDsRed, HA-Parkin and stained with anti-Lamp2 to label lysosomes. Arrowheads show colocalizing puncta. Scale bars=20 µm. **(e,f)** Quantification of Lamp2 positive puncta **(e)** and their colocalization **(f)** with MitoDsRed in *Atg5*$^{-/-}$ MEFs in response to 25 µM FCCP (n=40 cells scored for number of puncta in 3 independent experiments, *p<0.05,**p<0.01 vs 0 h). Nuclei were counterstained with Hoechst 33342 (blue). All values are means±s.e.m from independent experiments. Statistical significance was calculated using ANOVA followed by Dunnett's test for multiple comparison.

CHAPTER 5: REMOVAL OF MITOCHONDRIA VIA THE ENDOSOMAL PATHWAY PROTECTS AGAINST CELL DEATH

5.1 Introduction

As a response to stress, autophagy is activated fairly rapidly, and autophagic degradation is initiated in MEFs on the order of a few hours (Figure 3.1) (Narendra et al., 2008). However, this is limited by the fact that autophagosomes need to be generated *de novo* once there is demand. For instance, in PINK1/Parkin-mediated mitophagy, LC3-II-positive autophagosomes can be observed anywhere between 1 to 9 hours after CCCP or FCCP treatment, depending on the cell type (Figure 3.1) (Hollville et al., 2014; Narendra et al., 2008). This is followed by mitochondrial clearance via mitophagy anywhere between 12 to 48 hours (Figures 3.2, 3.3) (Hollville et al., 2014; Narendra et al., 2008). In contrast to autophagosomes, an entire network of endosomes is present in the cell at any given moment. In addition, the identity and function of an individual endosome can be rapidly altered by the exchange of particular Rab proteins on the endosomal surface (Stenmark, 2009). For example, a Rab5-positive early endosome can become a fast recycling endosome by the gain of Rab4. In regards to degradation capacity and speed, endosomes are responsible for the internalization and degradation of EGFR, and this undergoes measurable degradation within 1 to 2 hours (Sigismund et al., 2008). Thus, endosomes could potentially be redirected for quicker organelle clearance, before autophagosomes can be formed.

If damaged mitochondria are not rapidly cleared, they can cause an increase in cell death through the release of pro-death factors and excessive reactive oxygen

species (Honda et al., 2005; Kubli and Gustafsson, 2012). Thus, their clearance from the cell is critical. Myocytes within the heart are terminally differentiated, thus the loss of any one results in a permanent loss in cardiac function (Anversa et al., 2002). Furthermore, these myocytes also contain 30% mitochondria by volume, which means that there are many mitochondria which can produce ROS and release pro-death factors if damaged (Piquereau et al., 2013a). Also, the heart unlike MEFs, expresses endogenous Parkin and is heavily reliant on oxidative phosphorylation. Thus, impairment of efficient clearance of damaged mitochondria is detrimental to heart function (Kubli et al., 2013b). Given the importance of mitochondrial quality control in the heart, it is likely that there are multiple pathways that can compensate for one another in addition to mitophagy. In this chapter, I study the timing of activation of the endosomal pathway as well as determine this pathway's functional role in cardiac myocytes and the heart.

5.2 Results

5.2.1 Early Endosome Pathway is Activated Before Autophagy

Autophagy is triggered by cellular stress and takes a few hours to be in full effect (Bampton et al., 2005). We wanted to examine whether the activation of the autophagy and endosomal pathways was simultaneous or sequential in WT cells. In order to test this, we overexpressed GFP-LC3 and stained for Rab5, to monitor the formation of autophagosomes and early endosomes respectively, in WT MEFs which have both pathways intact. Interestingly, we observed a rapid, but transient, increase in the number of Rab5-positive endosomes in response to FCCP treatment, which peaked at

4 hours post FCCP treatment and then declined. In contrast, the number of autophagosomes increased progressively but more slowly over time (Figure 5.1). This indicates that the endosomal pathway might be activated as a first response in order to clear damaged mitochondria.

5.2.2 Endosomal Removal of Mitochondria Reduces Cell Death

Next we wanted to explore the functional importance of the endosomal degradation pathway, and what effects resulted if this pathway is inhibited. First, we utilized 3-MA and Bafilomycin A1 to pharmacologically inhibit the endosomal-lysosomal pathway. 3-MA is a PI3K inhibitor that inhibits Vps34 and disrupts formation of both endosomes and autophagosomes (Hirosako et al., 2004). Bafilomycin A1 is an inhibitor of the vacuolar proton ATPase in cells, which prevents vesicular fusion of both endosomes and autophagosomes with lysosomes (Drose and Altendorf, 1997). We found that inhibition of Vps34 by 3-MA or disrupting acidification of endosomes and lysosomes with Bafilomycin A1 led to increased cell death at baseline conditions (Figure 5.2 a-d). Interestingly, once paired with FCCP, 3-MA and Bafilomycin A1 both further increased susceptibility to cell death in WT and *Atg5*$^{-/-}$ MEFs (Figure 5.2 a-d). This suggests that mitochondrial depolarization coupled with inhibition of multiple clearance pathways is significantly detrimental to the cell. Next, we tested the hypothesis that knockdown of the late endosome protein Rab7 would increase cell death as mitochondria-containing endosomes would be unable to mature and fuse with lysosomes. Indeed, we found that knockdown of Rab7 led to increased FCCP-mediated cell death in WT and *Atg5*$^{-/-}$ MEFs (Figure 5.2 e-g). Subsequently, we wanted to test

whether abrogating Rab5 produced similar effects. Rab5 exists as three isoforms with overlapping functions and all three isoforms are expressed in MEFs (Figure 5.3 a,b), making it challenging to target with siRNA. There exists, though, a dominant negative form of Rab5, Rab5S34N, which targets all three isoforms of Rab5. Using Rab5S34N, we effectively reduced FCCP-mediated mitochondrial clearance in *Atg5*$^{-/-}$ MEFs (Figure 5.3 c,d). Overexpression of Rab5S34N also caused increased FCCP-mediated cell death in both WT and *Atg5*$^{-/-}$ MEFs. Intriguingly, the *Atg5*$^{-/-}$ MEFs were significantly more susceptible to Rab5 inhibition than WT cells (Figure 5.3 e). In addition, we observed that inhibition of the endosomal pathway alone led to an increase in cell death in both WT and *Atg5*$^{-/-}$ MEFs, confirming the importance of the endosomal pathway in cellular homeostasis. However, because the endosomal pathway is involved in many cellular processes, we cannot rule out the possibility that these results are influenced by other stresses induced by inhibition of the endosomal pathway.

To determine why WT cells were less susceptible to abrogation of the endosomal pathway, we examined the relationship between the autophagy and endosomal pathways in WT cells. Specifically, we wanted to test the hypothesis that WT cells are able to compensate for impaired endosomal activity by enhancing autophagic activity. Interestingly, inhibition of the endosomal pathway led to increased autophagic activity under both baseline conditions and after stress (Figure 5.4 a-c). This suggests that the endosomal pathway participates in significant degradative activity that can be compensated by the autophagy pathway. Although abrogating Rab5 alone led to increased autophagic activity, we did not observe an increase in mitophagic activity under baseline conditions (Figure 5.4 d,e). Thus, these data suggest that there is cross

talk between the two pathways and that the autophagy pathway can compensate when the endosomal pathway is impaired.

5.2.3 Neonatal Cardiomyocytes Utilize the Endosomal Pathway for Mitochondrial Clearance

Maintaining a functional population of mitochondria is critical for cardiac myocyte function. They are highly active cells that require large amounts of energy supplied by mitochondrial oxidative phosphorylation. Since myocytes are post-mitotic, it is critical for these cells to efficiently remove dysfunctional mitochondria before they can cause harm. Furthermore, cardiac myocytes express endogenous Parkin, unlike MEFs, making them a more physiologically relevant model. Therefore, I investigated if the endosomal pathway contributes to clearing damaged mitochondria in cardiac myocytes. Myocardial ischemia/reperfusion is associated with mitochondrial damage and activation of mitophagy (Hamacher-Brady et al., 2007), and is a more physiologic stress than treatment with FCCP. Interestingly, I found that simulated ischemia/reperfusion (sI/R) led to a rapid, transient increase in the number of Rab5-positive endosomes upon reperfusion (Figure 5.5 a,b). Simulated ischemia/reperfusion has many effects on the cell, so it is currently unclear if mitochondrial dysfunction is the only trigger for increased endosome formation. However, I observed that many of the endosomes colocalized with mitochondria in the myocytes (Figure 5.5 c). In addition, similar to MEFs, all three isoforms of Rab5 are expressed in the heart (Figure 5.5 d). Thus to abrogate Rab5 activity we overexpressed Rab5S34N and found that this led to increased sI/R-mediated cell death (Figure 5.5 e). We also confirmed that Beclin1 regulates endosomal activity in

myocytes in response to stress, as it does in the MEFs. Knockdown of Beclin1 using Ad-shRNA completely abrogated the increase in Rab5-positive endosomes and their colocalization with mitochondria in myocytes in response to sI/R or FCCP treatment (Figure 5.6). These data confirm that Rab5 and the endosomal pathway also contribute to clearing impaired mitochondria in cardiac myocytes.

5.2.4 Atg7 Conditional Knockout Mice Retain Normal Heart Function

I wanted to test whether the endosomal pathway has a role in mitochondrial quality control in cardiac myocytes *in vivo*. To do this, we crossed homozygous *Atg7*$^{flox/flox}$ mice with heterozygous mice expressing Cre recombinase driven by the cardiomyocyte-specific α-myosin heavy chain (αMHC) promoter to produce cardiac-specific, *Atg7* conditional knockouts (cKO) mice. While the *Atg7* cKO mice display slightly enlarged hearts compared to their WT littermates, they have normal cardiac function at 8 to 12 weeks of age (Figure 5.7). Isolated mitochondria from the hearts of WT and *Atg7* cKO mice also showed similar State 3 respiration with a variety of substrates (Figure 5.8). Succinate, a Complex II substrate, showed no impairment in respiration between either hearts indicating that Complexes II through V are able to respire normally (Figure 5.8 a). Cardiac myocytes preferably rely on fatty acid oxidation, and a switch to carbohydrate metabolism is indicative of either fetal or failing hearts (Razeghi et al., 2001). Thus, I tested both pyruvate, an end product of glycolysis, and palmitoyl-L-carnitine, a known intermediate in mitochondrial fatty acid oxidation, to determine if there was any difference in substrate respiration. Both of these substrates

showed comparable rates of oxygen consumption, confirming that *Atg7* cKO cardiac mitochondria have normal function even in the absence of autophagy (Figure 5.8 b,c).

Western blotting for LC3 confirms that *Atg7* cKO hearts are deficient in autophagy (Figure 5.9 a). Thus I wondered whether the endosomal pathway was able to compensate for a lack of autophagy since these hearts have normal function and mitochondrial respiration up to 12 weeks of age. While mRNA levels of all three Rab5 isoforms and Rab7 were similar between WT and *Atg7* cKO hearts, I found a significant increase in the protein levels of Rab7 in hearts in the absence of autophagy (Figure 5.9). This suggests that the endosomal pathway may be upregulated in autophagy-deficient hearts as a compensatory mechanism.

Autophagy is important for mitochondrial removal after myocardial infarction (MI), and this removal is crucial in the recovery process (Kubli et al., 2013b). We have previously found that lack of Parkin-mediated mitochondrial clearance leads to enhanced injury and susceptibility to MI. Interestingly, *Atg7* cKO hearts did not show exacerbated impairment in cardiac function at 7 days post MI compared to WT controls (Figure 5.10). This suggests that these hearts are utilizing some other compensatory pathway in the heart to repair cellular damage.

5.3 Discussion

In chapter 5, I have shown that activation of endosomal-mediated mitochondrial clearance precedes activation of the autophagy pathway. I propose that uptake of mitochondria into endosomes acts as a first line of defense to rapidly eliminate dysfunctional mitochondria. Early endosomes are continuously synthesized and exist in

a network in cells (Zeigerer et al., 2012), whereas autophagosomes are synthesized *de novo* upon demand (Rubinsztein et al., 2012). Therefore, dysfunctional mitochondria can be more rapidly sequestered by the early endosomes. However, it is likely that if the number of damaged mitochondria exceeds the capacity of endosomal-mediated degradation, then the autophagy pathway is also activated. A similar coordination and sequential activation has been observed for the traditional autophagy and chaperon-mediated autophagy (CMA) pathways in response to stress such as starvation and oxidative stress (Kaushik et al., 2008). Traditional autophagy is rapidly activated in response to stress but then there is a switch to CMA if the stress is prolonged. Future studies need to determine the context and timing of activation of these various pathways in cells. Our data also show that autophagic activity is increased when Rab5 activity is abrogated, suggesting that autophagic degradation is compensating when endosomal activity is impaired.

I have additionally demonstrated that neonatal cardiomyocytes also utilize the endosomal pathway when exposed to simulated ischemia-reperfusion. Inhibition of this pathway also led to increased cell death in WT MEFs, autophagy-deficient MEFs, and neonatal cardiomyocytes upon stress. Particularly considering the WT MEFs and neonatal cardiomyocytes, if autophagy were sufficient for removal of damaged mitochondria, then there should be no increase in the extent of cell death with endosomal inhibition. As expected, autophagy-deficient MEFs had even higher levels of cell death than WT MEFs. These data suggest that endosomal-mediated mitochondrial clearance is an important pathway through which damaged mitochondria may be removed from the cell, and may be a point of therapeutic intervention in the heart.

Previous studies have shown that inhibition of Parkin-mediated mitophagy is dispensable at baseline conditions (Kubli et al., 2013b). However, it is crucial for repair and heart function after myocardial infarction. Interestingly, *Atg7*-deficient hearts have normal function at baseline and are not more susceptible to MI than WT hearts, so it is possible that the endosomal pathway is compensating for impaired mitophagy *in vivo*. Additional studies need to be conducted to see if this is the case.

Interestingly, it seems that the autophagy pathway can at least partially compensate for impaired endosomal function. Since autophagy has not been studied in the context of endosomal-inhibition, it is unclear what contribution each pathway truly has in regards to protein and organelle quality control in the cell. The fact that Rab5S34N alone increases autophagic activity under baseline and stress conditions hints at this being the case. I propose that much of intracellular degradation that is fully attributed to autophagy instead has a significant component of clearance through the endosomal-lysosomal pathway. More studies are required to tease apart the role of each of these pathways, and the conditions that drive them.

Parts of Chapter 5 were originally published in *Nature Communications*. Hammerling, B. C., Najor, R. H., Cortez, M. Q., Shires, S. E., Leon, L. J., Gonzalez, E. R., Boassa, D., Phan, S., Thor, A., Jimenez, R. E., Li, H., Kitsis, R. N., Dorn II, G. W., Sadoshima, J., Ellisman, M. H., Gustafsson, A. G. A Rab5 Endosomal Pathway Mediates Parkin-Dependent Mitochondrial Clearance. *Nature Communications*. 8: 14050, 2017; doi:10.1038/ncomms14050 © 2017 Nature Publishing Group. The dissertation author was the primary investigator and author of this paper.

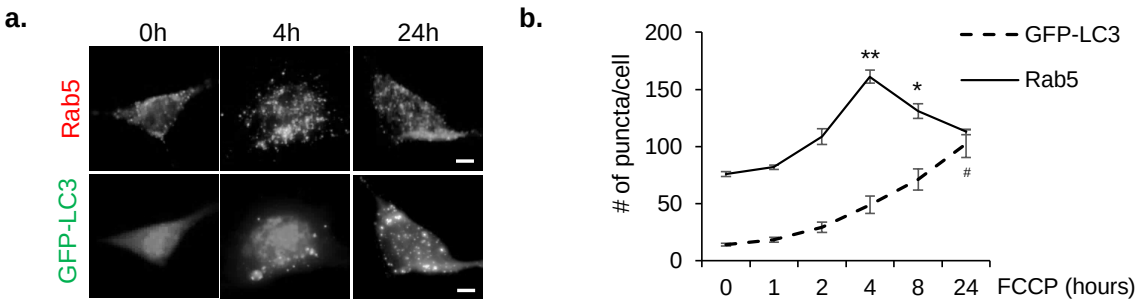

Figure 5.1. Endosomal clearance is activated prior to autophagy.
(a) Representative images of WT MEFs overexpressing GFP-LC3, treated with 25 µM FCCP for the indicated time, and stained with anti-Rab5. Scale bars=20 µm. **(b)** Quantification of Rab5 and GFP-LC3 positive vesicles in WT cells (n=40 cells scored for number of puncta in 3 independent experiments, *p<0.05, **p<0.01 vs 0 hours for Rab5, #p<0.05 vs 0 h for GFP-LC3). All values are means±s.e.m from independent experiments. Statistical significance was calculated using ANOVA followed by Dunnett's test for multiple comparison.

Figure 5.2. Abrogation of the endosomal-lysosomal degradation pathway increases susceptibility to cell death.

(a,b) Quantification of cell death in response to FCCP +/- 3-MA treatment. WT **(a)** or *Atg5*$^{-/-}$ **(b)** MEFs expressing Parkin were incubated with 5 mM 3-MA and DMSO or FCCP (25 µM) for 24 h. Cell death was assessed by Yo-Pro-1 uptake (n=350 cells screened for cell death in 3 independent experiments, *p<0.05, **p<0.01, ***p<0.001). **(c,d)** Quantification of cell death in response to FCCP +/- Baf A1 treatment. WT (**c**) or *Atg5*$^{-/-}$ (**d**) MEFs were incubated with 50 nM Bafilomycin A1 and DMSO or FCCP (25 µM) for 24 h. Cell death was assessed by Yo-Pro-1 uptake (n=350 cells screened for cell death in 3 independent experiments, *p<0.05, **p<0.01, ***p<0.001). **(e)** Western blot of Rab7 in *Atg5*$^{-/-}$ MEFs after siRNA transfection. **(f,g)** Quantification of cell death WT **(f)** or *Atg5*$^{-/-}$ **(g)** or cells were exposed to DMSO or FCCP (25 µM) for 24 h after siRNA knockdown and then stained with Yo-Pro-1 (**f**: n=470, **g**: n=175 cells, screened for cell death in 3 independent experiments, *p<0.05, **p<0.01, ***p<0.001). All values are means±s.e.m from independent experiments. Statistical significance was calculated using ANOVA followed by Dunnett's test for multiple comparison.

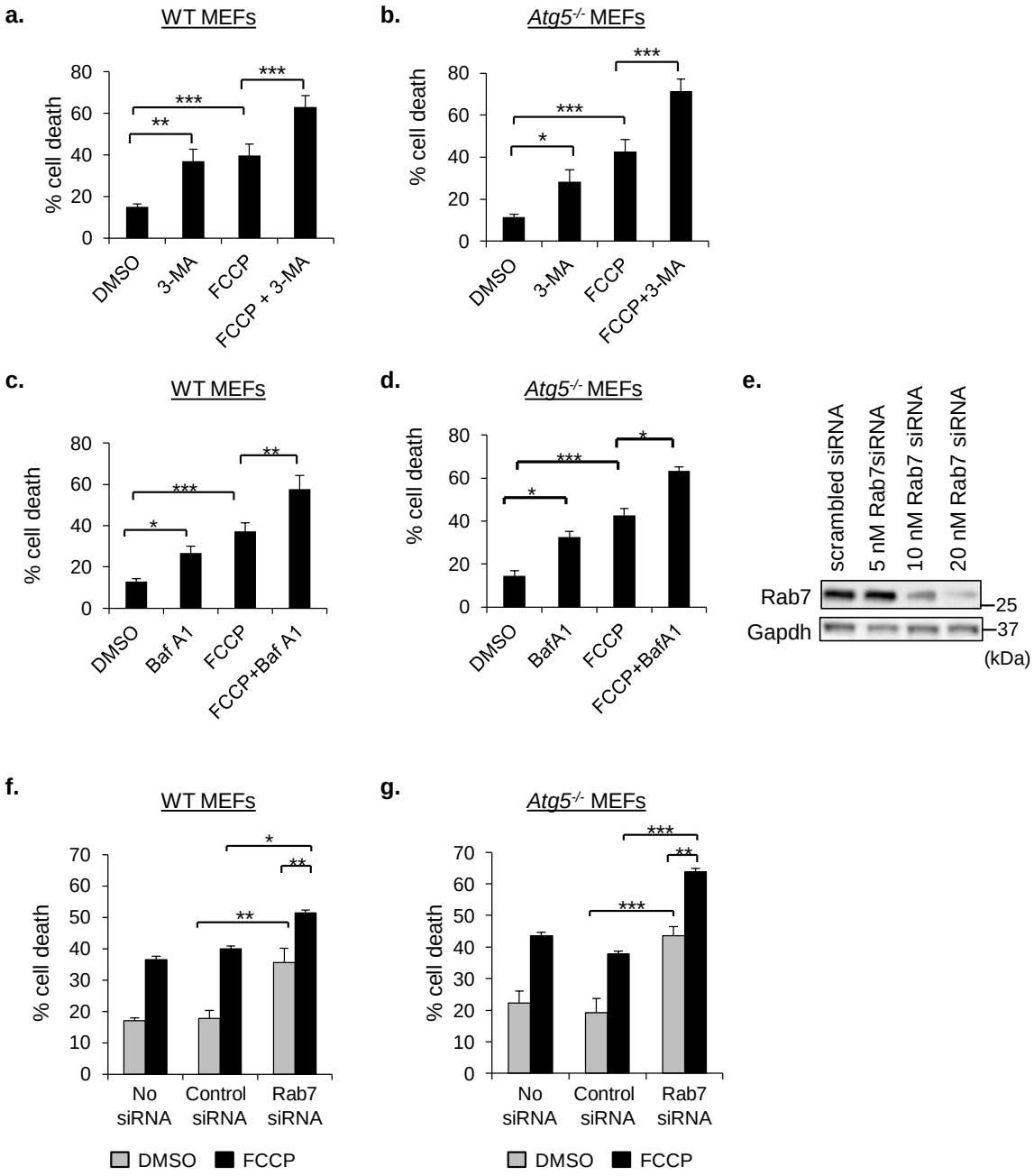
a.
WT MEFs
% cell death
DMSO
3-MA
FCCP
FCCP + 3-MA
b.
Atg5-/- MEFs
% cell death
DMSO
3-MA
FCCP
FCCP+3-MA
c.
WT MEFs
% cell death
DMSO
Baf A1
FCCP
FCCP+Baf A1
d.
Atg5-/- MEFs
% cell death
DMSO
BafA1
FCCP
FCCP+BafA1
e.
scrambled siRNA
5 nM Rab7siRNA
10 nM Rab7 siRNA
20 nM Rab7 siRNA
Rab7
Gapdh
25
37
(kDa)
f.
WT MEFs
% cell death
No siRNA
Control siRNA
Rab7 siRNA
DMSO
FCCP
g.
Atg5-/- MEFs
% cell death
No siRNA
Control siRNA
Rab7 siRNA
DMSO
FCCP

Figure 5.3. Dominant-negative Rab5S34N overexpression impairs FCCP-mediated mitochondrial clearance.

(a,b) qPCR for Rab5 isoforms in WT MEFs **(a)**, and *Atg5*$^{-/-}$ MEFs **(b)**. **(c)** Representative images of *Atg5*$^{-/-}$ MEFs expressing Parkin infected with GFP or GFP-Rab5S34N, treated with 25 µM FCCP (0 or 12 h), and stained with anti-COX IV and Hoechst 33342 (blue). Scale bars=20 µm. **(d)** Quantification of cells undergoing mitochondria clearance (n=85 cells screen for mitochondria in 3 independent experiments, *p<0.05). **(e)** Quantification of cell death in WT and *Atg5*$^{-/-}$ MEFs infected with myc-Parkin and βgal (con) or Rab5S34N. Cells were exposed to DMSO or FCCP (25 µM) for 24 h. Cell death was assessed by Po-Pro-3 uptake (n=160 cells screened for cell death in 4 independent experiments, **p<0.01, ****p<0.0001). All values are means±s.e.m from independent experiments. Statistical significance was calculated using ANOVA followed by Dunnett's test for multiple comparison.

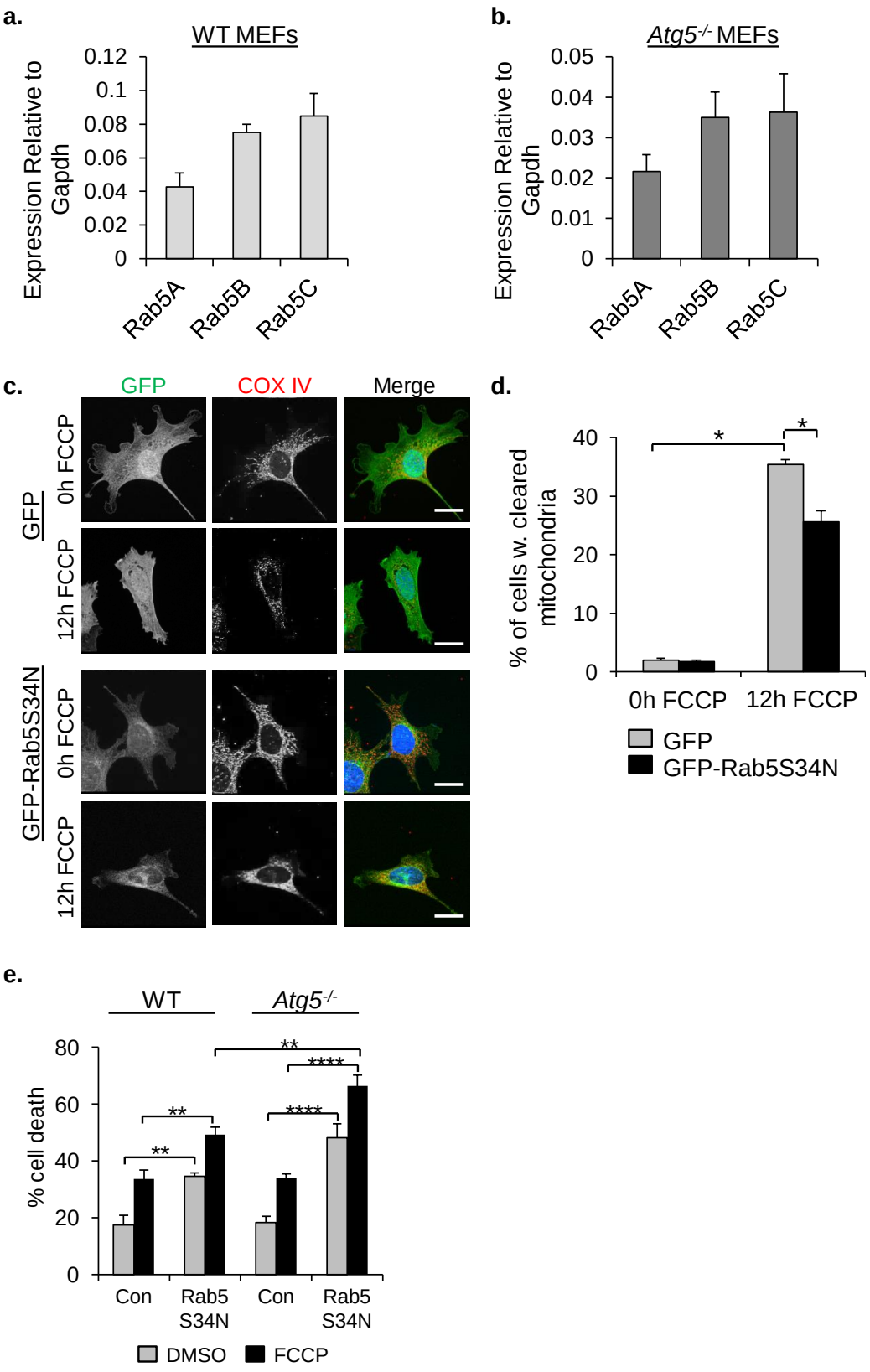
a.
WT MEFs
Expression Relative to Gapdh
0.12
0.1
0.08
0.06
0.04
0.02
0
Rab5A
Rab5B
Rab5C
b.
Atg5-/- MEFs
Expression Relative to Gapdh
0.05
0.04
0.03
0.02
0.01
0
Rab5A
Rab5B
Rab5C
c.
GFP
COX IV
Merge
GFP
0h FCCP
12h FCCP
GFP-Rab5S34N
0h FCCP
12h FCCP
d.
% of cells w. cleared mitochondria
40
30
20
10
0
*
*
0h FCCP
12h FCCP
GFP
GFP-Rab5S34N
e.
WT
Atg5-/-
% cell death
80
60
40
20
0
**
**
**
****
****
Con
Rab5 S34N
Con
Rab5 S34N
DMSO
FCCP

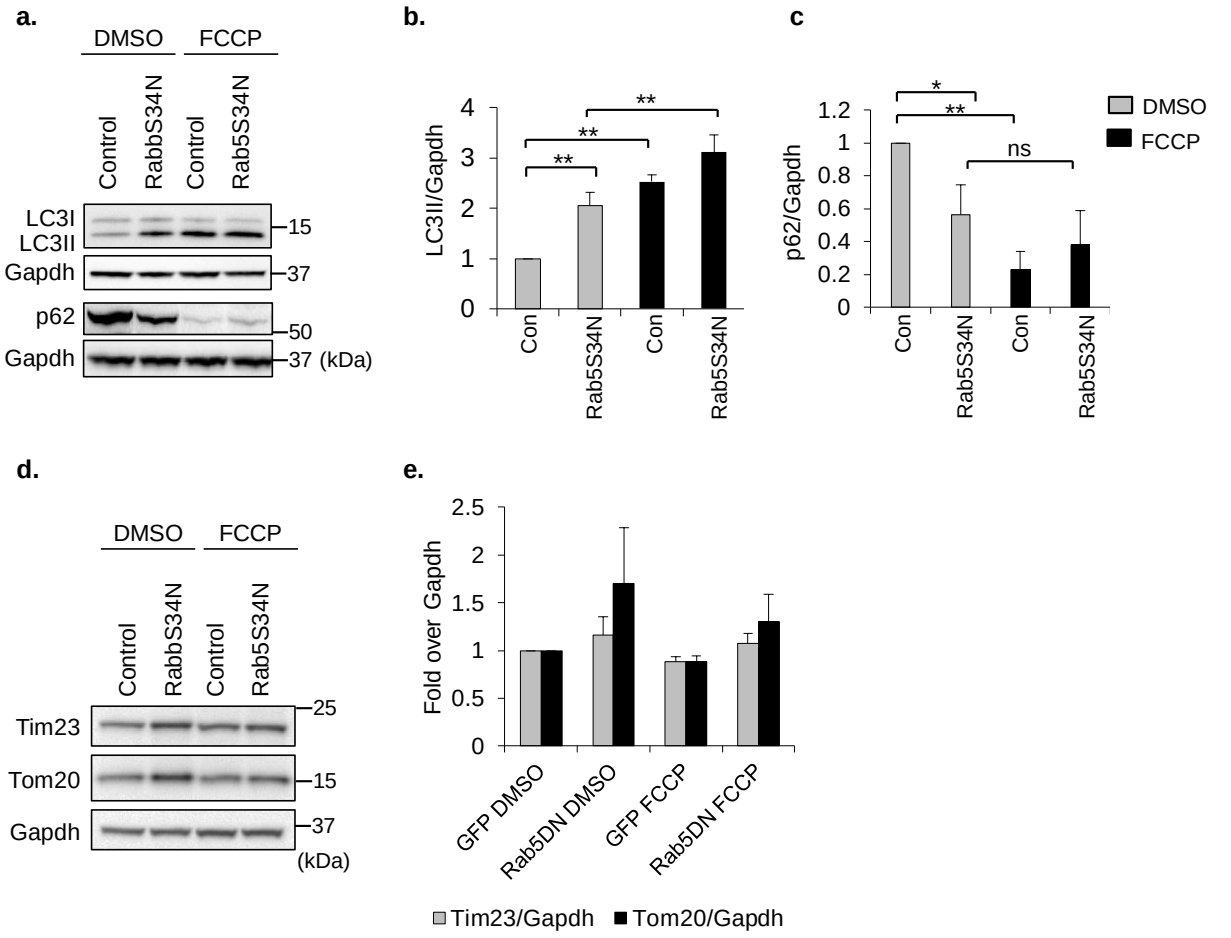

Figure 5.4. Endosomal inhibition increases autophagic, but not mitophagic, activity under baseline and after stress.
(a) Western blot for LC3 and p62 levels in WT MEFs expressing Parkin infected with β-gal (control) or Rab5S34N and treated with DMSO or FCCP (25 µM) for 4 h. **(b,c)** Band densitometry of LC3II **(b)** and p62 **(c)** protein levels (n=3, *p<0.05, **p<0.01, ns=not significant). **(d)** Western blot for Tim23 and Tom20 protein levels in WT MEFs expressing Parkin infected with β-gal (control) or Rab5S34N and treated with DMSO or FCCP (25 µM) for 4 h. **(e)** Band densitometry of Tim23 and Tom20 proteins levels from panel **d** (n=3, data are not significant). All values are means±s.e.m from independent experiments. Statistical significance was calculated using ANOVA followed by Dunnett's test for multiple comparison.

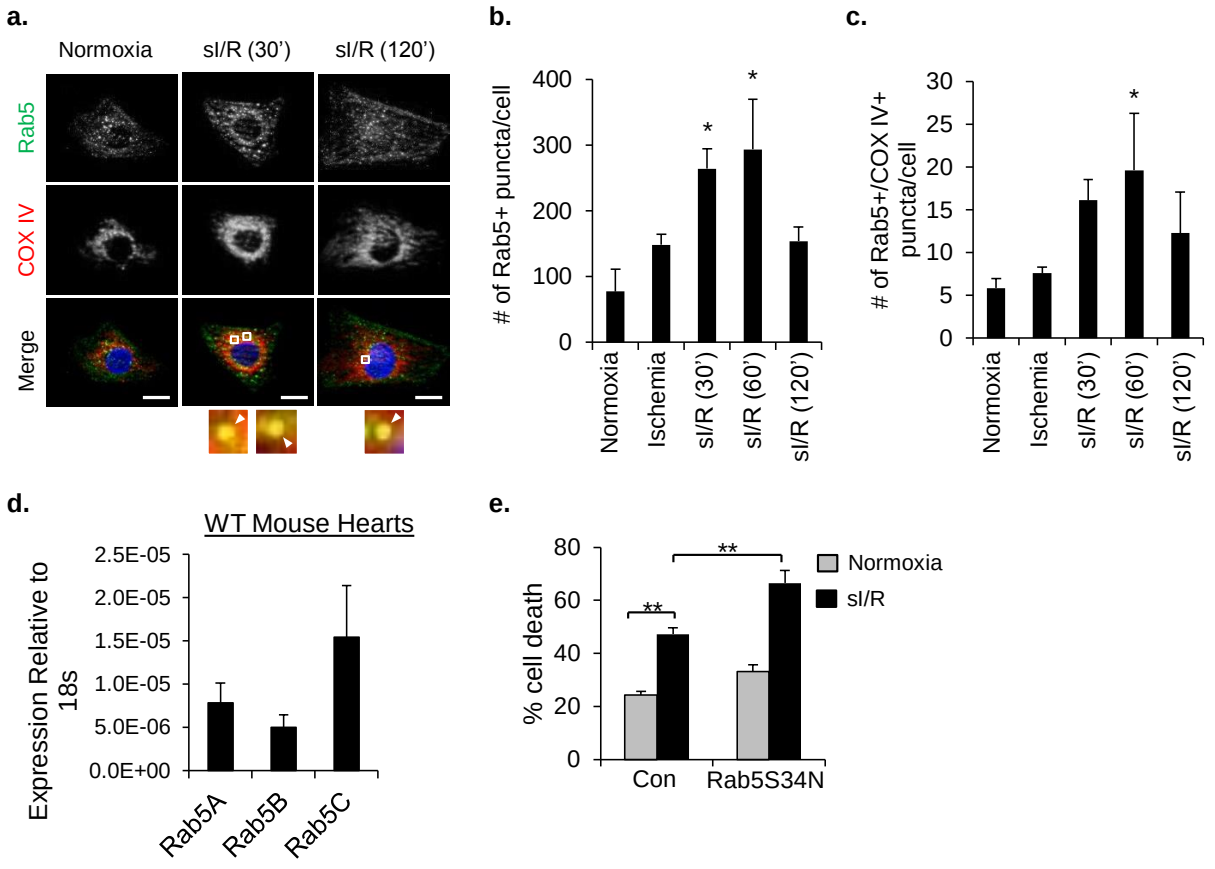

Figure 5.5. Activation of endosomal-mediated mitochondrial degradation in cardiac myocytes.

(a) Representative images of neonatal myocytes subjected to normoxia or simulated ischemia/reperfusion (sI/R). After the treatment, cells were fixed and stained with anti-Rab5 and anti-COX IV. Arrowheads show colocalizing puncta. Scale bar=10 µm. **(b,c)** Quantification of Rab5 positive puncta **(b)** and their colocalization **(c)** with COX IV labeled mitochondria in neonatal cardiac myocytes (n=36 cells scored for number of puncta in 3 independent experiments, *p<0.05 vs normoxia). **(d)** qPCR for Rab5 isoforms in WT mouse hearts. **(e)** Quantification of cell death. Cells were exposed to normoxia or 2 h of simulated ischemia plus 8 h of reperfusion. Cell death was assessed by propidium iodide staining (n=170 cells screened for cell death in 3 independent experiments, **p<0.01). Nuclei were counterstained with Hoechst 33342 (blue). All values are means±s.e.m from independent experiments. Statistical significance was calculated using ANOVA followed by Dunnett's test for multiple comparison.

Figure 5.6. Knockdown of Beclin1 in neonatal cardiomyocytes impairs mitochondrial clearance after FCCP or sI/R.

(a) Western blot of Beclin1 knockdown in myocytes. (un=uninfected, scr=scramble shRNA, parentheses indicate MOI). **(b)** Representative images of neonatal myocytes after Beclin1 knockdown. After treatment, cells were stained with anti-Rab5 and anti-COX IV. Scale bar=10 μm. Arrowheads show colocalization. Enlarged boxes without arrowheads show non-colocalizing puncta. **(c,d)** Quantification of Rab5 positive puncta **(c)** and their colocalization **(d)** with COX IV labeled mitochondria in neonatal cardiac myocytes. Cells were treated with scramble (scr) or Beclin1 shRNA (MOI=50) and subjected to normoxia or 2 h of simulated ischemia plus 60 min of reperfusion before fixation and staining with anti-Rab5 and anti-COX IV (n=30 cells scored for number of puncta in 3 independent experiments, ***$p<0.001$). **(e,f)** Quantification of Rab5 positive puncta **(e)** and their colocalization with COX IV labeled mitochondria **(f)** in neonatal cardiac myocytes. Cells were subjected to FCCP (10 μM) for 6 h before fixation and staining with anti-Rab5 and anti-COX IV (n=30 cells scored for number of puncta in 3 independent experiments, *$p<0.05$, **$p<0.01$, ****$p<0.0001$). Nuclei were counterstained with Hoechst 33342 (blue). All values are means±s.e.m from independent experiments. Statistical significance was calculated using ANOVA followed by Dunnett's test for multiple comparison.

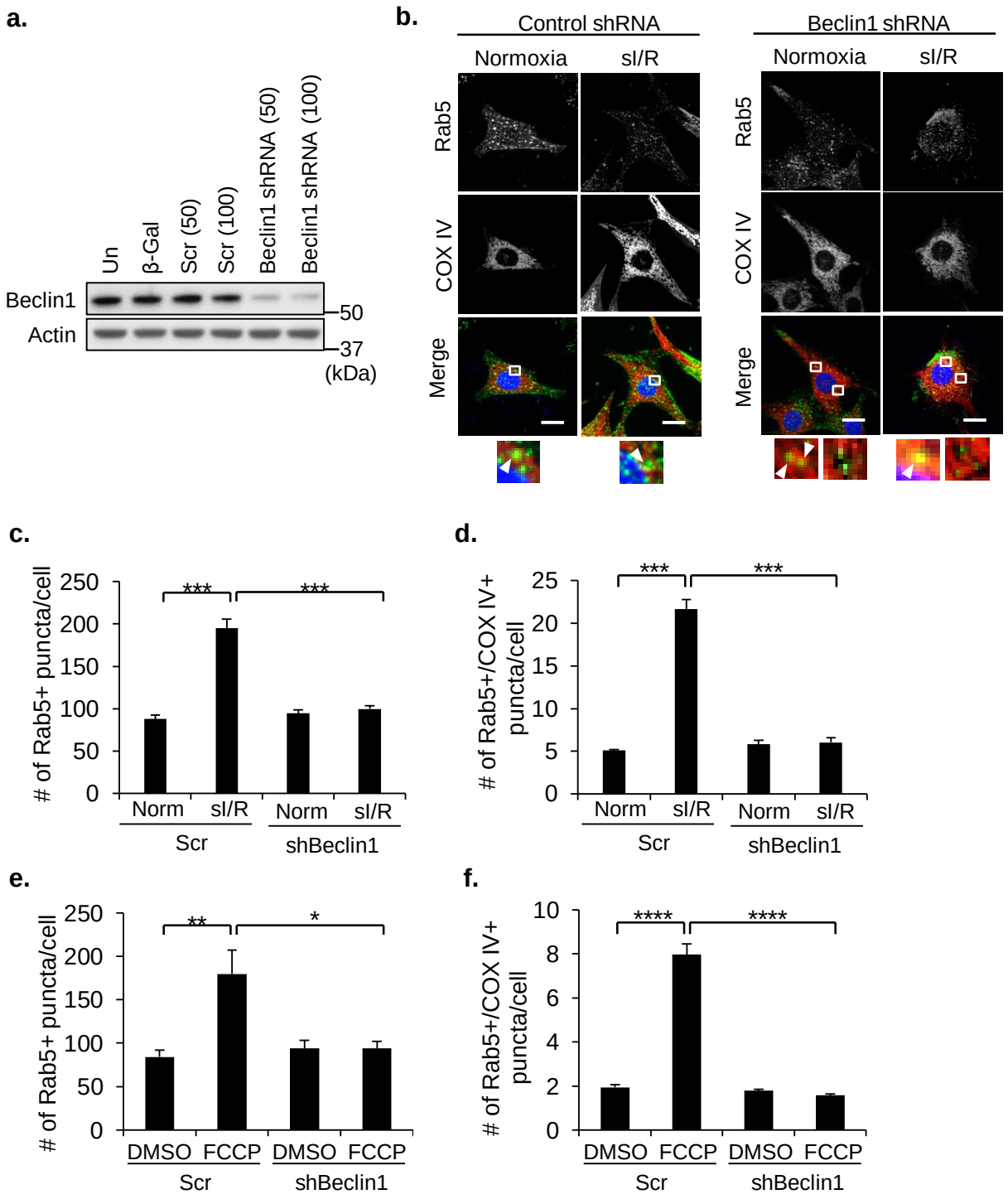
a.
Un
β-Gal
Scr (50)
Scr (100)
Beclin1 shRNA (50)
Beclin1 shRNA (100)
Beclin1
Actin
50
37
(kDa)
b.
Control shRNA
Beclin1 shRNA
Normoxia
sI/R
Rab5
COX IV
Merge
c.
# of Rab5+ puncta/cell
Norm
sI/R
Scr
shBeclin1
d.
# of Rab5+/COX IV+ puncta/cell
e.
DMSO
FCCP
f.

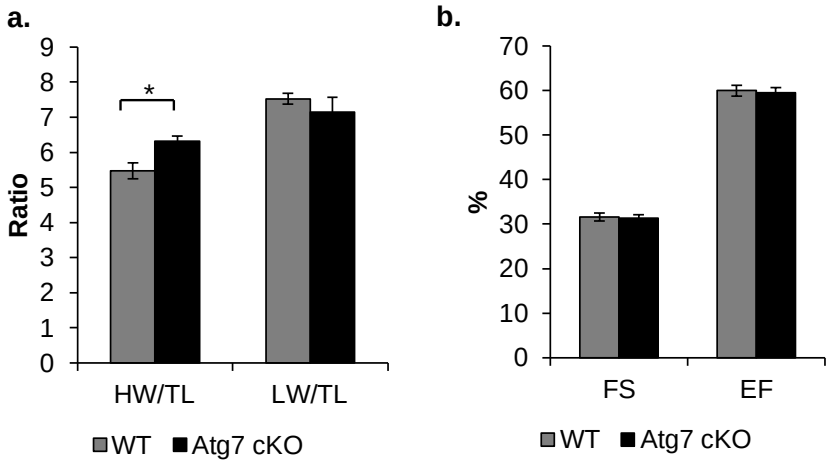

Figure 5.7. Autophagy-deficient hearts are larger than WT but are functionally comparable.

(a) Heart weight (HW, in mg) and lung weight (LW, in mg) to tibia length (TL, in mm) ratios in both WT and *Atg7* cKO hearts (n= 5 WT, 8 *Atg7* cKO, *p<0.05). **(b)** Percent fractional shortening (FS) and ejection fraction (EF) in WT and *Atg7* cKO hearts at 8 to 12 weeks of age (n=12 WT, 10 *Atg7* cKO, data are not significant). All values are means±s.e.m from independent experiments. Statistical significance was calculated using Student's t-test.

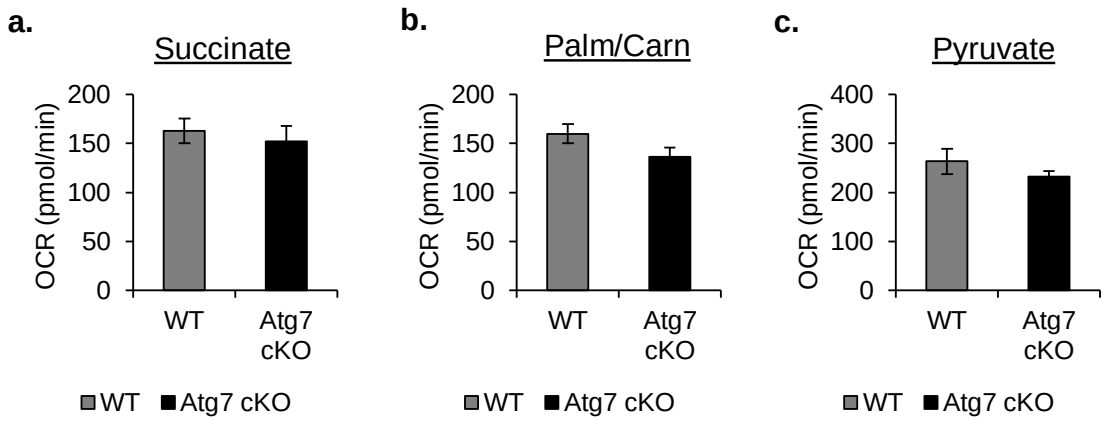

Figure 5.8. Maximal mitochondrial respiration in WT and autophagy-deficient mouse hearts.

(a,b,c) Maximal oxygen consumption rates (OCR) in mitochondria isolated from WT and *Atg7* cKO hearts. Mitochondria were give either succinate (n=6 WT, 6 *Atg7* cKO) **(a)**, palmitoyl-L-carnitine (n= 5 WT, 5 *Atg7* cKO) **(b)**, or pyruvate (n= 6 WT, 6 *Atg7* cKO) **(c)** as oxidative phosphorylation substrates (data are not significant). All values are means±s.e.m from independent experiments. Statistical significance was calculated using Student's t-test.

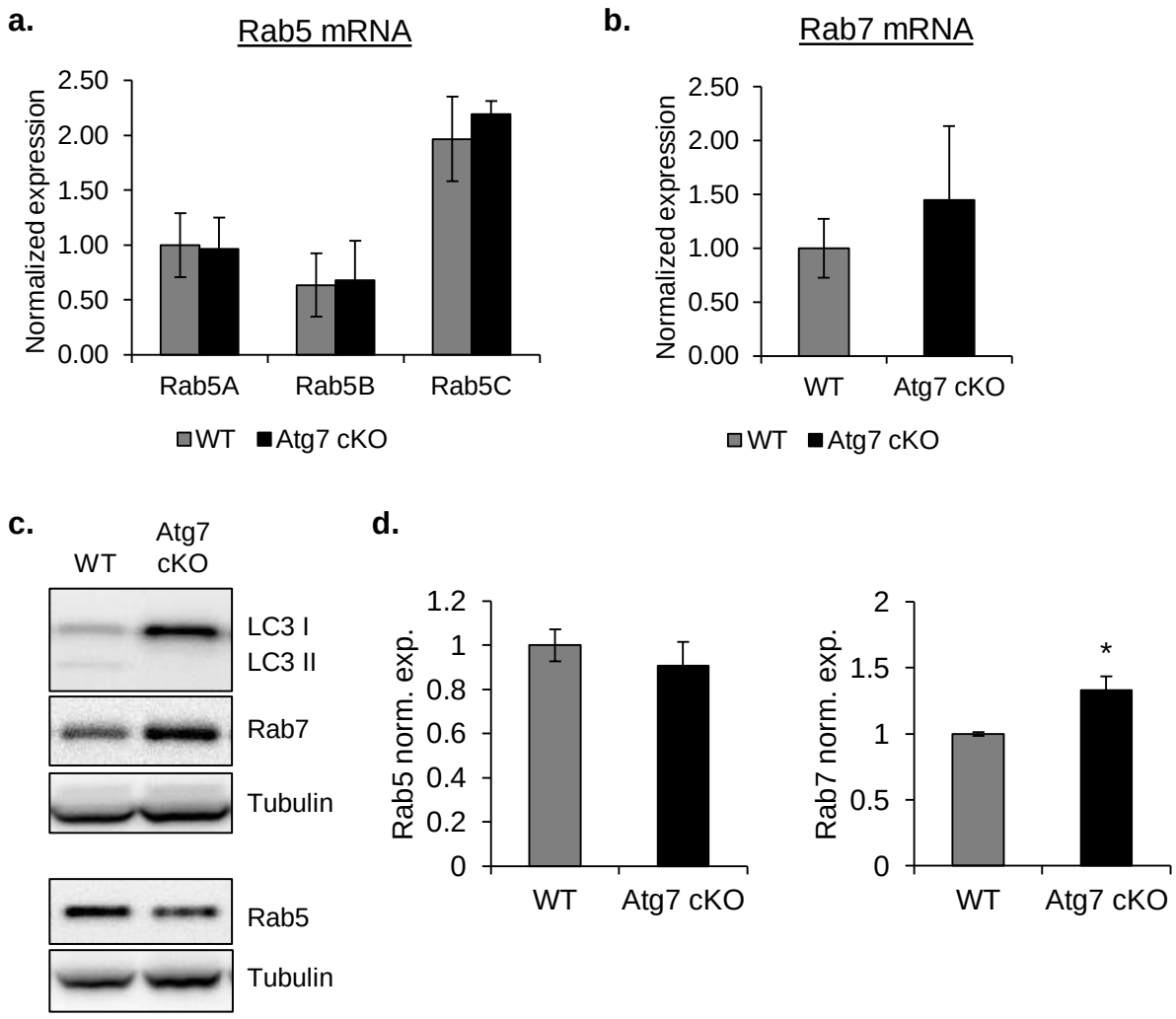

Figure 5.9. Rab7 protein levels are upregulated in autophagy-deficient hearts. **(a,b)** Rab5 isoforms **(a)** or Rab7 **(b)** mRNA levels in WT and *Atg7* cKO hearts. **(c)** Representative Western blots for LC3, Rab7, Rab5, and Tubulin in WT and *Atg7* cKO hearts. **(d)** Band densitometry of Rab5 and Rab7 levels (n= 5 WT, 8 *Atg7* cKO, *p<0.05). All values are means±s.e.m from independent experiments. Statistical significance was calculated using ANOVA followed by Dunnett's test for multiple comparison **(a)** or by Student's t-test **(b,d).**

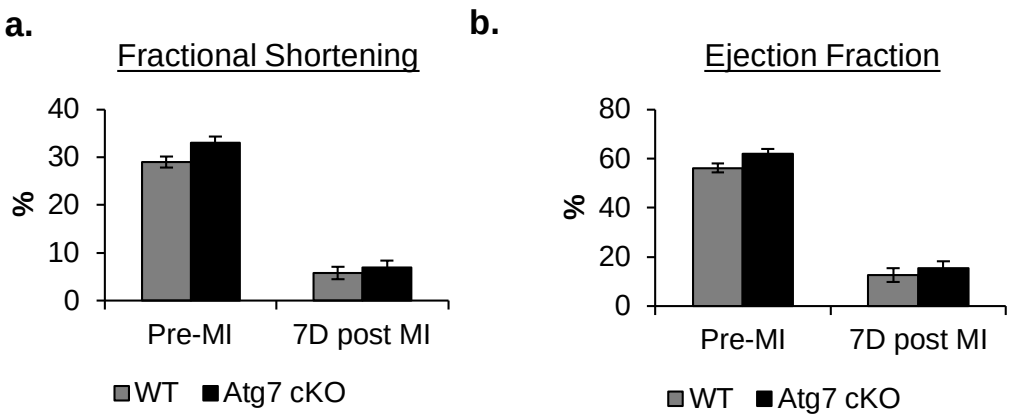

Figure 5.10. Autophagy-deficient hearts are no more susceptible to MI injury than WT hearts.

(a,b) Percent fractional shortening **(a)** and ejection fraction **(b)** in WT and *Atg7* cKO hearts prior to or 7 days after myocardial infarction (MI) (n=13 WT, 7 *Atg7* cKO, data are not significant). All values are means±s.e.m from independent experiments. Statistical significance was calculated using Student's t-test.

CHAPTER 6: MITOPHAGY RECEPTOR BNIP3 CAN UTILIZE THE ENDOSOMAL-LYSOSOMAL PATHWAY TO ELIMINATE MITOCHONDRIA

6.1 Introduction

In addition to Parkin-mediated mitophagy, mitochondrial clearance can also be directly mediated by mitophagy receptors such as Nix and BNIP3 (Ney, 2015). These proteins do not rely on the ubiquitination of mitochondria in order to promote clearance. Instead, these proteins localize to the outer mitochondrial membrane where they directly bind LC3 on autophagosomal membranes. This binding event causes sequestration of the mitochondria into the autophagosome (Figure 1.3 b). Initially well known for its role in cell death, BNIP3 was found to activate autophagy in MEFs undergoing hypoxia (Zhang et al., 2008). In the heart where BNIP3 exhibits high levels of expression, BNIP3 is activated in response to ischemia/reperfusion injury, and increases autophagy in HL-1 myocytes subjected to ischemia/reperfusion (Hamacher-Brady et al., 2007). Additionally, mere overexpression of either Nix or BNIP3 in the cell promotes mitochondrial clearance (Ding et al., 2010; Hanna et al., 2012). It is unknown whether these receptor proteins are also able to utilize the endosomal-lysosomal pathway. In this chapter, I examine whether BNIP3 overexpression is able to induce mitochondrial clearance in autophagy-deficient cells.

6.2 Results

6.2.1 BNIP3 Overexpression Causes Mitochondrial Clearance in Autophagy-Deficient Cells

I wondered whether mitophagy receptors like BNIP3 were able to promote mitochondrial clearance in the absence of autophagy. Indeed, I found that both WT and autophagy-deficient *Atg5*$^{-/-}$ MEFs were able to clear mitochondria upon overexpression of BNIP3 alone (Figure 6.1). The mutant BNIP3W18A contains a tryptophan to alanine amino-acid substitution in the LC3-interacting region (Hanna et al., 2012). This abrogates its ability to interact with LC3 and is unable to dock mitochondria to autophagosomes. Overexpression of BNIP3 and BNIP3W18A led to increased colocalization between p40PX-EGFP and Rab5 in *Atg5*$^{-/-}$ MEFs (Figure 6.2). P40PX-EGFP binds PI(3)P at early endosomes, providing a readout for VPS34 PI3K activity (Kanai et al., 2001). This suggests that both WT and mutant BNIP3 are able to promote activation of the endosomal pathway in autophagy-deficient cells.

6.2.2 BNIP3 Utilizes the Endosomal-Lysosomal Pathway to Clear Mitochondria

Our data show that BNIP3 is able to promote mitochondrial clearance in autophagy-deficient cells. I next wanted to test whether BNIP3 was also able to utilize the endosomal-lysosomal pathway for the mitochondrial clearance. First, I confirmed the accumulation of mitochondria inside enlarged Rab5Q79L-positive endosomes in both WT and *Atg5*$^{-/-}$ MEFs overexpressing BNIP3 (Figure 6.3). This suggests that mitophagy receptors can also utilize the endosomal pathway to clear mitochondria. Furthermore, BNIP3 is known to induce mitochondrial dysfunction and cell death when overexpressed in cells (Regula et al., 2002; Rikka et al., 2011; Vande et al., 2000). Therefore, to

examine whether removal of mitochondria by Rab5-positive endosomes was a protective response activated by the cell, we examined the effects of modulating Rab5 activity on cell viability. We found that overexpression of BNIP3 caused a significant increase in cell death as measured by BOBO-3 uptake in cells with compromised plasma membranes in both WT and *Atg5*$^{-/-}$ MEFs (Figure 6.4). We also found that the presence of GFP-Rab5Q79L did not change BNIP3-mediated cell death in either WT or *Atg5*$^{-/-}$ MEFs (Figure 6.4 a), suggesting that merely sequestering mitochondria in vesicles is not sufficient to protect against cell death. In contrast, overexpression of BNIP3 plus the Rab5 dominant negative, Rab5S34N, led to a significant increase in BNIP3-mediated cell death in *Atg5*$^{-/-}$ MEFs but not in WT MEFs (Figure 6.4 b). This is most likely due to the fact that the WT cells still have intact autophagy to clear mitochondria. These data indicate that BNIP3 is able to cause the sequestration of mitochondria inside Rab5-positive early endosomes, and that coupling BNIP3 overexpression with inhibition of the endosomal pathway is toxic to the cell.

6.3 Discussion

In this chapter, I have shown that the mitophagy receptor BNIP3 is also able to utilize the endosomal pathway for mitochondrial clearance. However, how BNIP3 causes engulfment of mitochondria into Rab5-positive endosomes is currently unknown. The ESCRT machinery is responsible for engulfing cargo into the endosome but these complexes recognize ubiquitinated cargo. BNIP3 is not an E3 ubiquitin ligase, therefore it is possible that BNIP3 is activating one of the resident mitochondrial E3 ubiquitin ligases to label mitochondria with ubiquitin. There are two mitochondrial ubiquitin

ligases on the cytosolic side of the OMM: March5 and MULAN/MAPL (Kotiadis et al., 2014; Zhong et al., 2005). It is possible that either, or both, of these ubiquitinates mitochondria to be bound by ESCRTs and sequestered into endosomes. More studies would have to be conducted to determine whether mitochondria are ubiquitinated in this form of BNIP3-mediated mitochondrial clearance.

Alternatively, given that BNIP3 can directly tether mitochondria to autophagosomes, ubiquitination of mitochondria may not be required. There is evidence in the literature that cargo can be sequestered inside endosomes in an ESCRT-independent, and thus ubiquitin-independent, manner (Babst, 2011). For instance, BNIP3 may directly tether mitochondria to endosomes through an unknown protein interaction. More studies are required to determine how BNIP3 promotes the sequestration of damaged mitochondria inside early endosomes.

Parts of Chapter 6 were originally published in *Nature Communications*. Hammerling, B. C., Najor, R. H., Cortez, M. Q., Shires, S. E., Leon, L. J., Gonzalez, E. R., Boassa, D., Phan, S., Thor, A., Jimenez, R. E., Li, H., Kitsis, R. N., Dorn II, G. W., Sadoshima, J., Ellisman, M. H., Gustafsson, A. G. A Rab5 Endosomal Pathway Mediates Parkin-Dependent Mitochondrial Clearance. *Nature Communications*. 8: 14050, 2017; doi:10.1038/ncomms14050 © 2017 Nature Publishing Group. The dissertation author was the primary investigator and author of this paper.

Parts of Chapter 6 were originally published in *Small GTPases*. Hammerling, B. C., Shires, S. E., Leon, L. J., Cortez, M. Q., Gustafsson, A. G. Isolation of Rab5-Positive Endosomes Reveals a New Mitochondrial Degradation Pathway Utilized by BINP3 and

Parkin. *Small GTPases*. 1-8, 2017; doi: doi:10.1080/21541248.2017.1342749. © 2017 Taylor & Francis Online. The dissertation author was the primary investigator and author of this paper.

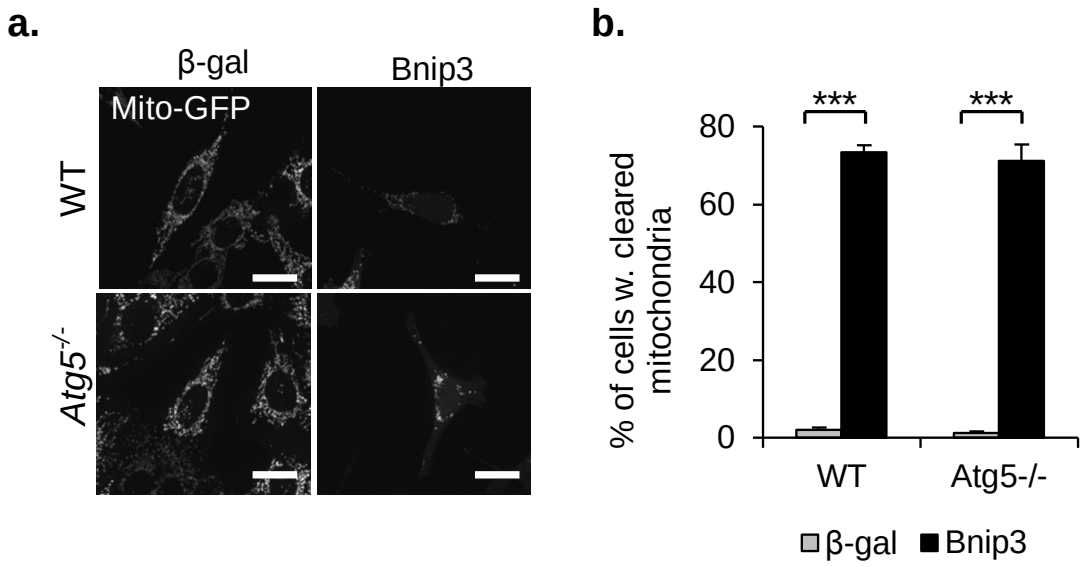

Figure 6.1. BNIP3 overexpression results in mitochondrial clearance in *Atg5*$^{-/-}$ MEFs.

(a) Representative images of mitochondrial clearance in WT or *Atg5*$^{-/-}$ MEFs infected with mito-GFP plus β-gal or BNIP3 for 24 h. Scale bars=20 μm. **(b)** Quantification of mitochondrial clearance in response to BNIP3 (n=100 cells screened for mitochondria in 3 independent experiments, ***p<0.001 vs β-gal). Scale bars=20 μm. All values are means±s.e.m from independent experiments. Statistical significance was calculated using ANOVA followed by Dunnett's test for multiple comparison.

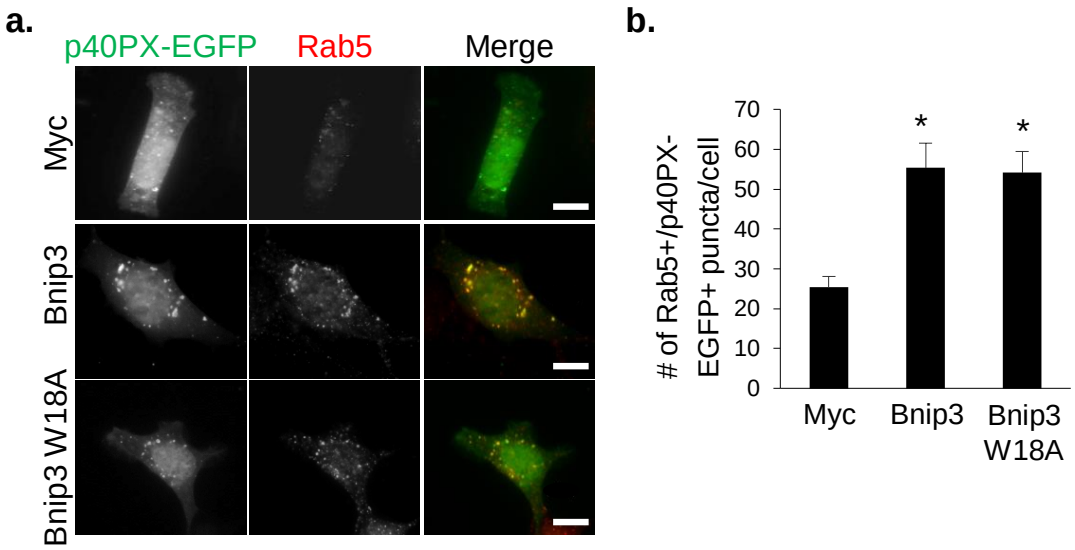

Figure 6.2. BNIP3 overexpression induces Rab5 activation.
(a) Representative images of *Atg5*$^{-/-}$ MEFs transfected with myc, BNIP3, or BNIP3W18A plus p40PX-EGFP for 24 h and stained with anti-Rab5. Scale bars=10 μm. **(b)** Quantification of puncta positive for p40PX-EGFP and Rab5 in *Atg5*$^{-/-}$ cells (n=35 cells scored for number of puncta in 4 independent experiments, *p<0.05 vs myc). All values are means±s.e.m from independent experiments. Statistical significance was calculated using ANOVA followed by Dunnett's test for multiple comparison.

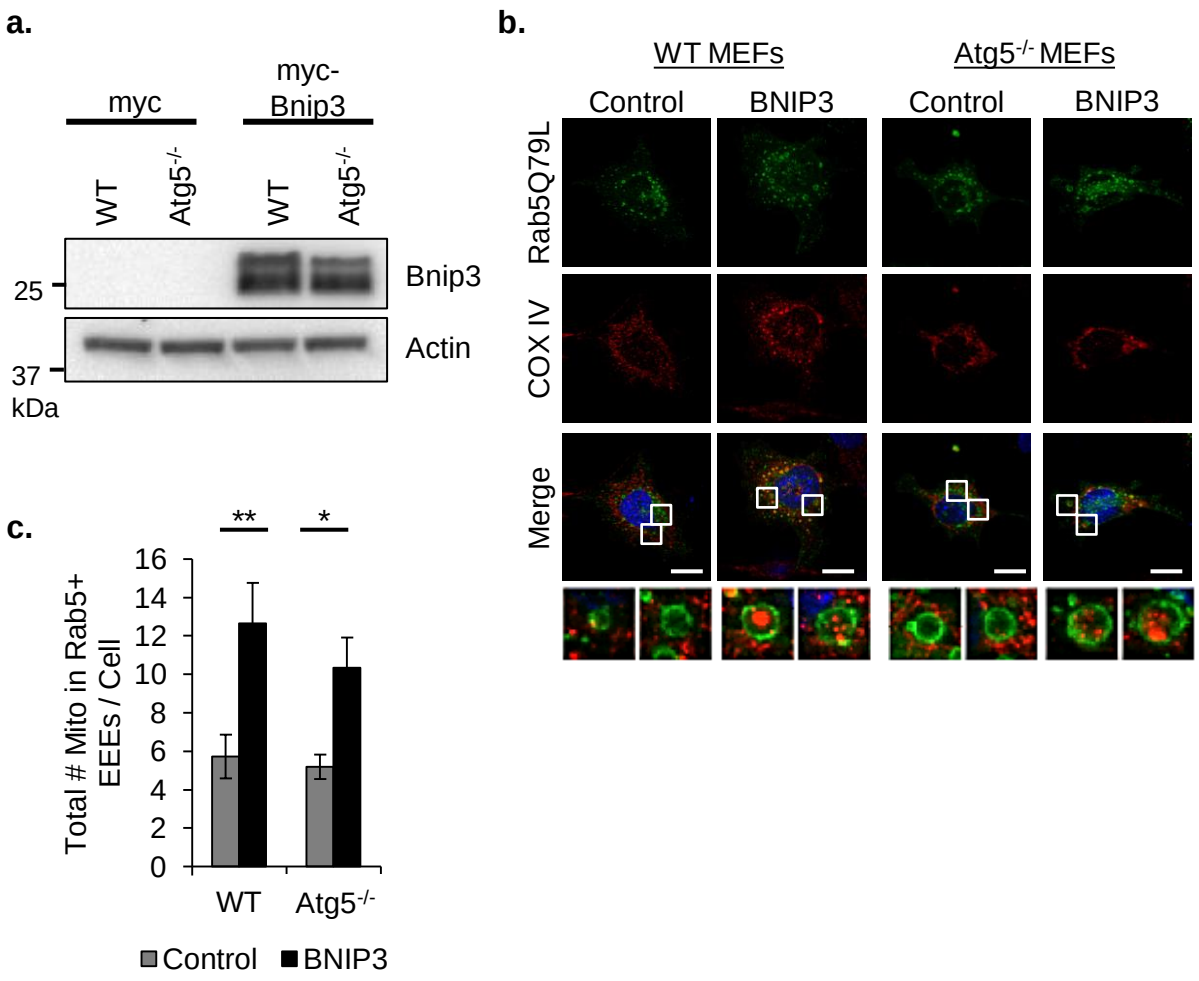

Figure 6.3. Mitochondria are sequestered in Rab5-positive enlarged endosomes in BNIP3 overexpressing cells.
(a) Western blot for BNIP3 in WT and *Atg5*$^{-/-}$ MEFs overexpressing myc or myc-BNIP3. **(b)** Representative images of WT and *Atg5*$^{-/-}$ MEFs overexpressing GFP-Rab5Q79L plus empty vector or BNIP3. 24 h post-transfection, the cells were fixed and stained with anti-COX IV to label mitochondria. **(c)** Quantification of mitochondria inside GFP-Rab5Q79L positive vesicles in (n=4, *p<0.05, **p<0.01 vs Control). EEE=enlarged early endosomes. All values are means±s.e.m from independent experiments. Statistical significance was calculated using ANOVA followed by Dunnett's test for multiple comparison.

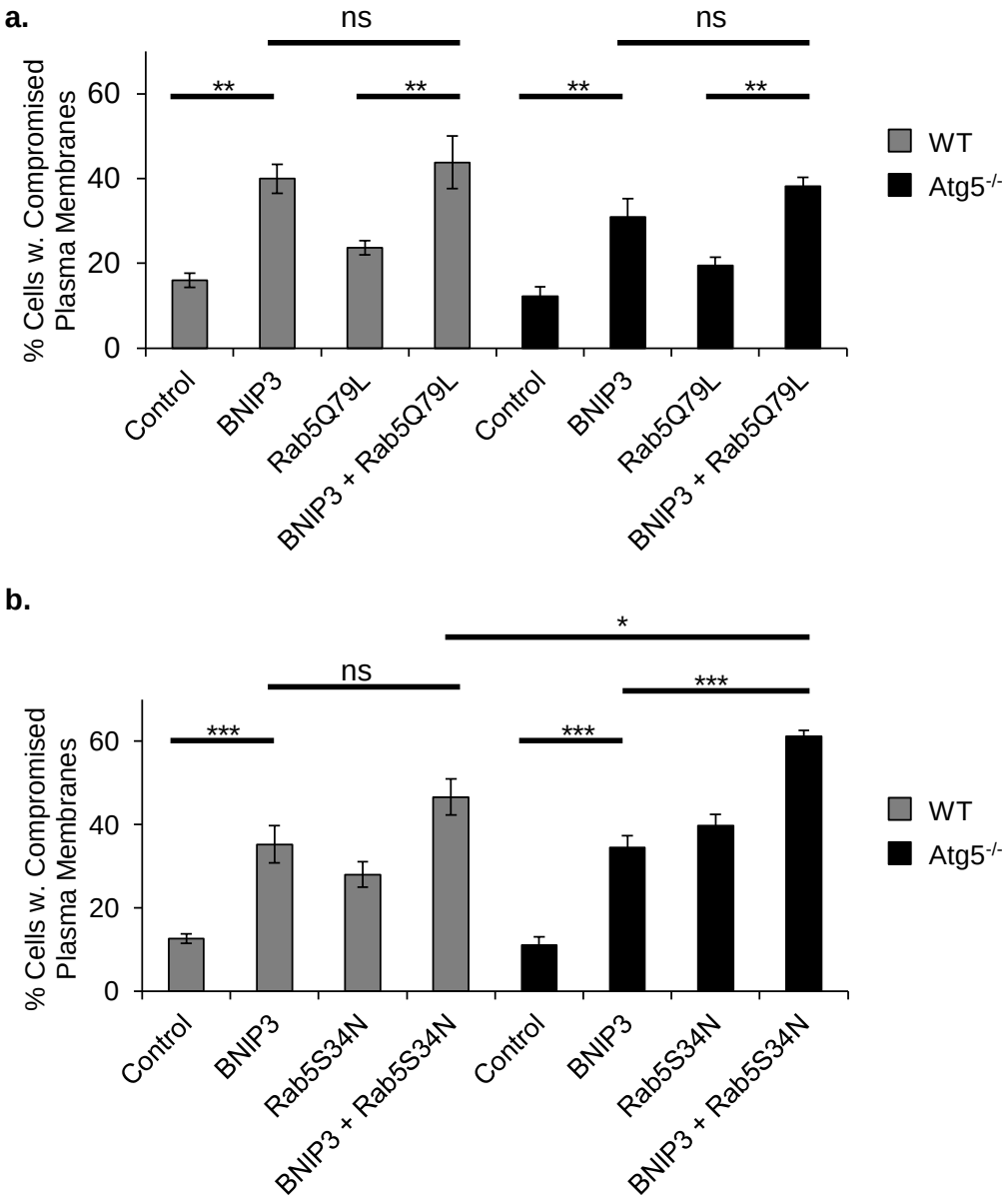

Figure 6.4. BNIP3 overexpression increases cell death.
(a) Quantification of BOBO-3 positive (dead) cells. Sequestration of mitochondria in Rab5Q79L-positive vesicles has no effect on BNIP3-mediated cell death in WT and *Atg5*$^{-/-}$ MEFs. **(b)** Quantification of BOBO-3 positive (dead) cells. Abrogation of Rab5 activity increases susceptibility to BNIP3-mediated cell death in *Atg5*$^{-/-}$ MEFs. Cell death was assessed by BOBO-3 Iodide uptake in cells overexpressing the indicated constructs (n=3, *p<0.05, **p<0.01, ***p<0.001). All values are means±s.e.m from independent experiments. Statistical significance was calculated using ANOVA followed by Dunnett's test for multiple comparison.

CHAPTER 7: DISCUSSION

7.1 Introduction

Autophagy has been extensively studied since its first description in the 1960s (Deter and De Duve, 1967). Its importance is highlighted by the founding of the journal *Autophagy* in 2005, which is dedicated to its study, and by the 2016 Nobel Prize in Physiology or Medicine awarded to Dr. Yoshinori Ohsumi for his discoveries of the mechanisms of autophagy (Nobelprize.org, 2016). This pathway is critical under a variety of conditions including starvation and immunity (Tanida, 2011). Defects in this pathway contribute to various disease conditions such as neurodegenerative diseases, diabetes, and cancer. Autophagy has been shown to be essential for the early neonatal starvation period (Kuma et al., 2004) and under homeostatic conditions (Nakai et al., 2007). Autophagy is also dysregulated in a variety of cardiovascular diseases (Tanida, 2011) and is critical for the removal of damaged mitochondria in the borderzone after myocardial infarction (Kubli et al., 2013b).

For a long time, it was believed that autophagy was the only pathway involved in degrading organelles such as mitochondria. In my dissertation research, I have uncovered a previously unidentified mechanism of mitochondrial clearance that exists in cells. My data show that autophagy-deficient cells are still able to efficiently clear their mitochondria through the endosomal-lysosomal degradation pathway. This clearance is dependent upon functional Parkin and the upstream regulator Beclin1, yet is not mediated through alternative autophagy. These mitochondria are sequestered into Rab5-positive early endosomes via the ESCRT complexes, which mature and fuse with

lysosomes for degradation. Interestingly, this pathway is activated prior to autophagy and is utilized by neonatal cardiac myocytes. Inhibition of this pathway increases stress-mediated cell death. Lastly, the mitophagy receptor BNIP3 is also able to utilize this pathway for the removal of mitochondria.

Further study of endosomal-mediated mitochondrial clearance will be important. Now that we understand that this pathway can clear organelles such as damaged mitochondria, it will be important to investigate if this pathway is utilized under other conditions or whether it is altered in disease states. As such, this pathway has the potential to be therapeutically targeted to manipulate or mitigate these states.

7.2 Identification of the Endosomal Pathway in the Degradation of Mitochondria by Parkin and BNIP3

The data presented here show that the delivery of mitochondria into the endosomes is distinct from autophagic engulfment. First, we find mitochondria within single-membrane, not double-membrane, vesicles. Second, these mitochondria can be sequestered in the absence of core autophagy genes: *Atg5* or *Atg7*. Third, in contrast to both autophagy and *Atg5/7*-independent alternative autophagy, this pathway is not dependent on Ulk1/2. Fourth, sequestration of damaged mitochondria requires the ESCRT complexes. Furthermore, while Rab5-positive endosomes are typically described as being 20-50 nm in size in the literature (Hopkins and Trowbridge, 1983), it was surprisingly to find that these vesicles can enlarge to 500-700 nm in size (Figures 4.9, 4.10) in order to accommodate the larger mitochondria. This suggests a greater versatility of endosomes than was previously thought. Moreover, 3D reconstruction of

electron tomographic volumes clearly shows that mitochondria are engulfed via a process involving invagination of the vesicle membrane. The data also show that mitochondria inside the vesicles are surrounded by intraluminal membranes. These are produced by the invagination and scission of the limiting membrane and this is reminiscent of ESCRT-dependent processes. The ESCRT complexes are responsible for cargo capturing and sorting as well as membrane invagination and scission (Henne et al., 2011). This is in contrast to autophagy, where a cup-shaped phagophore membrane binds to ubiquitinated cargo via autophagy receptors such as p62 and Nbr1, and then encloses around the cargo to form a double-membrane autophagosome (Kubli and Gustafsson, 2012).

In chapter 5, I show that activation of endosomal-mediated mitochondrial clearance precedes activation of the autophagy pathway. I propose that uptake of mitochondria into endosomes acts as a first line of defense to rapidly eliminate dysfunctional mitochondria. Early endosomes are continuously synthesized and exist in a network in cells (Zeigerer et al., 2012), whereas autophagosomes are synthesized *de novo* upon demand (Rubinsztein et al., 2012). Therefore, dysfunctional mitochondria can be more rapidly sequestered by the early endosomes. However, it is likely that if the number of damaged mitochondria exceeds the capacity of endosomal-mediated degradation, then the autophagy pathway is also activated. A similar coordination and sequential activation has been observed for the traditional autophagy and chaperon-mediated autophagy (CMA) pathways in response to stress such as starvation and oxidative stress (Kaushik et al., 2008). Traditional autophagy is rapidly activated in response to stress but then there is a switch to CMA if the stress is prolonged. Our data

also show that autophagic activity is increased when Rab5 activity is abrogated, suggesting that autophagic degradation is compensating when endosomal activity is impaired. However, it still needs to be determined if the endosomal pathway is increased when autophagy is abrogated. Moreover, future studies need to determine the context and timing of activation of these various pathways in cells.

In the absence of *Atg5/7*, alternative autophagy has been shown to play a role in degradation of specific organelles and proteins. I have also shown that alternative autophagy is not responsible for the mitochondrial clearance seen in our model. This suggests that there are multiple pathways by which damaged organelles can be cleared from the cell. It is also quite possible that in addition to conventional autophagy, alternative autophagy, and endosomal-mediated clearance, there are mechanisms of clearance that have yet to be discovered. A recent study reported that mitochondria can also be directly delivered to lysosomes via catalytically inactivated GAPDH (Hwang et al., 2015). An impairment in this process, which is also known as microautophagy (Li et al., 2012), plays a role in Huntington's disease (Hwang et al., 2015). In addition, when there is limited damage, the mitochondrion can repair itself by eliminating damaged lipids and protein via mitochondrial-derived vesicles that bud off from mitochondria and then fuse with the lysosomes (Soubannier et al., 2012a). Interestingly, it has been shown that transcellular degradation of mitochondria exists in certain areas in the CNS where mitochondria are internalized and degraded by adjacent astrocytes (Davis et al., 2014). Thus, it is clear that multiple quality control mechanisms exist to ensure rapid clearance of dysfunctional mitochondria. This redundancy ensures that mitochondria can be removed before they cause unnecessary cell death even if one of the pathways

is impaired or not functioning properly. Alternatively, different stressors may trigger different downstream clearance pathways, specific to their mode of effect. Our data suggest that the endosomal-lysosomal system is but one pathway through which mitochondria can be eliminated. Clearly, multiple levels of mitochondrial quality control exist to ensure mitochondrial health and it is very possible that additional, currently unidentified, pathways of mitochondrial quality control exist in cells.

Protein and mitochondrial quality control has proven to be pivotal in Parkinson's disease. Parkinson's disease can be broken into rare, familial or more common, sporadic cases. The protein Parkin is mutated in some forms of familial Parkinson's, whereas the endosomal pathway has been found to be defective in several sporadic forms as well (Hattori and Mizuno, 2004; Perrett et al., 2015). Both of these lead to abrogated mitochondrial clearance, which suggests that the accumulation of damaged mitochondria might be a link in their pathogenesis. Sporadic cases of Parkinson's are thought to be due to age-related or environmentally-induced defects (Benmoyal-Segal and Soreq, 2006). Thus, it is possible that age-related factors, such as increased ROS, impair proteins involved in regulating the endosomal pathway.

In agreement with the physiologic importance of the endosomal pathway in Parkinson's disease, I also provide evidence that blocking the endosomal pathway leads to increased cell death, particularly in cells that are deficient in autophagy. Moreover, I show that neonatal cardiac myocytes also utilize this pathway for mitochondrial clearance, and too are susceptible to cell death in its absence upon stress. Not only does this suggest that the endosomal pathway has an underappreciated function in protein and organelle homeostasis, but it shows that

energy-intensive cells like myocytes rely on this pathway. Since the heart has a vast number of mitochondria, and its myocytes are terminally differentiated with limited capacity to self-renew (Anversa et al., 2002), it is unsurprisingly then that there are several mechanisms by which damaged mitochondria can be removed before cell death is induced. This notion is supported by the fact that mice lacking autophagy in the heart develop normally, do not accumulate dysfunctional mitochondria, and display normal cardiac function up to 12 weeks of age or after stress. More studies are needed to determine the effects of endosomal inhibition on development, in response to stress, and its role in the heart.

One limitation of the experiments presented here is the use of FCCP to induce mitochondrial clearance. FCCP is reported to de-acidify all the compartments within the cell, including endosomes (Yamashiro et al., 1983). As such, it is possible that maturation of endosomes would be impaired, as one of the hallmarks of maturation involves vesicle acidification (Huotari and Helenius, 2011). However, we confirmed that endosomal maturation is not affected. Not only are mitochondria found to colocalize with Rab7-positive late endosomes and Lamp2-positive lysosomes, but the number of colocalization events increases along a time course, suggesting that progression through the pathway is uninhibited (Figure 4.13). This agrees with the various reports using CCCP to induce mitophagy as well (Choubey et al., 2014; Narendra et al., 2008; Tanaka et al., 2010). CCCP or FCCP would similarly be expected to inhibit lysosomal acidification and thus mitochondrial degradation through PINK1-Parkin-mediated mitophagy, but this does not appear to be the case.

7.3 Molecular Mechanism

Furthermore, it is clear that many of the proteins involved in cellular quality control regulate multiple quality control pathways. For instance, Beclin1 appears to be a central regulator of the endosomal, traditional and alternative autophagy pathways (McKnight et al., 2014; Nishida et al., 2009). Similarly, the Rab proteins are well known for their roles in regulating endosomal trafficking, but recent studies have found that some of the Rab proteins can also regulate autophagy (Jean et al., 2015; Roy et al., 2013). Parkin is known to mark mitochondria for autophagic degradation and here we demonstrate that Parkin also labels mitochondria for the endosomes. Both endosomes and autophagosomes recognize ubiquitinated targets (Raiborg and Stenmark, 2009). Parkin is also involved in the formation of a subset of MDVs that are destined for delivery to late endosomes/lysosomes (McLelland et al., 2014). Although the Rab5 pathway described in our study and formation of MDVs both utilize the endosomal-lysosomal degradation pathway and are independent of Atg5, these are clearly two distinct mechanisms of mitochondrial quality control. First, we observe that entire mitochondria are sequestered inside large (~500 nm) single membrane Rab5-positive early endosomes. In contrast, MDVs are small vesicles (70-150 nm) containing select mitochondrial proteins and lipids that bud off the outer mitochondrial membrane mitochondria which are then delivered directly to LAMP1-positive late endosomes/lysosomes. Finally, our data show that the mitochondria are captured by the early endosomes through ESCRT-mediated membrane invagination and subsequent scission, whereas MDVs directly fuse with late endosomes/lysosomes via Stx17 and SNARE complexes to deliver their content (McLelland and Lee, 2016). Thus, it is likely

that formation of MDVs occurs when there is limited damage in an attempt to avoid degradation of the entire mitochondrion. However, when the damage is too extensive, then the entire mitochondrion is sequestered inside a Rab5-positive early endosome.

The data presented in chapter 4 illustrate that the endosomes can sequester damaged mitochondria via the ESCRT complexes, mature into late endosomes, and fuse with lysosomes for cargo degradation. Furthermore, the endosomal degradation pathway seems to be under the regulation of Beclin1. As an upstream regulator of both the autophagy and endosomal pathways, it may simultaneously activate both pathways equally, or there may be other levels of regulation that drive either autophagy or endosomal-degradation depending on the specific cellular conditions. For instance, Beclin1 could form different protein complexes, each of which would drive one particular downstream pathway. Alternatively, Beclin1 may undergo various posttranslational modifications that would favor activation of either the endosomal or autophagy pathways. Future studies should investigate the extent of each pathway's activation and whether this can be shifted. If such a shift could be induced, it may prove to be a useful therapeutic option in patients or cell types with impaired or insufficient activity.

Up until this point, I have shown that Parkin, a mediator of mitophagy, is also capable of recruiting the endosomal pathway to induce mitochondrial clearance. In chapter 6, I have also confirmed that the mitophagy receptor BNIP3 can promote sequestration of mitochondria into Rab5-positive endosomes and that this process occurs independently of autophagy. I also found that abrogation of Rab5 led to increased susceptibility to BNIP3-mediated cell death in both WT and autophagy-deficient MEFs, suggesting that this is a protective mechanism activated by cells. BNIP3

is known to induce autophagy and mitophagy when overexpressed in cells (Hamacher-Brady et al., 2007; Rikka et al., 2011; Zhang et al., 2016). Thus, additional studies are needed to examine if BNIP3 simultaneously activates autophagy and endosomal-mediated mitochondrial clearance or if their timing of activation is different. Moreover, the mechanism by which BNIP3 can activate the endosomal pathway needs to be further examined. BNIP3 may directly tether mitochondria to endosomes, or it may activate a residential mitochondrial ubiquitin ligase, such as March5 or MULAN/MAPL. This ligase could then ubiquitinate mitochondria to be bound and sequestered by ESCRTs. Lastly, these studies illustrate that there are several mechanisms of activating the endosomal pathway for protein and organelle homeostasis. Thus far I have shown that both Parkin and BNIP3 can activate the endosomal pathway to clear damaged mitochondria. This underscores the idea that there are several redundant pathways for protein and organelle quality control within the cell to remove critically damaged organelles such as mitochondria.

While the work I have presented here is both exciting and novel, there are a few limitations to this study. Although overexpression of proteins is very useful tool to study protein function and signaling pathways, there is always the concern that the overexpression interferes with normal cell function. To study Parkin-mediated mitochondrial degradation, we relied on overexpression of Parkin in cells. One advantage is that we can study Parkin and mutants in cells such as MEFs that have no detectable levels of endogenous Parkin. Second, using fluorescently tagged Parkin has allowed us and numerous other investigators (Chen and Dorn, 2013; Geisler et al., 2010; Narendra et al., 2008) to monitor translocation of Parkin to mitochondria in live

cells in response to stress. The disadvantages are that to visualize and study Parkin in cells, the protein is expressed at levels that are well above the normal physiological levels in cells and tissues.

7.4 Model

In light of the new findings illustrating a novel Parkin-mediated mitochondrial clearance pathway through the endosomal-lysosomal pathway, I propose a model of endosomal-mediated mitochondrial degradation (Figure 7.1). In this model, stress associated with mitochondrial damage induces Parkin recruitment and ubiquitination of proteins on the outer mitochondrial membrane. The ubiquitinated mitochondrion is recognized and captured by the ESCRT complexes on the early endosome. The ESCRT machinery then induces invagination and subsequent scission of the endosomal membrane, leading to internalization of the mitochondrion in the lumen of the endosome. The early endosome then matures and fuses with a lysosome for cargo degradation. Thus, damaged mitochondria may either be degraded through the endosomal-lysosomal pathway as a first response or through the autophagy pathway when the stress is prolonged (Figure 7.2).

7.5 Relevance to Disease and Therapeutic Potential

While the endosomal pathway has a role in receptor recycling and degradation, it has not until now, been implicated in larger scale levels of protein and organelle quality control such as the removal of mitochondria. As such, it is unknown if there are any diseases that are a direct result of impairment of this pathway, or if impairment

contributes to already known pathologies, such as in Parkinson's patients with Parkin mutations. Now that we know the full capabilities of the endosomal pathway, this pathway can be studied in the context of diseases states.

It is known that heart function is intricately linked to mitochondrial health. Thus, clearance of damaged mitochondria is critical to the continued survival of individual cardiac myocytes. Our studies here show not only that the endosomal pathway can help in the clearance of damaged mitochondria, but that cardiac myocytes *in vitro* utilize this mechanism in response to mitochondrial damage. Future studies need to examine the role of the endosomal-lysosomal degradation pathway *in vivo*, and determine whether any dysfunctions in this pathway result or contribute to known cardiovascular diseases.

Furthermore, it is possible that one can therapeutically target the endosomal-lysosomal pathway to compensate for other diseases states, such as impaired autophagy. However, to address this, some remaining questions need to be answered. For instance, if the endosomal-lysosomal pathway can be driven by overexpression of a protein or the presence of a drug, this may compensate for defects caused by impaired of insufficient autophagy. Given that I obtained similar results with endogenous Rab5 and overexpression of GFP-Rab5 indicates that Rab5 is not a rate-limiting step. However, if other downstream proteins, such as Rab7, are rate-limiting, these can then be targeted. Further studies are required so that we can better understand the interplay between the endosomal and other pathways, and test ways to alter its function.

7.6 Future Studies

The work presented here adds significant impact to the fields of autophagy, mitochondrial quality control, and endosomal function. It also highlights the coordination between multiple mitochondrial quality control pathways. However, this work raises several new questions that need to be explored in future studies.

In this work, I have described a new phenomenon of mitochondrial clearance that uses the endosomal-lysosomal pathway. In addition, I have also identified some details in regards to the downstream steps of the mechanism from Beclin1 involvement, to Parkin-mediated ubiquitination, ESCRT-mediated sequestration, endosome maturation, and fusion with lysosomes. However, I have not yet examined the signaling pathways upstream of this process. Damaged mitochondria can affect ATP levels and production of ROS. Studies must be performed to determine if either, or both, of these are responsible for the activation of the endosomal pathway. Furthermore, it would be of interest to see if the trigger or triggers is specific for endosomal degradation or if both autophagy and endosomal degradation are activated concurrently by the same stimuli. Additionally, more experiments need to be performed in order to determine how BNIP3 overexpression activates endosomal engulfment of mitochondria. Whether ESCRT complexes are involved, and if not, what is involved, also needs to be determined.

The electron microscopy data clearly show that mitochondria are contained within intraluminal vesicles, within the endosomes. Given that ILVs can be released as exosomes, the question is raised whether these mitochondria can be expelled into the extracellular space as large exosomes. Large membrane-bound vesicles which can contain mitochondria, have been reported to be released from touch neurons in *c. elegans* (Melentijevic et al., 2017). Whether these two mechanisms are related has yet

to be determined. Moreover, if these mitochondria can be released as exosomes, the next question becomes what is their final destination? In the brain, neurons can pass their mitochondria to glia cells for degradation (Davis et al., 2014), so perhaps a similar mechanism exists in the heart and other tissues. Perhaps several mechanisms of clearance are activated under severe stress in order to clear the damage as quickly as possible, thus implementing mitophagy, endosomal-mediated clearance, and extracellular release simultaneously. Extracellular release also raises its own questions including how does this affect the immune system and a systemic inflammatory response. More studies need to be performed to determine to what extent, and under what conditions a mitochondrion may be degraded through any one of these pathways.

At the level of the whole organism, we have yet to explore whether this phenomena exists outside of MEFs or the heart. Since the brain is also highly metabolically active like the heart, it may also make use of this pathway. Already there are some links between these two organs. For instance, Parkin plays an important role in mitochondrial maintenance in both tissues (Kubli et al., 2013b; Palacino et al., 2004). Several neurodegenerative diseases, like Huntington's disease, epilepsy, and amyotrophic lateral sclerosis, also display cardiac abnormalities (Finsterer and Wahbi, 2014; Mielcarek et al., 2014). Thus, studying the regulation and dysregulation of the endosomal pathway may bring to light the mechanism for some neuropathologies. In both the brain and the heart, more work must also be done to study the role of endosomal-mediated degradation in development and in response to stress.

7.7 Concluding Remarks

Quality control pathways are important for cellular health, and defects in these pathways contribute to several disease states. Specifically, mitochondrial dysfunction contributes both to heart failure and the aging process (Baker and Haynes, 2011; Kujoth et al., 2005; Marin-Garcia and Goldenthal, 2002). With an aging population and a high incidence of cardiovascular diseases, accounting for 30% of all deaths (Mozaffarian et al., 2016), it is critical that we understand the underlying mechanisms in order to combat them. The work presented here introduces a new pathway of mitochondrial quality control that adds to the list of existing quality control mechanisms, and may provide an avenue for tackling diseases.

Parts of Chapter 7 were originally published in *Nature Communications*. Hammerling, B. C., Najor, R. H., Cortez, M. Q., Shires, S. E., Leon, L. J., Gonzalez, E. R., Boassa, D., Phan, S., Thor, A., Jimenez, R. E., Li, H., Kitsis, R. N., Dorn II, G. W., Sadoshima, J., Ellisman, M. H., Gustafsson, A. G. A Rab5 Endosomal Pathway Mediates Parkin-Dependent Mitochondrial Clearance. *Nature Communications*. 8: 14050, 2017; doi:10.1038/ncomms14050 © 2017 Nature Publishing Group. The dissertation author was the primary investigator and author of this paper.

Parts of Chapter 7 were originally published in *Small GTPases*. Hammerling, B. C., Shires, S. E., Leon, L. J., Cortez, M. Q., Gustafsson, A. G. Isolation of Rab5-Positive Endosomes Reveals a New Mitochondrial Degradation Pathway Utilized by BINP3 and Parkin. *Small GTPases*. 1-8, 2017; doi: doi:10.1080/21541248.2017.1342749. © 2017 Taylor & Francis Online. The dissertation author was the primary investigator and author of this paper.

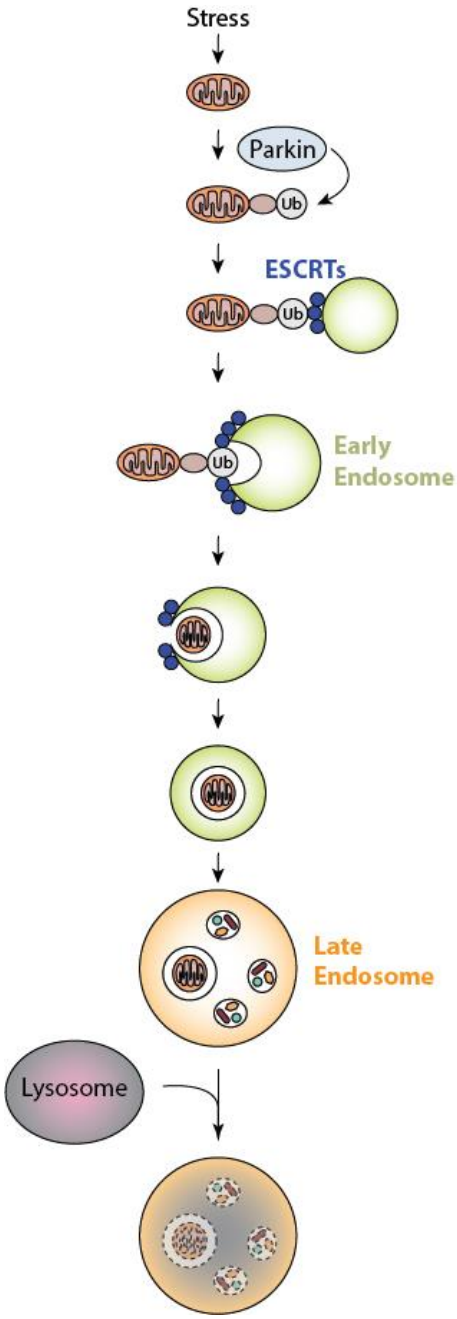

Figure 7.1. Model of endosomal sequestration and degradation of a damaged mitochondrion.
Stress, such as FCCP or sI/R, induces Parkin recruitment and ubiquitination of proteins in the outer mitochondrial membrane. The ubiquitinated mitochondrion is captured by the ESCRT complexes on the early endosome. The ESCRT machinery induces invagination and subsequent scission of the endosome membrane, leading to internalization of the mitochondrion in the lumen of the endosome.

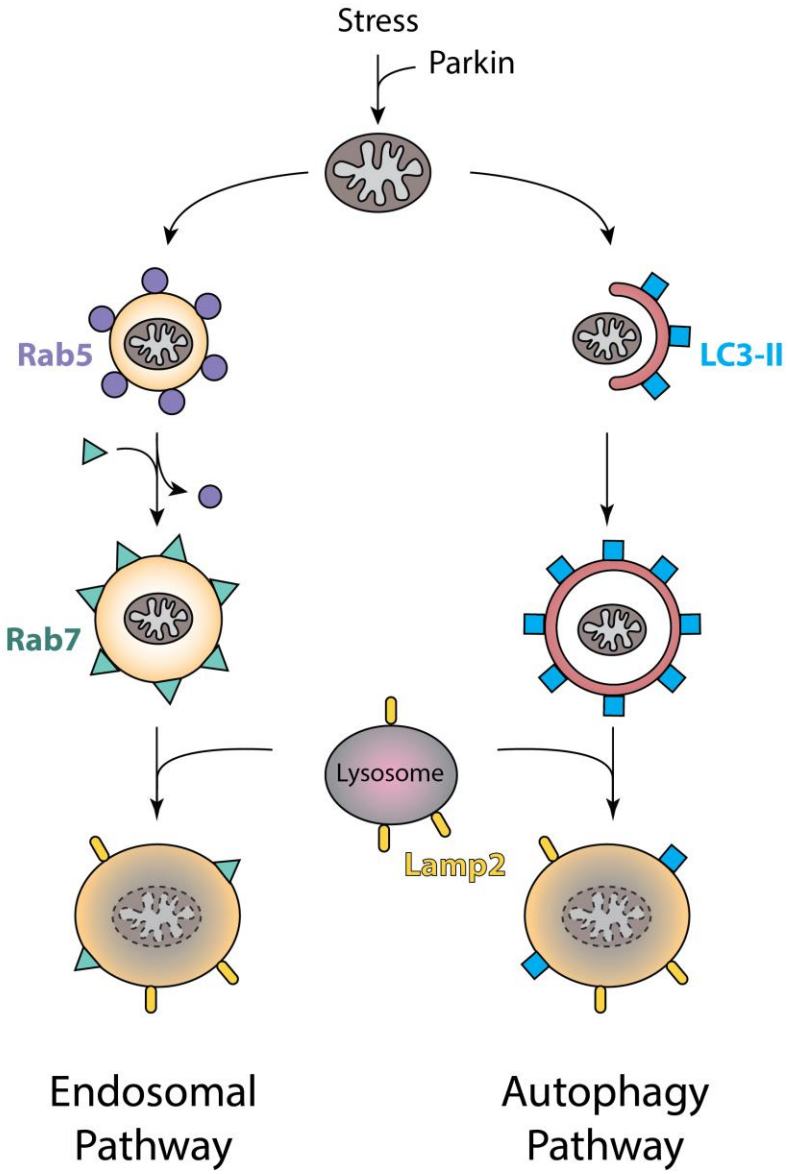

Figure 7.2. Endosomal- or autophagy-mediated degradation of mitochondria. Stress-induced mitochondrial damage can promote clearance of mitochondria through the endosomal pathway (left) or autophagy (right). Both pathways result in the mitochondria-containing vesicle fusing with a lysosome for degradation.

REFERENCES

Anversa, P., A. Leri, J. Kajstura, and B. Nadal-Ginard. 2002. Myocyte growth and cardiac repair. *Journal of molecular and cellular cardiology*. 34:91-105.

Augustin, S., M. Nolden, S. Muller, O. Hardt, I. Arnold, and T. Langer. 2005. Characterization of peptides released from mitochondria: evidence for constant proteolysis and peptide efflux. *The Journal of biological chemistry*. 280:2691-2699.

Babst, M. 2011. MVB vesicle formation: ESCRT-dependent, ESCRT-independent and everything in between. *Current opinion in cell biology*. 23:452-457.

Baker, B.M., and C.M. Haynes. 2011. Mitochondrial protein quality control during biogenesis and aging. *Trends in biochemical sciences*. 36:254-261.

Bampton, E.T., C.G. Goemans, D. Niranjan, N. Mizushima, and A.M. Tolkovsky. 2005. The dynamics of autophagy visualized in live cells: from autophagosome formation to fusion with endo/lysosomes. *Autophagy*. 1:23-36.

Benmoyal-Segal, L., and H. Soreq. 2006. Gene-environment interactions in sporadic Parkinson's disease. *Journal of neurochemistry*. 97:1740-1755.

Bhandari, P., M. Song, Y. Chen, Y. Burelle, and G.W. Dorn, 2nd. 2014. Mitochondrial contagion induced by Parkin deficiency in Drosophila hearts and its containment by suppressing mitofusin. *Circulation research*. 114:257-265.

Billia, F., L. Hauck, F. Konecny, V. Rao, J. Shen, and T.W. Mak. 2011. PTEN-inducible kinase 1 (PINK1)/Park6 is indispensable for normal heart function. *P Natl Acad Sci USA*. 108:9572-9577.

Bota, D.A., and K.J. Davies. 2002. Lon protease preferentially degrades oxidized mitochondrial aconitase by an ATP-stimulated mechanism. *Nature cell biology*. 4:674-680.

Bota, D.A., J.K. Ngo, and K.J. Davies. 2005. Downregulation of the human Lon protease impairs mitochondrial structure and function and causes cell death. *Free radical biology & medicine*. 38:665-677.

Bota, D.A., H. Van Remmen, and K.J. Davies. 2002. Modulation of Lon protease activity and aconitase turnover during aging and oxidative stress. *FEBS letters*. 532:103-106.

Cadete, V.J., S. Deschenes, A. Cuillerier, F. Brisebois, A. Sugiura, A. Vincent, D. Turnbull, M. Picard, H.M. McBride, and Y. Burelle. 2016. Formation of mitochondrial-derived vesicles is an active and physiologically relevant mitochondrial quality control process in the cardiac system. *The Journal of physiology*. 594:5343-5362.

Campsteijn, C., M. Vietri, and H. Stenmark. 2016. Novel ESCRT functions in cell biology: spiraling out of control? *Current opinion in cell biology*. 41:1-8.

Chan, D.C. 2012. Fusion and fission: interlinked processes critical for mitochondrial health. *Annual review of genetics*. 46:265-287.

Chen, H., S.A. Detmer, A.J. Ewald, E.E. Griffin, S.E. Fraser, and D.C. Chan. 2003. Mitofusins Mfn1 and Mfn2 coordinately regulate mitochondrial fusion and are essential for embryonic development. *The Journal of cell biology*. 160:189-200.

Chen, L., T. Liu, A. Tran, X. Lu, A.A. Tomilov, V. Davies, G. Cortopassi, N. Chiamvimonvat, D.M. Bers, M. Votruba, and A.A. Knowlton. 2012. OPA1 mutation and late-onset cardiomyopathy: mitochondrial dysfunction and mtDNA instability. *Journal of the American Heart Association*. 1:e003012.

Chen, Y., and G.W. Dorn. 2013. PINK1-phosphorylated Mitofusin 2 Is a Parkin receptor for culling damaged mitochondria. *Science*. 340:471-475.

Chen, Y., Y.Q. Liu, and G.W. Dorn. 2011. Mitochondrial fusion is essential for organelle function and cardiac homeostasis. *Circulation research*. 109:1327-U1336.

Chen, Y.R., and J.L. Zweier. 2014. Cardiac mitochondria and reactive oxygen species generation. *Circulation research*. 114:524-537.

Chiong, M., Z.V. Wang, Z. Pedrozo, D.J. Cao, R. Troncoso, M. Ibacache, A. Criollo, A. Nemchenko, J.A. Hill, and S. Lavandero. 2011. Cardiomyocyte death: mechanisms and translational implications. *Cell death & disease*. 2:e244.

Choubey, V., M. Cagalinec, J. Liiv, D. Safiulina, M.A. Hickey, M. Kuum, M. Liiv, T. Anwar, E.L. Eskelinen, and A. Kaasik. 2014. BECN1 is involved in the initiation of mitophagy: it facilitates PARK2 translocation to mitochondria. *Autophagy*. 10:1105-1119.

Choudhury, A., M. Dominguez, V. Puri, D.K. Sharma, K. Narita, C.L. Wheatley, D.L. Marks, and R.E. Pagano. 2002. Rab proteins mediate Golgi transport of caveola-internalized glycosphingolipids and correct lipid trafficking in Niemann-Pick C cells. *The Journal of clinical investigation*. 109:1541-1550.

Colman, R.J., R.M. Anderson, S.C. Johnson, E.K. Kastman, K.J. Kosmatka, T.M. Beasley, D.B. Allison, C. Cruzen, H.A. Simmons, J.W. Kemnitz, and R. Weindruch. 2009. Caloric restriction delays disease onset and mortality in rhesus monkeys. *Science*. 325:201-204.

Cook, K.L., D.R. Soto-Pantoja, M. Abu-Asab, P.A. Clarke, D.D. Roberts, and R. Clarke. 2014. Mitochondria directly donate their membrane to form autophagosomes during a novel mechanism of parkin-associated mitophagy. *Cell & bioscience*. 4:16.

Cuervo, A.M. 2008. Autophagy and aging: keeping that old broom working. *Trends Genet*. 24:604-612.

Curran, J., M.A. Makara, S.C. Little, H. Musa, B. Liu, X. Wu, I. Polina, J.S. Alecusan, P. Wright, J. Li, G.E. Billman, P.A. Boyden, S. Gyorke, H. Band, T.J. Hund, and P.J. Mohler. 2014. EHD3-dependent endosome pathway regulates cardiac membrane excitability and physiology. *Circulation research*. 115:68-78.

Davis, C.H., K.Y. Kim, E.A. Bushong, E.A. Mills, D. Boassa, T. Shih, M. Kinebuchi, S. Phan, Y. Zhou, N.A. Bihlmeyer, J.V. Nguyen, Y. Jin, M.H. Ellisman, and N. Marsh-Armstrong. 2014. Transcellular degradation of axonal mitochondria. *Proceedings of the National Academy of Sciences of the United States of America*. 111:9633-9638.

Day, R.N., and M.W. Davidson. 2009. The fluorescent protein palette: tools for cellular imaging. *Chemical Society reviews*. 38:2887-2921.

Delaval, E., M. Perichon, and B. Friguet. 2004. Age-related impairment of mitochondrial matrix aconitase and ATP-stimulated protease in rat liver and heart. *European journal of biochemistry / FEBS*. 271:4559-4564.

Deter, R.L., and C. De Duve. 1967. Influence of glucagon, an inducer of cellular autophagy, on some physical properties of rat liver lysosomes. *The Journal of cell biology*. 33:437-449.

Ding, W.X., H.M. Ni, M. Li, Y. Liao, X.Y. Chen, D.B. Stolz, G.W. Dorn, and X.M. Yin. 2010. Nix is critical to two distinct phases of mitophagy, reactive oxygen species-mediated autophagy induction and Parkin-ubiquitin-p62-mediated mitochondrial priming. *Journal of Biological Chemistry*. 285:27879-27890.

Dorn, G.W., 2nd, and R.N. Kitsis. 2015. The mitochondrial dynamism-mitophagy-cell death interactome: multiple roles performed by members of a mitochondrial molecular ensemble. *Circulation research*. 116:167-182.

Doyotte, A., M.R. Russell, C.R. Hopkins, and P.G. Woodman. 2005. Depletion of TSG101 forms a mammalian "Class E" compartment: a multicisternal early endosome with multiple sorting defects. *J Cell Sci*. 118:3003-3017.

Drose, S., and K. Altendorf. 1997. Bafilomycins and concanamycins as inhibitors of V-ATPases and P-ATPases. *J Exp Biol*. 200:1-8.

Dunn, W.A., Jr., J.M. Cregg, J.A. Kiel, I.J. van der Klei, M. Oku, Y. Sakai, A.A. Sibirny, O.V. Stasyk, and M. Veenhuis. 2005. Pexophagy: the selective autophagy of peroxisomes. *Autophagy*. 1:75-83.

Edgar, D., I. Shabalina, Y. Camara, A. Wredenberg, M.A. Calvaruso, L. Nijtmans, J. Nedergaard, B. Cannon, N.G. Larsson, and A. Trifunovic. 2009. Random point mutations with major effects on protein-coding genes are the driving force behind premature aging in mtDNA mutator mice. *Cell metabolism*. 10:131-138.

Finsterer, J., and K. Wahbi. 2014. CNS-disease affecting the heart: brain-heart disorders. *Journal of the neurological sciences*. 345:8-14.

Funderburk, S.F., Q.J. Wang, and Z. Yue. 2010. The Beclin 1-VPS34 complex--at the crossroads of autophagy and beyond. *Trends in cell biology*. 20:355-362.

Geisler, S., K.M. Holmstrom, D. Skujat, F.C. Fiesel, O.C. Rothfuss, P.J. Kahle, and W. Springer. 2010. PINK1/Parkin-mediated mitophagy is dependent on VDAC1 and p62/SQSTM1. *Nature cell biology*. 12:119-131.

Gispert, S., D. Parganlija, M. Klinkenberg, S. Drose, I. Wittig, M. Mittelbronn, P. Grzmil, S. Koob, A. Hamann, M. Walter, F. Buchel, T. Adler, M. Hrabe de Angelis, D.H. Busch, A. Zell, A.S. Reichert, U. Brandt, H.D. Osiewacz, M. Jendrach, and G. Auburger. 2013. Loss of mitochondrial peptidase Clpp leads to infertility, hearing loss plus growth retardation via accumulation of CLPX, mtDNA and inflammatory factors. *Human molecular genetics*. 22:4871-4887.

Go, A.S., D. Mozaffarian, V.L. Roger, E.J. Benjamin, J.D. Berry, W.B. Borden, D.M. Bravata, S. Dai, E.S. Ford, C.S. Fox, S. Franco, H.J. Fullerton, C. Gillespie, S.M. Hailpern, J.A. Heit, V.J. Howard, M.D. Huffman, B.M. Kissela, S.J. Kittner, D.T. Lackland, J.H. Lichtman, L.D. Lisabeth, D. Magid, G.M. Marcus, A. Marelli, D.B. Matchar, D.K. McGuire, E.R. Mohler, C.S. Moy, M.E. Mussolino, G. Nichol, N.P. Paynter, P.J. Schreiner, P.D. Sorlie, J. Stein, T.N. Turan, S.S. Virani, N.D. Wong, D. Woo, and M.B. Turner. 2013. Heart disease and stroke statistics--2013 update: a report from the American Heart Association. *Circulation*. 127:e6-e245.

Goldman, A., L. Leinwand, and D. Spector. 1998. Cells: A Laboratory Manual. Cold Spring Harbor Laboratory Press, Cold Spring Harbor, NY. 14.

Gomes, L.C., G. Di Benedetto, and L. Scorrano. 2011. During autophagy mitochondria elongate, are spared from degradation and sustain cell viability. *Nature cell biology*. 13:589-598.

Gong, G., M. Song, G. Csordas, D.P. Kelly, S.J. Matkovich, and G.W. Dorn, 2nd. 2015. Parkin-mediated mitophagy directs perinatal cardiac metabolic maturation in mice. *Science*. 350:aad2459.

Goo, H.G., M.K. Jung, S.S. Han, H. Rhim, and S. Kang. 2013. HtrA2/Omi deficiency causes damage and mutation of mitochondrial DNA. *Biochimica et biophysica acta*. 1833:1866-1875.

Hamacher-Brady, A., N.R. Brady, S.E. Logue, M.R. Sayen, M. Jinno, L.A. Kirshenbaum, R.A. Gottlieb, and A.B. Gustafsson. 2007. Response to myocardial ischemia/reperfusion injury involves Bnip3 and autophagy. *Cell death and differentiation*. 14:146-157.

Hammerling, B.C., and A.B. Gustafsson. 2014. Mitochondrial quality control in the myocardium: cooperation between protein degradation and mitophagy. *Journal of molecular and cellular cardiology*. 75:122-130.

Hanna, R.A., M.N. Quinsay, A.M. Orogo, K. Giang, S. Rikka, and A.B. Gustafsson. 2012. Microtubule-associated protein 1 light chain 3 (LC3) interacts with Bnip3 protein to selectively remove endoplasmic reticulum and mitochondria via autophagy. *The Journal of biological chemistry*. 287:19094-19104.

Hariharan, N., Y. Ikeda, C. Hong, R.R. Alcendor, S. Usui, S. Gao, Y. Maejima, and J. Sadoshima. 2013. Autophagy plays an essential role in mediating regression of hypertrophy during unloading of the heart. *Plos One*. 8:e51632.

Hartleben, B., M. Godel, C. Meyer-Schwesinger, S. Liu, T. Ulrich, S. Kobler, T. Wiech, F. Grahammer, S.J. Arnold, M.T. Lindenmeyer, C.D. Cohen, H. Pavenstadt, D. Kerjaschki, N. Mizushima, A.S. Shaw, G. Walz, and T.B. Huber. 2010. Autophagy influences glomerular disease susceptibility and maintains podocyte homeostasis in aging mice. *J Clin Invest*. 120:1084-1096.

Hattori, N., and Y. Mizuno. 2004. Pathogenetic mechanisms of parkin in Parkinson's disease. *Lancet (London, England)*. 364:722-724.

Hayashida, K., P.D. Stahl, and P.W. Park. 2008. Syndecan-1 ectodomain shedding is regulated by the small GTPase Rab5. *The Journal of biological chemistry*. 283:35435-35444.

Haynes, C.M., Y. Yang, S.P. Blais, T.A. Neubert, and D. Ron. 2010. The matrix peptide exporter HAF-1 signals a mitochondrial UPR by activating the transcription factor ZC376.7 in C. elegans. *Mol Cell*. 37:529-540.

Henne, W.M., N.J. Buchkovich, and S.D. Emr. 2011. The ESCRT pathway. *Developmental cell*. 21:77-91.

Hirosako, K., H. Imasato, Y. Hirota, T. Kuronita, N. Masuyama, M. Nishioka, A. Umeda, H. Fujita, M. Himeno, and Y. Tanaka. 2004. 3-Methyladenine specifically inhibits retrograde transport of cation-independent mannose 6-phosphate/insulin-like growth factor II receptor from the early endosome to the TGN. *Biochemical and biophysical research communications*. 316:845-852.

Hirota, Y., S. Yamashita, Y. Kurihara, X. Jin, M. Aihara, T. Saigusa, D. Kang, and T. Kanki. 2015. Mitophagy is primarily due to alternative autophagy and requires the MAPK1 and MAPK14 signaling pathways. *Autophagy*. 11:332-343.

Hollville, E., R.G. Carroll, S.P. Cullen, and S.J. Martin. 2014. Bcl-2 family proteins participate in mitochondrial quality control by regulating Parkin/PINK1-dependent mitophagy. *Mol Cell*. 55:451-466.

Honda, H.M., P. Korge, and J.N. Weiss. 2005. Mitochondria and ischemia/reperfusion injury. *Annals of the New York Academy of Sciences*. 1047:248-258.

Honda, S., S. Arakawa, Y. Nishida, H. Yamaguchi, E. Ishii, and S. Shimizu. 2014. Ulk1-mediated Atg5-independent macroautophagy mediates elimination of mitochondria from embryonic reticulocytes. *Nature communications*. 5:4004.

Hopkins, C.R., and I.S. Trowbridge. 1983. Internalization and processing of transferrin and the transferrin receptor in human carcinoma A431 cells. *The Journal of cell biology*. 97:508-521.

Hoshino, A., Y. Mita, Y. Okawa, M. Ariyoshi, E. Iwai-Kanai, T. Ueyama, K. Ikeda, T. Ogata, and S. Matoba. 2013. Cytosolic p53 inhibits Parkin-mediated mitophagy and promotes mitochondrial dysfunction in the mouse heart. *Nature communications*. 4:2308.

Hoshino, A., Y. Okawa, M. Ariyoshi, S. Kaimoto, M. Uchihashi, K. Fukai, E. Iwai-Kanai, and S. Matoba. 2014. Oxidative post-translational modifications develop LONP1 dysfunction in pressure overload heart failure. *Circulation. Heart failure*. 7:500-509.

Huang, C., A.M. Andres, E.P. Ratliff, G. Hernandez, P. Lee, and R.A. Gottlieb. 2011. Preconditioning involves selective mitophagy mediated by Parkin and p62/SQSTM1. *Plos One*. 6:e20975.

Huang, C., X. Zhang, J.M. Ramil, S. Rikka, L. Kim, Y. Lee, N.A. Gude, P.A. Thistlethwaite, M.A. Sussman, R.A. Gottlieb, and A.B. Gustafsson. 2010. Juvenile exposure to anthracyclines impairs cardiac progenitor cell function and vascularization resulting in greater susceptibility to stress-induced myocardial injury in adult mice. *Circulation*. 121:675-683.

Huotari, J., and A. Helenius. 2011. Endosome maturation. *The EMBO journal*. 30:3481-3500.

Hwang, S., M.H. Disatnik, and D. Mochly-Rosen. 2015. Impaired GAPDH-induced mitophagy contributes to the pathology of Huntington's disease. *EMBO molecular medicine*. 7:1307-1326.

Jean, S., S. Cox, S. Nassari, and A.A. Kiger. 2015. Starvation-induced MTMR13 and RAB21 activity regulates VAMP8 to promote autophagosome-lysosome fusion. *Embo Rep*. 16:297-311.

Jin, S.M., M. Lazarou, C. Wang, L.A. Kane, D.P. Narendra, and R.J. Youle. 2010. Mitochondrial membrane potential regulates PINK1 import and proteolytic destabilization by PARL. *The Journal of cell biology*. 191:933-942.

Kabeya, Y., N. Mizushima, T. Ueno, A. Yamamoto, T. Kirisako, T. Noda, E. Kominami, Y. Ohsumi, and T. Yoshimori. 2000. LC3, a mammalian homologue of yeast Apg8p, is localized in autophagosome membranes after processing. *The EMBO journal*. 19:5720-5728.

Kanai, F., H. Liu, S.J. Field, H. Akbary, T. Matsuo, G.E. Brown, L.C. Cantley, and M.B. Yaffe. 2001. The PX domains of p47phox and p40phox bind to lipid products of PI(3)K. *Nature cell biology*. 3:675-678.

Kang, S., J.P. Louboutin, P. Datta, C.P. Landel, D. Martinez, A.S. Zervos, D.S. Strayer, T. Fernandes-Alnemri, and E.S. Alnemri. 2013. Loss of HtrA2/Omi activity in non-neuronal tissues of adult mice causes premature aging. *Cell death and differentiation*. 20:259-269.

Kang, S.G., M.N. Dimitrova, J.Q. Ortega, A. Ginsburg, and M.R. Maurizi. 2005. Human mitochondrial ClpP is a stable heptamer that assembles into a tetradecamer in the presence of ClpX. *Journal of Biological Chemistry*. 280:35424-35432.

Karwatowska-Prokopczuk, E., J.A. Nordberg, H.L. Li, R.L. Engler, and R.A. Gottlieb. 1998. Effect of vacuolar proton ATPase on pHi, Ca2+, and apoptosis in neonatal cardiomyocytes during metabolic inhibition/recovery. *Circulation research*. 82:1139-1144.

Kaushik, S., A.C. Massey, N. Mizushima, and A.M. Cuervo. 2008. Constitutive activation of chaperone-mediated autophagy in cells with impaired macroautophagy. *Molecular biology of the cell*. 19:2179-2192.

Kirchhofer, A., J. Helma, K. Schmidthals, C. Frauer, S. Cui, A. Karcher, M. Pellis, S. Muyldermans, C.S. Casas-Delucchi, M.C. Cardoso, H. Leonhardt, K.P. Hopfner, and U. Rothbauer. 2010. Modulation of protein properties in living cells using nanobodies. *Nature structural & molecular biology*. 17:133-138.

Kirkin, V., D.G. McEwan, I. Novak, and I. Dikic. 2009. A role for ubiquitin in selective autophagy. *Mol Cell*. 34:259-269.

Komatsu, M., S. Waguri, M. Koike, Y.S. Sou, T. Ueno, T. Hara, N. Mizushima, J. Iwata, J. Ezaki, S. Murata, J. Hamazaki, Y. Nishito, S. Iemura, T. Natsume, T. Yanagawa, J. Uwayama, E. Warabi, H. Yoshida, T. Ishii, A. Kobayashi, M. Yamamoto, Z. Yue, Y. Uchiyama, E. Kominami, and K. Tanaka. 2007. Homeostatic levels of p62 control cytoplasmic inclusion body formation in autophagy-deficient mice. *Cell*. 131:1149-1163.

Komatsu, M., S. Waguri, T. Ueno, J. Iwata, S. Murata, I. Tanida, J. Ezaki, N. Mizushima, Y. Ohsumi, Y. Uchiyama, E. Kominami, K. Tanaka, and T. Chiba. 2005. Impairment of starvation-induced and constitutive autophagy in Atg7-deficient mice. *The Journal of cell biology*. 169:425-434.

Kotiadis, V.N., M.R. Duchen, and L.D. Osellame. 2014. Mitochondrial quality control and communications with the nucleus are important in maintaining mitochondrial function and cell health. *Biochimica et biophysica acta*. 1840:1254-1265.

Kremer, J.R., D.N. Mastronarde, and J.R. McIntosh. 1996. Computer visualization of three-dimensional image data using IMOD. *Journal of structural biology*. 116:71-76.

Kubli, D.A., and A.B. Gustafsson. 2012. Mitochondria and mitophagy: the yin and yang of cell death control. *Circulation research*. 111:1208-1221.

Kubli, D.A., M.N. Quinsay, and A.B. Gustafsson. 2013a. Parkin deficiency results in accumulation of abnormal mitochondria in aging myocytes. *Communicative & integrative biology*. 6:e24511.

Kubli, D.A., M.N. Quinsay, C. Huang, Y. Lee, and A.B. Gustafsson. 2008. Bnip3 functions as a mitochondrial sensor of oxidative stress during myocardial ischemia and reperfusion. *American journal of physiology. Heart and circulatory physiology*. 295:H2025-2031.

Kubli, D.A., J.E. Ycaza, and A.B. Gustafsson. 2007. Bnip3 mediates mitochondrial dysfunction and cell death through Bax and Bak. *The Biochemical journal*. 405:407-415.

Kubli, D.A., X. Zhang, Y. Lee, R.A. Hanna, M.N. Quinsay, C.K. Nguyen, R. Jimenez, S. Petrosyan, A.N. Murphy, and A.B. Gustafsson. 2013b. Parkin protein deficiency exacerbates cardiac injury and reduces survival following myocardial infarction. *The Journal of biological chemistry*. 288:915-926.

Kujoth, G.C., A. Hiona, T.D. Pugh, S. Someya, K. Panzer, S.E. Wohlgemuth, T. Hofer, A.Y. Seo, R. Sullivan, W.A. Jobling, J.D. Morrow, H. Van Remmen, J.M. Sedivy, T. Yamasoba, M. Tanokura, R. Weindruch, C. Leeuwenburgh, and T.A. Prolla. 2005. Mitochondrial DNA mutations, oxidative stress, and apoptosis in mammalian aging. *Science*. 309:481-484.

Kuma, A., M. Hatano, M. Matsui, A. Yamamoto, H. Nakaya, T. Yoshimori, Y. Ohsumi, T. Tokuhisa, and N. Mizushima. 2004. The role of autophagy during the early neonatal starvation period. *Nature*. 432:1032-1036.

Kundu, M., T. Lindsten, C.Y. Yang, J. Wu, F. Zhao, J. Zhang, M.A. Selak, P.A. Ney, and C.B. Thompson. 2008. Ulk1 plays a critical role in the autophagic clearance of mitochondria and ribosomes during reticulocyte maturation. *Blood*. 112:1493-1502.

Lam, S.S., J.D. Martell, and K.J. Kamer. 2015. Directed evolution of APEX2 for electron microscopy and proximity labeling. *Nat. Methods*. 12:51-54.

Lau, E., D. Wang, J. Zhang, H. Yu, M.P. Lam, X. Liang, N. Zong, T.Y. Kim, and P. Ping. 2012. Substrate- and isoform-specific proteome stability in normal and stressed cardiac mitochondria. *Circulation research*. 110:1174-1178.

Lee, I.H., Y. Kawai, M.M. Fergusson, Rovira, II, A.J. Bishop, N. Motoyama, L. Cao, and T. Finkel. 2012. Atg7 modulates p53 activity to regulate cell cycle and survival during metabolic stress. *Science*. 336:225-228.

Li, W.W., J. Li, and J.K. Bao. 2012. Microautophagy: lesser-known self-eating. *Cellular and molecular life sciences : CMLS*. 69:1125-1136.

Livnat-Levanon, N., and M.H. Glickman. 2011. Ubiquitin-proteasome system and mitochondria - reciprocity. *Biochimica et biophysica acta*. 1809:80-87.

Ma, T., J. Li, Y. Xu, C. Yu, T. Xu, H. Wang, K. Liu, N. Cao, B.M. Nie, S.Y. Zhu, S. Xu, K. Li, W.G. Wei, Y. Wu, K.L. Guan, and S. Ding. 2015. Atg5-independent autophagy regulates mitochondrial clearance and is essential for iPSC reprogramming. *Nature cell biology*. 17:1379-1387.

Marchese, A., M.M. Paing, B.R. Temple, and J. Trejo. 2008. G protein-coupled receptor sorting to endosomes and lysosomes. *Annual review of pharmacology and toxicology*. 48:601-629.

Marin-Garcia, J., and M.J. Goldenthal. 2002. Understanding the impact of mitochondrial defects in cardiovascular disease: a review. *Journal of cardiac failure*. 8:347-361.

Martin, S.J., S.V. Lennon, A.M. Bonham, and T.G. Cotter. 1990. Induction of apoptosis (programmed cell death) in human leukemic HL-60 cells by inhibition of RNA or protein synthesis. *Journal of immunology (Baltimore, Md. : 1950)*. 145:1859-1867.

Martins, L.M., A. Morrison, K. Klupsch, V. Fedele, N. Moisoi, P. Teismann, A. Abuin, E. Grau, M. Geppert, G.P. Livi, C.L. Creasy, A. Martin, I. Hargreaves, S.J. Heales, H. Okada, S. Brandner, J.B. Schulz, T. Mak, and J. Downward. 2004. Neuroprotective role of the Reaper-related serine protease HtrA2/Omi revealed by targeted deletion in mice. *Mol Cell Biol*. 24:9848-9862.

Matsuda, N., S. Sato, K. Shiba, K. Okatsu, K. Saisho, C.A. Gautier, Y.S. Sou, S. Saiki, S. Kawajiri, F. Sato, M. Kimura, M. Komatsu, N. Hattori, and K. Tanaka. 2010. PINK1 stabilized by mitochondrial depolarization recruits Parkin to damaged mitochondria and activates latent Parkin for mitophagy. *The Journal of cell biology*. 189:211-221.

Maxfield, F.R., and T.E. McGraw. 2004. Endocytic recycling. *Nature reviews. Molecular cell biology*. 5:121-132.

McKnight, N.C., Y. Zhong, M.S. Wold, S. Gong, G.R. Phillips, Z. Dou, Y. Zhao, N. Heintz, W.X. Zong, and Z. Yue. 2014. Beclin 1 is required for neuron viability and regulates endosome pathways via the UVRAG-VPS34 complex. *PLoS genetics*. 10:e1004626.

McLelland, G.L., and S.A. Lee. 2016. Syntaxin-17 delivers PINK1/parkin-dependent mitochondrial vesicles to the endolysosomal system. *The Journal of cell biology*. 214:275-291.

McLelland, G.L., V. Soubannier, C.X. Chen, H.M. McBride, and E.A. Fon. 2014. Parkin and PINK1 function in a vesicular trafficking pathway regulating mitochondrial quality control. *The EMBO journal*. 33:282-295.

Melentijevic, I., M.L. Toth, M.L. Arnold, R.J. Guasp, G. Harinath, K.C. Nguyen, D. Taub, J.A. Parker, C. Neri, C.V. Gabel, D.H. Hall, and M. Driscoll. 2017. C. elegans neurons jettison protein aggregates and mitochondria under neurotoxic stress. *Nature*. 542:367-371.

Mielcarek, M., L. Inuabasi, M.K. Bondulich, T. Muller, G.F. Osborne, S.A. Franklin, D.L. Smith, A. Neueder, J. Rosinski, I. Rattray, A. Protti, and G.P. Bates. 2014. Dysfunction of the CNS-heart axis in mouse models of Huntington's disease. *PLoS genetics*. 10:e1004550.

Mizushima, N., T. Yoshimori, and Y. Ohsumi. 2011. The role of Atg proteins in autophagosome formation. *Annual review of cell and developmental biology*. 27:107-132.

Mozaffarian, D., E.J. Benjamin, A.S. Go, D.K. Arnett, M.J. Blaha, M. Cushman, S.R. Das, S. de Ferranti, J.P. Despres, H.J. Fullerton, V.J. Howard, M.D. Huffman, C.R. Isasi, M.C. Jimenez, S.E. Judd, B.M. Kissela, J.H. Lichtman, L.D. Lisabeth, S. Liu, R.H. Mackey, D.J. Magid, D.K. McGuire, E.R. Mohler, 3rd, C.S. Moy, P. Muntner, M.E. Mussolino, K. Nasir, R.W. Neumar, G. Nichol, L. Palaniappan, D.K. Pandey, M.J. Reeves, C.J. Rodriguez, W. Rosamond, P.D. Sorlie, J. Stein, A. Towfighi, T.N. Turan, S.S. Virani, D. Woo, R.W. Yeh, and M.B. Turner. 2016. Heart disease and stroke statistics-2016 update: a report from the American Heart Association. *Circulation*. 133:e38-360.

Nakai, A., O. Yamaguchi, T. Takeda, Y. Higuchi, S. Hikoso, M. Taniike, S. Omiya, I. Mizote, Y. Matsumura, M. Asahi, K. Nishida, M. Hori, N. Mizushima, and K. Otsu. 2007. The role of autophagy in cardiomyocytes in the basal state and in response to hemodynamic stress. *Nature medicine*. 13:619-624.

Narendra, D., A. Tanaka, D.F. Suen, and R.J. Youle. 2008. Parkin is recruited selectively to impaired mitochondria and promotes their autophagy. *The Journal of cell biology*. 183:795-803.

Neuspiel, M., A.C. Schauss, E. Braschi, R. Zunino, P. Rippstein, R.A. Rachubinski, M.A. Andrade-Navarro, and H.M. McBride. 2008. Cargo-selected transport from the mitochondria to peroxisomes is mediated by vesicular carriers. *Current Biology*. 18:102-108.

Ney, P.A. 2015. Mitochondrial autophagy: Origins, significance, and role of BNIP3 and NIX. *Biochimica et biophysica acta*. 1853:2775-2783.

Nishida, Y., S. Arakawa, K. Fujitani, H. Yamaguchi, T. Mizuta, T. Kanaseki, M. Komatsu, K. Otsu, Y. Tsujimoto, and S. Shimizu. 2009. Discovery of Atg5/Atg7-independent alternative macroautophagy. *Nature*. 461:654-658.

Nobelprize.org. 2016. The Nobel Prize in Physiology or Medicine 2016. *In* Nobelprize.org. Vol. 2017. Nobel Media AB 2014.

Novak, I., V. Kirkin, D.G. McEwan, J. Zhang, P. Wild, A. Rozenknop, V. Rogov, F. Lohr, D. Popovic, A. Occhipinti, A.S. Reichert, J. Terzic, V. Dotsch, P.A. Ney, and I. Dikic. 2010. Nix is a selective autophagy receptor for mitochondrial clearance. *Embo Rep*. 11:45-51.

Okatsu, K., S. Iemura, F. Koyano, E. Go, M. Kimura, T. Natsume, K. Tanaka, and N. Matsuda. 2012. Mitochondrial hexokinase HKI is a novel substrate of the Parkin ubiquitin ligase. *Biochemical and biophysical research communications*. 428:197-202.

Okatsu, K., K. Saisho, M. Shimanuki, K. Nakada, H. Shitara, Y.S. Sou, M. Kimura, S. Sato, N. Hattori, M. Komatsu, K. Tanaka, and N. Matsuda. 2010. p62/SQSTM1 cooperates with Parkin for perinuclear clustering of depolarized mitochondria. *Genes to cells : devoted to molecular & cellular mechanisms*. 15:887-900.

Omodei, D., and L. Fontana. 2011. Calorie restriction and prevention of age-associated chronic disease. *FEBS Lett*. 585:1537-1542.

Palacino, J.J., D. Sagi, M.S. Goldberg, S. Krauss, C. Motz, M. Wacker, J. Klose, and J. Shen. 2004. Mitochondrial dysfunction and oxidative damage in parkin-deficient mice. *The Journal of biological chemistry*. 279:18614-18622.

Pankiv, S., T.H. Clausen, T. Lamark, A. Brech, J.A. Bruun, H. Outzen, A. Overvatn, G. Bjorkoy, and T. Johansen. 2007. p62/SQSTM1 binds directly to Atg8/LC3 to facilitate degradation of ubiquitinated protein aggregates by autophagy. *The Journal of biological chemistry*. 282:24131-24145.

Perrett, R.M., Z. Alexopoulou, and G.K. Tofaris. 2015. The endosomal pathway in Parkinson's disease. *Mol Cell Neurosci*. 66:21-28.

Phan, S., D. Boassa, P. Nguyen, X. Wan, J. Lanman, A. Lawrence, and M.H. Ellisman. 2017. 3D reconstruction of biological structures: automated procedures for alignment and reconstruction of multiple tilt series in electron tomography. *Advanced structural and chemical imaging*. 2:8.

Piquereau, J., F. Caffin, M. Novotova, C. Lemaire, V. Veksler, A. Garnier, R. Ventura-Clapier, and F. Joubert. 2013a. Mitochondrial dynamics in the adult cardiomyocytes: which roles for a highly specialized cell? *Frontiers in physiology*. 4:102.

Piquereau, J., R. Godin, S. Deschenes, V.L. Bessi, M. Mofarrahi, S.N. Hussain, and Y. Burelle. 2013b. Protective role of PARK2/Parkin in sepsis-induced cardiac contractile and mitochondrial dysfunction. *Autophagy*. 9:1837-1851.

Plun-Favreau, H., V.S. Burchell, K.M. Holmstrom, Z. Yao, E. Deas, K. Cain, V. Fedele, N. Moisoi, M. Campanella, L. Miguel Martins, N.W. Wood, A.V. Gourine, and A.Y. Abramov. 2012. HtrA2 deficiency causes mitochondrial uncoupling through the F(1)F(0)-ATP synthase and consequent ATP depletion. *Cell death & disease*. 3:e335.

Raiborg, C., and H. Stenmark. 2009. The ESCRT machinery in endosomal sorting of ubiquitylated membrane proteins. *Nature*. 458:445-452.

Rana, A., M. Rera, and D.W. Walker. 2013. Parkin overexpression during aging reduces proteotoxicity, alters mitochondrial dynamics, and extends lifespan. *Proceedings of the National Academy of Sciences of the United States of America*. 110:8638-8643.

Razeghi, P., M.E. Young, J.L. Alcorn, C.S. Moravec, O.H. Frazier, and H. Taegtmeyer. 2001. Metabolic gene expression in fetal and failing human heart. *Circulation*. 104:2923-2931.

Razi, M., and C.E. Futter. 2006. Distinct roles for Tsg101 and Hrs in multivesicular body formation and inward vesiculation. *Molecular biology of the cell*. 17:3469-3483.

Regula, K.M., K. Ens, and L.A. Kirshenbaum. 2002. Inducible expression of BNIP3 provokes mitochondrial defects and hypoxia-mediated cell death of ventricular myocytes. *Circ Res*. 91:226-231.

Rikka, S., M.N. Quinsay, R.L. Thomas, D.A. Kubli, X. Zhang, A.N. Murphy, and A.B. Gustafsson. 2011. Bnip3 impairs mitochondrial bioenergetics and stimulates mitochondrial turnover. *Cell death and differentiation*. 18:721-731.

Rink, J., E. Ghigo, Y. Kalaidzidis, and M. Zerial. 2005. Rab conversion as a mechanism of progression from early to late endosomes. *Cell*. 122:735-749.

Roy, S.G., M.W. Stevens, L. So, and A.L. Edinger. 2013. Reciprocal effects of rab7 deletion in activated and neglected T cells. *Autophagy*. 9:1009-1023.

Rubinsztein, D.C., T. Shpilka, and Z. Elazar. 2012. Mechanisms of autophagosome biogenesis. *Current biology : CB*. 22:R29-34.

Saelens, X., N. Festjens, L. Vande Walle, M. van Gurp, G. van Loo, and P. Vandenabeele. 2004. Toxic proteins released from mitochondria in cell death. *Oncogene*. 23:2861-2874.

Schaper, J., E. Meiser, and G. Stammler. 1985. Ultrastructural morphometric analysis of myocardium from dogs, rats, hamsters, mice, and from human hearts. *Circulation research*. 56:377-391.

Schmittgen, T.D., and K.J. Livak. 2008. Analyzing real-time PCR data by the comparative C(T) method. *Nature protocols*. 3:1101-1108.

Schwarten, M., J. Mohrluder, P.X. Ma, M. Stoldt, Y. Thielmann, T. Stangler, N. Hersch, B. Hoffmann, R. Merkel, and D. Willbold. 2009. Nix directly binds to GABARAP A possible crosstalk between apoptosis and autophagy. *Autophagy*. 5:690-698.

Seglen, P.O., P.B. Gordon, and I. Holen. 1990. Non-selective autophagy. *Seminars in cell biology*. 1:441-448.

Siddall, H.K., D.M. Yellon, S.B. Ong, U.A. Mukherjee, N. Burke, A.R. Hall, P.R. Angelova, M.H. Ludtmann, E. Deas, S.M. Davidson, M.M. Mocanu, and D.J. Hausenloy. 2013. Loss of PINK1 increases the heart's vulnerability to ischemia-reperfusion injury. *Plos One*. 8:e62400.

Sigismund, S., E. Argenzio, D. Tosoni, E. Cavallaro, S. Polo, and P.P. Di Fiore. 2008. Clathrin-mediated internalization is essential for sustained EGFR signaling but dispensable for degradation. *Developmental cell*. 15:209-219.

Singh, R., S. Kaushik, Y. Wang, Y. Xiang, I. Novak, M. Komatsu, K. Tanaka, A.M. Cuervo, and M.J. Czaja. 2009. Autophagy regulates lipid metabolism. *Nature*. 458:1131-1135.

Smirnova, E., L. Griparic, D.L. Shurland, and A.M. van der Bliek. 2001. Dynamin-related protein Drp1 is required for mitochondrial division in mammalian cells. *Molecular biology of the cell*. 12:2245-2256.

Song, M., K. Mihara, Y. Chen, L. Scorrano, and G.W. Dorn, 2nd. 2015. Mitochondrial fission and fusion factors reciprocally orchestrate mitophagic culling in mouse hearts and cultured fibroblasts. *Cell metabolism*. 21:273-285.

Soubannier, V., G.L. McLelland, R. Zunino, E. Braschi, P. Rippstein, E.A. Fon, and H.M. McBride. 2012a. A vesicular transport pathway shuttles cargo from mitochondria to lysosomes. *Current biology : CB*. 22:135-141.

Soubannier, V., P. Rippstein, B.A. Kaufman, E.A. Shoubridge, and H.M. McBride. 2012b. Reconstitution of mitochondria derived vesicle formation demonstrates selective enrichment of oxidized cargo. *Plos One*. 7:e52830.

Sriram, S.R., X. Li, H.S. Ko, K.K. Chung, E. Wong, K.L. Lim, V.L. Dawson, and T.M. Dawson. 2005. Familial-associated mutations differentially disrupt the solubility, localization, binding and ubiquitination properties of parkin. *Human molecular genetics*. 14:2571-2586.

Stenmark, H. 2009. Rab GTPases as coordinators of vesicle traffic. *Nature reviews. Molecular cell biology*. 10:513-525.

Stenmark, H., R.G. Parton, O. Steele-Mortimer, A. Lutcke, J. Gruenberg, and M. Zerial. 1994a. Inhibition of rab5 GTPase activity stimulates membrane fusion in endocytosis. *The EMBO journal*. 13:1287-1296.

Stenmark, H., A. Valencia, O. Martinez, O. Ullrich, B. Goud, and M. Zerial. 1994b. Distinct structural elements of rab5 define its functional specificity. *The EMBO journal*. 13:575-583.

Sudhof, T.C. 2004. The synaptic vesicle cycle. *Annual review of neuroscience*. 27:509-547.

Sullivan, P.G., N.B. Dragicevic, J.H. Deng, Y. Bai, E. Dimayuga, Q. Ding, Q. Chen, A.J. Bruce-Keller, and J.N. Keller. 2004. Proteasome inhibition alters neural mitochondrial homeostasis and mitochondria turnover. *The Journal of biological chemistry*. 279:20699-20707.

Sun, L., C.K. Macgowan, J.G. Sled, S.J. Yoo, C. Manlhiot, P. Porayette, L. Grosse-Wortmann, E. Jaeggi, B.W. McCrindle, J. Kingdom, E. Hickey, S. Miller, and M. Seed. 2015. Reduced fetal cerebral oxygen consumption is associated with smaller brain size in fetuses with congenital heart disease. *Circulation*. 131:1313-1323.

Sun, Q., W. Westphal, K.N. Wong, I. Tan, and Q. Zhong. 2010. Rubicon controls endosome maturation as a Rab7 effector. *Proceedings of the National Academy of Sciences of the United States of America*. 107:19338-19343.

Tanaka, A., M.M. Cleland, S. Xu, D.P. Narendra, D.F. Suen, M. Karbowski, and R.J. Youle. 2010. Proteasome and p97 mediate mitophagy and degradation of mitofusins induced by Parkin. *The Journal of cell biology*. 191:1367-1380.

Taneike, M., O. Yamaguchi, A. Nakai, S. Hikoso, T. Takeda, I. Mizote, T. Oka, T. Tamai, J. Oyabu, T. Murakawa, K. Nishida, T. Shimizu, M. Hori, I. Komuro, T.S. Takuji Shirasawa, N. Mizushima, and K. Otsu. 2010. Inhibition of autophagy in the heart induces age-related cardiomyopathy. *Autophagy*. 6:600-606.

Tanida, I. 2011. Autophagy basics. *Microbiology and immunology*. 55:1-11.

Thomas, R.L., D.J. Roberts, D.A. Kubli, Y. Lee, M.N. Quinsay, J.B. Owens, K.M. Fischer, M.A. Sussman, S. Miyamoto, and A.B. Gustafsson. 2013. Loss of MCL-1 leads to impaired autophagy and rapid development of heart failure. *Genes & development*. 27:1365-1377.

Thornburg, K., S. Jonker, P. O'Tierney, N. Chattergoon, S. Louey, J. Faber, and G. Giraud. 2011. Regulation of the cardiomyocyte population in the developing heart. *Progress in biophysics and molecular biology*. 106:289-299.

Twig, G., A. Elorza, A.J. Molina, H. Mohamed, J.D. Wikstrom, G. Walzer, L. Stiles, S.E. Haigh, S. Katz, G. Las, J. Alroy, M. Wu, B.F. Py, J. Yuan, J.T. Deeney, B.E. Corkey, and O.S. Shirihai. 2008. Fission and selective fusion govern mitochondrial segregation and elimination by autophagy. *The EMBO journal*. 27:433-446.

van Buchem, M.A., G.J. Biessels, H.P. Brunner la Rocca, A.J. de Craen, W.M. van der Flier, M.A. Ikram, L.J. Kappelle, P.J. Koudstaal, S.P. Mooijaart, W. Niessen, R. van Oostenbrugge, A. de Roos, A.C. van Rossum, and M.J. Daemen. 2014. The heart-brain connection: a multidisciplinary approach targeting a missing link in the pathophysiology of vascular cognitive impairment. *Journal of Alzheimer's disease : JAD*. 42 Suppl 4:S443-451.

van der Bliek, A.M., Q. Shen, and S. Kawajiri. 2013. Mechanisms of mitochondrial fission and fusion. *Cold Spring Harbor perspectives in biology*. 5.

Vande, V.C., J. Cizeau, D. Dubik, J. Alimonti, T. Brown, S. Israels, R. Hakem, and A.H. Greenberg. 2000. BNIP3 and genetic control of necrosis-like cell death through the mitochondrial permeability transition pore. *Mol.Cell Biol.* 20:5454-5468.

Wai, T., J. Garcia-Prieto, M.J. Baker, C. Merkwirth, P. Benit, P. Rustin, F.J. Ruperez, C. Barbas, B. Ibanez, and T. Langer. 2015. Imbalanced OPA1 processing and mitochondrial fragmentation cause heart failure in mice. *Science*. 350:aad0116.

Wang, K., and D.J. Klionsky. 2011. Mitochondria removal by autophagy. *Autophagy*. 7:297-300.

Wang, X., and J. Robbins. 2014. Proteasomal and lysosomal protein degradation and heart disease. *Journal of molecular and cellular cardiology*. 71c:16-24.

Wang, X., D. Winter, G. Ashrafi, J. Schlehe, Y.L. Wong, D. Selkoe, S. Rice, J. Steen, M.J. LaVoie, and T.L. Schwarz. 2011. PINK1 and Parkin target Miro for phosphorylation and degradation to arrest mitochondrial motility. *Cell*. 147:893-906.

Williams, R.L., and S. Urbe. 2007. The emerging shape of the ESCRT machinery. *Nature reviews. Molecular cell biology*. 8:355-368.

Wu, C., M.R. Jain, Q. Li, S. Oka, W. Li, A.N. Kong, N. Nagarajan, J. Sadoshima, W.J. Simmons, and H. Li. 2014. Identification of novel nuclear targets of human thioredoxin 1. *Molecular & cellular proteomics : MCP*. 13:3507-3518.

Xu, W., A.M. Weissmiller, J.A. White, 2nd, F. Fang, X. Wang, Y. Wu, M.L. Pearn, X. Zhao, M. Sawa, S. Chen, S. Gunawardena, J. Ding, W.C. Mobley, and C. Wu. 2016. Amyloid precursor protein-mediated endocytic pathway disruption induces

axonal dysfunction and neurodegeneration. *The Journal of clinical investigation*. 126:1815-1833.

Yamashiro, D.J., S.R. Fluss, and F.R. Maxfield. 1983. Acidification of endocytic vesicles by an ATP-dependent proton pump. *The Journal of cell biology*. 97:929-934.

Yoshii, S.R., C. Kishi, N. Ishihara, and N. Mizushima. 2011. Parkin mediates proteasome-dependent protein degradation and rupture of the outer mitochondrial membrane. *The Journal of biological chemistry*. 286:19630-19640.

Youle, R.J., and D.P. Narendra. 2011. Mechanisms of mitophagy. *Nature reviews. Molecular cell biology*. 12:9-14.

Zeigerer, A., J. Gilleron, R.L. Bogorad, G. Marsico, H. Nonaka, S. Seifert, H. Epstein-Barash, S. Kuchimanchi, C.G. Peng, V.M. Ruda, P. Del Conte-Zerial, J.G. Hengstler, Y. Kalaidzidis, V. Koteliansky, and M. Zerial. 2012. Rab5 is necessary for the biogenesis of the endolysosomal system in vivo. *Nature*. 485:465-470.

Zhang, H., M. Bosch-Marce, L.A. Shimoda, Y.S. Tan, J.H. Baek, J.B. Wesley, F.J. Gonzalez, and G.L. Semenza. 2008. Mitochondrial autophagy is an HIF-1-dependent adaptive metabolic response to hypoxia. *The Journal of biological chemistry*. 283:10892-10903.

Zhang, T., L. Xue, L. Li, C. Tang, Z. Wan, R. Wang, J. Tan, Y. Tan, H. Han, R. Tian, T.R. Billiar, W.A. Tao, and Z. Zhang. 2016. BNIP3 protein suppresses PINK1 kinase proteolytic cleavage to promote mitophagy. *The Journal of biological chemistry*. 291:21616-21629.

Zhang, Y., J. Gao, K.K. Chung, H. Huang, V.L. Dawson, and T.M. Dawson. 2000. Parkin functions as an E2-dependent ubiquitin- protein ligase and promotes the degradation of the synaptic vesicle-associated protein, CDCrel-1. *Proceedings of the National Academy of Sciences of the United States of America*. 97:13354-13359.

Zhong, Q., W. Gao, F. Du, and X. Wang. 2005. Mule/ARF-BP1, a BH3-only E3 ubiquitin ligase, catalyzes the polyubiquitination of Mcl-1 and regulates apoptosis. *Cell*. 121:1085-1095.